VOLUME 33 FEBRUARY 1955 NUMBER 2

Canadian Journal of Physics

Editor: G. M. VOLKOFF

Associate Editors:

L. G. ELLIOTT, *Atomic Energy of Canada, Ltd., Chalk River*
J. S. FOSTER, *McGill University*
G. HERZBERG, *National Research Council of Canada*
L. LEPRINCE-RINGUET, *Ecole Polytechnique, Paris*
D. W. R. McKINLEY, *National Research Council of Canada*
B. W. SARGENT, *Queen's University*
Sir FRANCIS SIMON, *Clarendon Laboratory, University of Oxford*
W. H. WATSON, *University of Toronto*

Published by THE NATIONAL RESEARCH COUNCIL
OTTAWA CANADA

CANADIAN JOURNAL OF PHYSICS

(*Formerly Section A, Canadian Journal of Research*)

Under the authority of the Chairman of the Committee of the Privy Council on Scientific and Industrial Research, the National Research Council issues THE CANADIAN JOURNAL OF PHYSICS and six other journals devoted to the publication of the results of original scientific research. Matters of general policy concerning these journals are the responsibility of a joint Editorial Board consisting of: members representing the National Research Council of Canada; the Editors of the Journals; and members representing the Royal Society of Canada and four other scientific societies.

EDITORIAL BOARD

Representatives of the National Research Council

A. N. Campbell, *University of Manitoba*
G. E. Hall, *University of Western Ontario*
E. G. D. Murray, *McGill University*
D. L. Thomson, *McGill University*
W. H. Watson (Chairman), *University of Toronto*

Editors of the Journals

D. L. Bailey, *University of Toronto*
J. B. Collip, *University of Western Ontario*
E. H. Craigie, *University of Toronto*
G. A. Ledingham, *National Research Council*
Léo Marion, *National Research Council*
R. G. E. Murray, *University of Western Ontario*
G. M. Volkoff, *University of British Columbia*

Representatives of Societies

D. L. Bailey, *University or Toronto*
Royal Society of Canada
J. B. Collip, *University of Western Ontario*
Canadian Physiological Society
E. H. Craigie, *University of Toronto*
Royal Society of Canada
R. G. E. Murray, *University of Western Ontario*
Canadian Society of Microbiologists
H. G. Thode, *McMaster University*
Chemical Institute of Canada
T. Thorvaldson, *University of Saskatchewan*
Royal Society of Canada
G. M. Volkoff, *University of British Columbia*
Royal Society of Canada; Canadian Association of Physicists

Ex officio

Léo Marion (Editor-in-Chief), *National Research Council*

Manuscripts for publication should be submitted to Dr. Léo Marion, Editor-in-Chief, Canadian Journal of Physics, National Research Council, Ottawa 2, Canada.
(For instructions on preparation of copy, see **Notes to Contributors** (inside back cover).)

Proof, correspondence concerning proof, and orders for reprints should be sent to the Manager, Editorial Office (Research Journals), Division of Administration, National Research Council, Ottawa 2, Canada.

Subscriptions, renewals, requests for single or back numbers, and all remittances should be sent to Division of Administration, National Research Council, Ottawa 2, Canada. Remittances should be made payable to the Receiver General of Canada, credit National Research Council.

The journals published, frequency of publication, and prices are:

Canadian Journal of Biochemistry and Physiology	Bimonthly	$3.00 a year
Canadian Journal of Botany	Bimonthly	$4.00 a year
Canadian Journal of Chemistry	Monthly	$5.00 a year
Canadian Journal of Microbiology*	Bimonthly	$3.00 a year
Canadian Journal of Physics	Monthly	$4.00 a year
Canadian Journal of Technology	Bimonthly	$3.00 a year
Canadian Journal of Zoology	Bimonthly	$3.00 a year

The price of single numbers of all journals is 75 cents.

*Volume 1 will combine three numbers published in 1954 with six published in 1955 and will be available at the regular annual subscription rate of $3.00.

"Reprinted in entirety by photo-offset from the original issue"

Canadian Journal of Physics

Issued by THE NATIONAL RESEARCH COUNCIL OF CANADA

VOLUME 33 FEBRUARY 1955 NUMBER 2

MASS SPECTROMETRIC STUDY OF NATURAL AND NEUTRON-IRRADIATED CHLORINE[1]

BY A. W. BOYD, F. BROWN, AND M. LOUNSBURY

ABSTRACT

Using a Nier-type mass spectrometer, the isotopic composition of chlorine gas obtained from natural potassium chloride has been measured to be 75.529 $\pm$0.016 atom per cent Cl^{35} and 24.471$\pm$0.016 atom per cent Cl^{37}, corresponding to a Cl^{35}/Cl^{37} atom ratio of 3.0865$\pm$0.0027. By comparison of this result with that for chlorine gas from potassium chloride irradiated for 14 months in a high flux position of the NRX reactor, the neutron capture cross-section of Cl^{36} has been determined to be 90$\pm$25 barns. This value has been calculated on the assumption that only (n, γ) reactions were significant in changing the isotopic composition of the chlorine.

INTRODUCTION

Aston (2) in 1931 measured the natural abundance ratio of the chlorine isotopes, Cl^{35}/Cl^{37}, and found values between 3.0 and 3.1. Kallman and Lazareff (6) in 1933 found the ratio to be 3.24. The ratio was measured in 1936 by Nier and Hanson (7) and they found a value of 3.07$\pm$0.03. Owen and Schaeffer (8) recently obtained the value of 3.13$\pm$0.03, and found no variation in the ratio for samples of marine, igneous, or sedimentary origin. This paper presents mass spectrometer data which give a more precise value of the isotopic abundance ratio for chlorine obtained from natural potassium chloride.

The neutron capture cross-section of the long-lived β-emitter Cl^{36} has not been measured previously. Cl^{36} is an odd–odd nuclide with 19 neutrons, one less than the "magic" 20-neutron configuration. It would be interesting to compare its neutron capture cross-section with that of Cl^{35} and Cl^{37}. By comparison of the mass spectrometer analyses of natural and neutron-irradiated chlorine, a value for the neutron capture cross-section of Cl^{36} has been obtained. A subsequent paper (3) will describe results relating to the determination of the half-life of Cl^{36}.

EXPERIMENTAL

A. Preparation of Gas Samples

The source of natural chlorine used was C.P. grade potassium chloride. A 10-gm. sample of this same material was irradiated for 14 months in a high flux position of the NRX reactor, and was used to prepare the radioactive gas samples.

[1]*Manuscript received September 29, 1954.*
Contribution from Chemistry Branch, Atomic Energy of Canada Limited, Chalk River, Ontario. Issued as A.E.C.L. No. 150.

For the unirradiated samples, the potassium chloride was recrystallized from distilled water. A 4-gm. sample was treated with hot concentrated sulphuric acid in a slow stream of air. The hydrogen chloride gas evolved was recovered quantitatively in ice-cold water and was then redistilled *in vacuo*. The product was converted to potassium chloride by titration with potassium carbonate solution, using methyl orange as an indicator. Potassium chloride was recovered from the solution by evaporation of most of the water, followed by the addition of alcohol. Finally the product was dried in an oven, and stored in a desiccator. Chlorine gas was prepared from this material by the method of Brown, Gillies, and Stevens (4). The preparation was carried out in triplicate, so that three separate samples, designated as A, B, and C, of natural chlorine gas were available for mass analysis. The high yield of this method of preparation should introduce negligible isotopic fractionation.

For the radioactive samples, the irradiated potassium chloride was again recrystallized from distilled water to ensure complete isotopic mixing, and then treated using the same procedure as described in the preceding paragraph. The three samples of irradiated chlorine which were prepared were designated as A′, B′, and C′.

B. Mass Spectrometry

A 90°-deflection, 6-in.-radius mass spectrometer was used for the analysis of the chlorine gas samples. This instrument is similar to one previously described (5). The sample inlet system consisted of a rotary fore pump, a silicone oil diffusion pump, and a liquid nitrogen-cooled trap. The gas sample pressure was adjusted by means of an evacuated expansion bulb. Apiezon high vacuum grease N was used for stopcocks and joints. Magnetic scanning of the mass region 70 to 74 was employed. The ion currents were amplified by a d-c. amplifier and recorded with a Leeds and Northrup Speedomax, Type G.

It was found that the mass spectrometer exhibited a pronounced memory effect in the analysis of the chlorine gas samples, so that it was not possible to alternate quickly between the natural and irradiated samples. After the large memory effect was discovered, no chlorine was admitted to the instrument for six months. Chlorine residuals were then no longer detectable. The instrument was then flushed for a day with radioactive sample B′, evacuated, and another volume of the same gas admitted and analyzed continuously during the course of several days. The procedure was repeated with radioactive sample A′. The instrument was then pumped for three months, and using the same procedure, the three samples of natural chlorine were analyzed in the order ABCBA. The presence of radioactive chlorine in the natural chlorine was monitored at masses 71 and 73, which occur only in the radioactive gas. In all cases, radioactive contamination was found to be negligible. When the analysis of the three natural samples was completed, the instrument was again pumped for three months, and then the third radioactive sample, C′, was analyzed. Agreement with the results of samples A′ and B′ indicated that the three-month pumping period was sufficient to reduce the natural chlorine residuals to negligible proportions.

RESULTS AND DISCUSSION

A. Natural Abundance of Chlorine Isotopes

The two stable isotopes of chlorine combine to form the following molecular species:

Mass	Composition
70	$Cl^{35}Cl^{35}$
72	$Cl^{35}Cl^{37}$
74	$Cl^{37}Cl^{37}$

Thus, the natural isotopic abundance ratio is given by

$$\frac{Cl^{35}}{Cl^{37}} = \frac{2(70)+(72)}{2(74)+(72)} \qquad [a]$$

where (70) is the height of the mass 70 peak, and similarly for the others.

In Table I are presented the results obtained from the three natural chlorine samples A, B, and C. Each of the 10 determinations listed is the average obtained from 10 or more spectrograms. The error quoted in each case is the standard deviation from the mean, and does not include any possible systematic error. However, precautions were taken so that errors arising from isotopic fractionation in sample preparation and in gas flow through the mass spectrometer, from mass discrimination in the ion source, and from non-linearity in ion current measurements either were not present, or were reduced to negligible proportions.

TABLE I

ISOTOPIC COMPOSITION OF NATURAL CHLORINE

Obs. No.	Sample	Atom % Cl^{35}	Atom % Cl^{37}	Atom ratio Cl^{35}/Cl^{37}
1	A	75.550 ±0.016	24.450 ±0.016	3.0900 ±0.0026
2	A	75.509 ±0.013	24.491 ±0.013	3.0831 ±0.0022
3	A	75.515 ±0.013	24.485 ±0.013	3.0842 ±0.0021
4	A	75.511 ±0.013	24.489 ±0.013	3.0834 ±0.0022
5	A	75.533 ±0.010	24.467 ±0.010	3.0871 ±0.0016
6	B	75.538 ±0.011	24.462 ±0.011	3.0880 ±0.0019
7	C	75.556 ±0.011	24.444 ±0.011	3.0910 ±0.0019
8	C	75.541 ±0.013	24.459 ±0.013	3.0884 ±0.0021
9	B	75.512 ±0.016	24.488 ±0.016	3.0837 ±0.0026
10	A	75.524 ±0.013	24.476 ±0.013	3.0856 ±0.0021
Grand mean		75.529	24.471	3.0865
Standard deviation		±0.016	±0.016	±0.0027

As may be seen from Table I, the grand mean for the natural isotopic abundance ratio Cl^{35}/Cl^{37} is 3.0865 ± 0.0027, which is within the limit of 3.07 ± 0.03 previously determined by Nier and Hanson (7) from a study of hydrogen chloride gas.

B. Isotopic Analysis of the Irradiated Chlorine

The three isotopes, masses 35, 36, and 37, of the irradiated chlorine combine to form the following molecular species:

Mass	Composition
70	$Cl^{35}Cl^{35}$
71	$Cl^{35}Cl^{36}$
72	$Cl^{36}Cl^{36}+Cl^{35}Cl^{37}$
73	$Cl^{36}Cl^{37}$
74	$Cl^{37}Cl^{37}$

If the mole fraction $[Cl^{36}Cl^{36}/(Cl^{36}Cl^{36}+Cl^{35}Cl^{37})]$ is represented by α, then the abundances of the three chlorine isotopes are given by:

[*b*] $$Cl^{35} = 2(70)+(71)+(1-\alpha)(72),$$

[*c*] $$Cl^{36} = (71)+2\alpha(72)+(73),$$

[*d*] $$Cl^{37} = (1-\alpha)(72)+(73)+2(74).$$

The mole fraction α may be evaluated using the following expressions:

[*e*] $$Cl^{36}/Cl^{35} = (71)/2(70) = y,$$

[*f*] $$Cl^{37}/Cl^{35} = \sqrt{(74)/(70)} = z,$$

which are exact if the isotopic distribution is determined by equal statistical weights. Then

[*g*] $$\alpha = \frac{Cl^{36}Cl^{36}}{Cl^{36}Cl^{36}+Cl^{35}Cl^{37}} = \frac{y^2}{y^2+2z}.$$

Using the mass spectrometer data for the irradiated chlorine, the mole fraction α was determined by equation [*g*] to be 0.001713. Small errors in α are insignificant because α is very small. Using this value of α and the mass spectrometer data, the isotopic abundances of the irradiated chlorine were calculated using equations [*b*], [*c*], and [*d*].

Table II shows the results obtained from the three irradiated chlorine samples A′, B′, and C′. Each of the eight determinations listed is the average obtained from about fifteen spectrograms. The errors quoted have the same significance as those in Table I. In terms of atom per cent, the grand mean is 72.962% Cl^{35}, 2.483% Cl^{36}, and 24.555% Cl^{37} for the irradiated chlorine.

TABLE II

ISOTOPIC COMPOSITION OF IRRADIATED CHLORINE

Obs. No.	Sample	Atom % Cl^{35}	Atom % Cl^{36}	Atom % Cl^{37}
1	B′	72.932 ±0.018	2.484 ±0.004	24.584 ±0.018
2	B′	72.990 ±0.010	2.479 ±0.005	24.531 ±0.010
3	B′	72.948 ±0.014	2.485 ±0.006	24.567 ±0.015
4	A′	72.978 ±0.014	2.490 ±0.004	24.532 ±0.015
5	A′	72.969 ±0.019	2.480 ±0.005	24.551 ±0.018
6	A′	72.937 ±0.012	2.484 ±0.007	24.579 ±0.013
7	C′	72.994 ±0.014	2.477 ±0.005	24.529 ±0.012
8	C′	72.948 ±0.015	2.484 ±0.003	24.568 ±0.014
	Grand mean	72.962	2.483	24.555
	Standard deviation	±0.022	±0.004	±0.021

C. The Cross-section for the Reaction $Cl^{36}(n, \gamma)Cl^{37}$ and Others

In Table III, the changes in isotopic composition resulting from the neutron irradiation of natural chlorine are shown.

TABLE III

COMPARISON OF ISOTOPIC COMPOSITION OF NATURAL AND IRRADIATED CHLORINE

Sample	Atom % Cl^{35}	Atom % Cl^{36}	Atom % Cl^{37}
Natural	75.529 ±0.016	—	24.471 ±0.016
Irradiated	72.962 ±0.022	2.483 ±0.004	24.555 ±0.021
Difference	−2.567 ±0.027	+2.483 ±0.004	+0.084 ±0.026

A value for the cross-section σ_{c6} of the reaction $Cl^{36}(n, \gamma)Cl^{37}$ and for the destruction cross-section σ_{d6} of Cl^{36} by other reactions excepting reversion to Cl^{35} can be obtained by considering possible decreases or increases in the atom percentage of Cl^{37}. It is first necessary to consider the cross-sections of reactions leading to or from the three isotopes of chlorine.

(n, γ) Reactions

The thermal neutron absorption cross-section for the element chlorine is 32 barns (10). It is reasonably certain that almost all this absorption is due to the reaction $Cl^{35}(n, \gamma)Cl^{36}$ ($Q = 8.56$ Mev.) with a cross-section of 40 barns, since the cross-sections for other known reactions are small (see below) and the activation cross-section for the reaction $Cl^{37}(n, \gamma)Cl^{38}$ ($Q = 6.25$ Mev.) is only 0.56 barns (10).

(n, p) Reactions

The reaction $Cl^{35}(n, p)S^{35}$ ($Q = 0.52$ Mev.) has a thermal neutron cross-section of 0.3 barns (10). This reaction is partially reversible during a long irradiation since the half-life for β^- decay of S^{35} is 87 days. It can be calculated that in the present experiment with an irradiation of 14 months and a decay period of 2 months before processing the amount of Cl^{35} finally destroyed by this reaction is 0.003 atom per cent (of all the chlorine). The resultant relative increase in the atom per cent of Cl^{37} will be $\sim$0.001, which is negligible. The reaction $Cl^{37}(n, p)S^{37}$ is totally reversible since the half-life for β^- decay of S^{37} is only five minutes. In any case the Q value of this reaction is -3.7 Mev. so that the cross-section would be extremely small for pile neutrons.

(n, α) Reactions

The cross-section for the reaction $Cl^{35}(n, \alpha)P^{32}$ ($Q = 0.97$ Mev.) is only 10 millibarns for 3 Mev. neutrons (1), 65 millibarns for 4 Mev. neutrons (1), and 165 millibarns for 14.5 Mev. neutrons (9) so that it would be negligibly small for pile neutrons. The cross-section for the reaction $Cl^{37}(n, \alpha)P^{34}$, which has a Q value of -1.3 Mev., is only 50 millibarns for 14.5 Mev. neutrons (9) and should also be negligibly small for pile neutrons. Another reaction of interest is $K^{39}(n, \alpha)Cl^{36}$, since the irradiated material was potassium chloride. The Q value for this reaction is 1.3 Mev., and considering that Z for potassium is two units higher than for chlorine there is good reason to suppose that the cross-section for this reaction can once again be neglected for the present purposes. The cross-section for $K^{39}(n, \gamma)K^{40}$ ($Q = 7.76$ Mev.) is only 2 barns (10); the cross section for $K^{41}(n, \alpha)Cl^{38}$ ($Q = -0.83$ Mev.) is only 30 millibarns for 14.5 Mev. neutrons (9).

(n, 2n) Reactions

These have thresholds in the order of 10 Mev. and although sometimes detectable for pile neutrons, the effective cross-sections will be negligible for the present purposes.

It may therefore be assumed that the only reaction leading to a decrease in Cl^{37} is the $Cl^{37}(n, \gamma)Cl^{38}$ reaction and the only reactions leading to an increase in Cl^{37} are (*a*) the $Cl^{36}(n, \gamma)Cl^{37}$ reaction ($Q = 9.95$ Mev.) and (*b*) destruction of Cl^{36} by other reactions, which would also cause an increase in the *atom percentage* of Cl^{37}.

Consider in the first place the possible increase of Cl^{37} due to the reaction $Cl^{36}(n, \gamma)Cl^{37}$ with a cross-section σ_{c6}. The observed increase is 0.084 ± 0.026 atom per cent. The expected decrease in Cl^{37} due to the reaction $Cl^{37}(n, \gamma)Cl^{38}$

can be calculated as 0.011 atom per cent (of total chlorine). Hence the production of Cl^{37} by the $Cl^{36}(n, \gamma)Cl^{37}$ process is $0.011+(0.084\pm0.026) = 0.095 \pm 0.026$ atom per cent. This amount so produced may be expressed with sufficient accuracy by:

[h] $$\tfrac{1}{2}[Cl^{36}]_t \, \sigma_{c6} \, nvt = 0.095\pm0.026 \text{ atom per cent}$$

where $[Cl^{36}]_t$ is the amount of Cl^{36} (atom per cent) present at the end of the irradiation and nvt is the integrated neutron flux. The quantity nvt can be calculated approximately by using the expression:

[i] $$[Cl^{35}]_t/[Cl^{35}]_0 = e^{-\sigma_{c5} nvt}$$

where $[Cl^{35}]_0$ and $[Cl^{35}]_t$ are respectively the amounts of Cl^{35} (in atom per cent) present at the beginning and at the end of the irradiation, and σ_{c5}, the cross-section for the reaction $Cl^{35}(n, \gamma)Cl^{36}$, equals 40 barns (10). The first two quantities are measured by the experiment. The value of nvt thus obtained is 8.65×10^{20} neutrons/cm.^{2}.

Substituting this value and the experimental value of $[Cl^{36}]_t$ in equation [h], one obtains the cross-section for the reaction $Cl^{36}(n, \gamma)Cl^{37}$

$$\sigma_{c6} = 90\pm25 \text{ barns},$$

if the destruction of Cl^{36} by reactions other than $Cl^{36}(n, \gamma)Cl^{37}$ is negligible.

Alternatively, one may assume that σ_{c6} is negligible and consider the destruction of Cl^{36} by reactions other than (n, γ). Such destruction would cause an increase in the *atom percentage* of Cl^{37} equal to one quarter of the Cl^{36} destroyed (since Cl^{37} is one quarter of total chlorine), and one may write:

[j] $$\tfrac{1}{2}[Cl^{36}]_t \, \sigma_{d6} \, nvt = 4(0.095\pm0.026) \text{ atom per cent},$$

where σ_{d6} is the destruction cross-section of Cl^{36} by reactions other than (n, γ). Using the same experimental data as before, one obtains

$$\sigma_{d6} = 360\pm100 \text{ barns},$$

but only if the capture cross-section, σ_{c6}, is zero.

However, the assumption that σ_{d6} is almost certainly very small is consistent with the present knowledge of cross-sections for reactor neutron-induced destruction reactions in this mass region. Therefore, on the assumption that only (n, γ) reactions were of significance in changing the isotopic composition of the chlorine, the neutron capture cross-section for the reaction $Cl^{36}(n, \gamma)Cl^{37}$ may be taken to be 90 ± 25 barns.

ACKNOWLEDGMENTS

The authors wish to acknowledge the assistance of Dr. W. B. Lewis in many valuable discussions of this work. They also wish to thank Mr. W. D. McKee and Mrs. R. M. Bartholomew for their help in recording and computing mass spectrometer data.

REFERENCES

1. ADLER, H., HUBER, P., and HÄLG, W. Helv. Phys. Acta, 26: 349. 1953.
2. ASTON, F. W. Proc. Roy. Soc.(London), A, 132: 487. 1931.

3. BARTHOLOMEW, R. M., BOYD, A. W., BROWN, F., HAWKINGS, R. C., LOUNSBURY, M., and MERRITT, W. F. Can. J. Phys. 33: 43. 1955.
4. BROWN, F., GILLIES, A., and STEVENS, W. H. Can. J. Chem. 31: 768. 1953.
5. GRAHAM, R. L., HARKNESS, A. L., and THODE, H. G. J. Sci. Instr. 24: 119. 1947.
6. KALLMAN, H. and LAZAREFF, W. Z. Physik, 80: 237. 1933.
7. NIER, A. O. and HANSON, E. E. Phys. Rev. 50: 722. 1936.
8. OWEN, H. R. and SCHAEFFER, O. A. Private communication.
9. PAUL, E. B. and CLARKE, R. L. Can. J. Phys. 31: 267. 1953.
10. United States Atomic Energy Commission Report AECU-2040. 1952.

THE HALF-LIFE OF Cl^{36} [1]

By Rosalie M. Bartholomew, A. W. Boyd, F. Brown, R. C. Hawkings, M. Lounsbury, and W. F. Merritt

ABSTRACT

Cl^{36} was prepared by neutron irradiation of C.P. grade potassium chloride for 14 months in the NRX reactor. The disintegration rate of a purified sample of the irradiated material was determined by absolute beta counting with a 4π methane flow-type proportional counter. The number of Cl^{36} atoms in the sample was determined by gravimetric and mass spectrometric analysis. A value of $(3.08 \pm 0.03) \times 10^5$ years was obtained for the half-life of Cl^{36}, assuming that the simple decay scheme is correct.

INTRODUCTION

The nuclide Cl^{36}, first described by Grahame and Walke (3), is reported by Wu and Feldman (2, 8) to be a pure negatron emitter with a simple beta-ray spectrum of maximum energy ~0.7 Mev. Values reported for the half-life of Cl^{36} range from 2×10^5 years (7) to 2×10^6 years (5, 6). Wu and co-workers (9), using an end-window G–M counter to determine the disintegration rate and a microwave spectrometer to determine the isotopic concentrations, obtained a value of $(4.4 \pm 0.5) \times 10^5$ years. This paper presents data from which a new value of the half-life of Cl^{36} has been obtained, based on absolute beta counting and mass spectrometric analysis of neutron-irradiated chlorine.

EXPERIMENTAL

A. Isotopic Analysis of Irradiated Chlorine

The potassium chloride containing Cl^{36} was taken from the stock used by Boyd, Brown, and Lounsbury (1) for the determination of the neutron capture cross-section of Cl^{36}. This material, analyzed mass spectrometrically in the form of chlorine gas, was found by them to have the following isotopic composition (in atom per cent): $72.962 \pm 0.022\%$ Cl^{35}, $2.483 \pm 0.004\%$ Cl^{36}, and $24.555 \pm 0.021\%$ Cl^{37}. In each case, the error quoted is the standard deviation from the mean, and does not include any possible systematic error.

B. Radiochemical Purity of Samples

The initial purification of the irradiated potassium chloride was undertaken approximately three months after its removal from the NRX reactor. During this interval all short-lived radioactive impurities should have decayed to negligible proportions, leaving S^{35}, produced in the reaction $Cl^{35}(n, p)S^{35}$, as the major radioactive impurity.

The entire sample of irradiated potassium chloride was recrystallized from water and dried. This step was taken to ensure a uniform isotopic distribution. A portion of the recrystallized material was then distilled from hot concentrated sulphuric acid and the evolved hydrogen chloride swept into ice water with a stream of air. The resulting aqueous solution was redistilled *in vacuo*

[1]*Manuscript received September 29, 1954.*
Contribution from Atomic Energy of Canada Limited, Chalk River, Ontario. Issued as A.E.C.L. No. 151.

and the hydrogen chloride titrated with potassium carbonate using methyl orange indicator. The solution was then evaporated to incipient crystallization, the potassium chloride precipitated by the addition of ethanol, the crystals filtered off, washed with alcohol, and finally dried in an oven. This material was used to prepare the samples for mass spectrometric analysis (1). A beta-ray absorption curve on this material using aluminum absorbers showed no abnormalities with the possible exception of a slight excess of low energy electrons ($E_{max} \sim 100$ kev.). After the initial counting rate had been recorded the source was treated with concentrated hydrochloric acid and taken to dryness. This procedure was repeated several times so that the Cl^{36} in the form of the chloride would be removed by isotopic exchange with normal chloride ions from the hydrochloric acid. The residual activity on the source was found to be 0.5% of the initial activity. In an effort to determine whether this residual activity was due to failure to completely remove Cl^{36} or in fact due to non-volatile impurities (e.g. S^{35}) the following experiment was carried out.

A sample of the purified potassium chloride (10 mgm.) was dissolved in 1 ml. of water. Potassium sulphite (10 mgm.) was added, followed by hydrogen peroxide (1 ml., 30%) to oxidize the $SO_3^=$ to $SO_4^=$. Any S^{35} remaining should then be present as $SO_4^=$ and therefore non-volatile. This solution was then subjected to repeated evaporations with hydrochloric acid and the final residue again made up to 1 ml. The residual activity of this solution was found to be 0.1% of the initial activity, thereby establishing the absence of non-volatile radiochemical impurities having a total activity greater than 0.1% of the total activity of the purified potassium chloride sample.

A second purification was then carried out which was designed to remove any remaining contaminants with the possible exception of other halogens. The chloride from approx. 300 mgm. of radioactive potassium chloride from the first purification was precipitated with silver nitrate from a solution of the salt in dilute nitric acid. The precipitate was digested on a steam bath in the dark for several hours, allowed to cool, washed several times with 0.1 *N* nitric acid by decantation, and finally dissolved in a minimum amount of ammonium hydroxide. The silver was then precipitated as the sulphide with hydrogen sulphide, the precipitate washed and discarded. The supernatant liquid and washings were then evaporated to dryness, taken up in a small volume of dilute nitric acid, and the whole procedure repeated. The final residue of ammonium chloride was transferred to a volumetric flask and made up to a known volume.

C. Absolute Cl^{36} Content of Samples

Two standard solutions were prepared from the active potassium chloride product of the first purification. These were designated as solutions A-1 and A-2. The solution from the second purification was designated as solution B-1. Portions of each of these standard solutions were used for absolute beta counting. Further portions of A-1 and of B-1 ($\sim$10 ml.) were weighed out in duplicate and the chloride ions precipitated as silver chloride using standard procedure. The precipitates were collected in sintered glass crucibles and dried

TABLE I

GRAVIMETRIC ANALYSIS OF ACTIVE AND INACTIVE POTASSIUM CHLORIDE

	First purification (A) (by distillation as HCl)				Second purification (B) (by precipitation as AgCl)			
	Active sample		Normal sample		Active sample		Normal sample	
Weight (gm.) salt taken for solution	0.2491		0.2502		———		0.2504	
Weight (gm.) of solution	25.0941		25.0825		25.5500		25.1385	
Volume (ml.) of solution	25.0		25.0		25.0		25.0	
Weight (gm.) of solution analyzed	10.0120	10.0161	10.0337	10.0411	10.1788	10.1022	10.0349	10.0162
Weight (gm.) AgCl calculated	———	———	0.1924	0.1926	———	———	0.1922	0.1918
Weight (gm.) AgCl formed	0.1903	0.1909	0.1934	0.1932	0.1941	0.1928	0.1920	0.1920
Corrected weight (gm.) of AgCl*	0.1895	0.1901	———	———	0.1941	0.1928	———	———
Weight (mgm.) Cl*/ml.†	4.7088±0.0065		———		4.8257±0.0020		———	
No. atoms Cl*/ml.	$(7.996\pm0.011)\times10^{19}$		———		$(8.194\pm0.003)\times10^{19}$		———	
No. atoms Cl^{36}/ml.‡	$(1.985\pm0.004)\times10^{18}$		———		$(2.035\pm0.003)\times10^{18}$		———	

†Atomic weight of irradiated chlorine, Cl, calculated from mass spectrometer analysis = 35.484.*
‡Error shown is the combined standard error of the mass spectrometric and gravimetric analyses.

TABLE II

ABSOLUTE BETA COUNTING OF ACTIVE POTASSIUM CHLORIDE

Solution	Observed rate (dis./sec./ml.)	Date counted	Remarks
A–1	$(1.421 \pm 0.005) \times 10^6$	July 23, 1953	Av. five samples prepared July 23, 1953
A–1	$(1.414 \pm 0.004) \times 10^6$	July 24, 1953	Av. two samples prepared July 24, 1953
A–1	$(1.416 \pm 0.006) \times 10^6$	Sept. 15, 1953	Av. five samples prepared July 23, 1953
A–1	$(1.415 \pm 0.001) \times 10^6$	Sept. 16, 1953	Av. two samples prepared Sept. 16, 1953
A–1	$(1.409 \pm 0.012) \times 10^6$	Nov. 6, 1953	Av. six samples prepared July 23–24, 1953
A–2	$(1.422 \pm 0.003) \times 10^6$	Dec. 1, 1953	Av. four samples prepared Dec. 1, 1953
Average for A =	$(1.416 \pm 0.004) \times 10^6$		
B–1	$(1.451 \pm 0.002) \times 10^6$	Dec. 1, 1953	Av. four samples prepared Dec. 1, 1953

to constant weight. All handling of the precipitates was done under red light. At the same time, an exactly similar analysis was carried out, in duplicate, on normal potassium chloride (C.P. grade, dried). The results of these gravimetric analyses are presented in Table I. The chloride ion content of solution A-2 was known from that of A-1 since both were prepared from the same material.

D. Absolute Disintegration Rate of Samples

All counting was done in a 4π methane flow-type proportional counter using techniques which have already been described in detail (4). The source holders consisted of thin films of laminated zapon–formvar of 100 μgm./cm.^{2}, sputtered on each side with gold of approx. 25 μgm./cm.^{2}. The films were supported on aluminum rings. Aliquots from the standard solution containing Cl^{36} were measured out with calibrated micropipettes and delivered to a slight excess of silver nitrate solution previously pipetted onto the film. A fine precipitate of silver chloride is thus formed and the growth of comparatively large potassium chloride crystals is prevented. Self-absorption in the sources was reduced to a minimum by counting aliquots from successive dilutions until no further increase in specific activity was observed. Absorption losses resulting from the finite size of crystal aggregates were estimated to be equal to or less than one per cent. The correction for losses in the supporting film as measured by the sandwich film technique was 0.7%. Corrections for resolving time losses were made wherever necessary and rarely exceeded 2%. The number of counts recorded was such that statistical errors in counting were negligible. The errors given are the standard errors and represent, for the most part, aliquoting errors. Possible systematic errors are not included. The results of absolute beta counting of sources prepared from two solutions (A-1, A-2) from the first purification and from one solution (B-1) from the second purification are given in Table II. The agreement between the observed half-lives (Table III) for samples from the first and second purifications indicates freedom from radioactive contaminants.

E. Half-life of Cl^{36}

The half-life of Cl^{36} is calculated from the relationship $dN/dt = -\lambda N$, where dN/dt is the disintegration rate of N atoms having a decay constant λ. In Table III, the data of Tables I and II are summarized and combined to give the half-life of Cl^{36}.

TABLE III

HALF-LIFE OF Cl^{36}

Solution	N (atoms Cl^{36}/ml.)	dN/dt (dis./sec./ml.)	Half-life (years)
A	$(1.985 \pm 0.004) \times 10^{18}$	$(1.416 \pm 0.004) \times 10^{5}$	$(3.080 \pm 0.010) \times 10^{5}$
B	$(2.035 \pm 0.003) \times 10^{18}$	$(1.451 \pm 0.002) \times 10^{5}$	$(3.080 \pm 0.006) \times 10^{5}$
		Mean	$(3.080 \pm 0.008) \times 10^{5}$

The error attached to the value of the half-life is the over-all standard error indicating the combined precision of all measurements. The over-all systematic error is rather difficult to assess but it is estimated to be not greater than $\pm 1\%$. The half-life of Cl^{36} may therefore be taken as $(3.08 \pm 0.03) \times 10^5$ years, assuming that the simple decay scheme (8) is correct.

ACKNOWLEDGMENT

The authors wish to thank Mr. W. D. McKee for his assistance in recording and computing mass spectrometer data.

REFERENCES

1. Boyd, A. W., Brown, F., and Lounsbury, M. Can. J. Phys. 33: 35. 1955.
2. Feldman, L. and Wu, C. S. Phys. Rev. 87: 1091. 1952.
3. Grahame, D. C. and Walke, H. J. Phys. Rev. 60: 909. 1941.
4. Hawkings, R. C., Merritt, W. F., and Craven, J. H. Proc. Symposium on "Recent Developments and Techniques in the Maintenance of Standards". Natl. Phys. Lab., England. May, 1951. *Reissued as* Atomic Energy Can. Ltd. Rept. AECL No. 43. 1952.
5. Hughes, D. J., Eggler, C., and Goldstein, N. U.S. Atomic Energy Comm. Rept. CP–3801. 1947.
6. Overman, R. T. U.S. Atomic Energy Comm. Rept. AECD–857. 1947.
7. Reynolds, S. A. U.S. Atomic Energy Comm. Rept. ORNL–286. 1949.
8. Wu, C. S. and Feldman, L. Phys. Rev. 76: 693. 1949.
9. Wu, C. S., Townes, C. H., and Feldman, L. Phys. Rev. 76: 692. 1949.

SURFACE TENSION OF He^3 [1]

By D. R. Lovejoy[2]

ABSTRACT

The surface tension of He^3 has been measured by a capillary rise method between 1.08° and 2.32°K. A decrease of more than 50% was observed in this range and this supports the ideas on which Atkins' theory of the surface tension of liquid helium is based. On the basis of this theory the surface tension has been extrapolated to 0°K., where it has the value 0.154 ± 0.005 erg $cm.^{-2}$. Above 2.3°K. it was extrapolated linearly to zero at the critical temperature. The Eötvös constant was calculated to be about 0.8.

1. INTRODUCTION

Since the zero-point energy of the atoms plays an important rôle in determining the surface energy of the liquid at very low temperatures, liquid He^3 would be expected to have a surface tension appreciably different from that of liquid He^4. Recently Atkins (1) (1953) has proposed a theory to account for the variation of surface tension of liquid helium with temperature near 0°K. It was therefore of interest to measure the surface tension of He^3, both for its own sake, and for comparison with the theory. This paper describes its measurement by a capillary rise method.

2. APPARATUS AND PROCEDURE

The apparatus is depicted in Fig. 1. It consisted of a 0.5 mm. bore Pyrex glass capillary tube in which about 10 cc. of He^3 gas at N.T.P. was condensed, the tube being in a standard helium cryostat. Along side it at its lower end was a piece of Pyrex glass capillary tube of 0.138 mm. bore and about 11 cm. long, opening to the 0.5 mm. capillary at either end. The fine bore capillary was made by drawing out a number of 0.5 mm. bore capillaries and choosing the center part of the one which appeared to be most uniform in bore. To measure the bore a mercury pellet was introduced after the experiments were finished and an X-ray shadowgraph of it was taken in each of two directions at right angles. As the capillary edges were not sharply defined in the shadowgraphs it was necessary to take a large number of measurements with a travelling microscope in the region on the photographic plate where the He^3 meniscus had been. In this way the bore was found to be 0.138 mm. with a probable error of 2%. The nominally 0.5 mm. bore capillary was also measured in this way and found to have a bore of 0.498 mm. with a probable error of 1%.

The surface tension of the liquid He^3 was deduced from the difference in height of the He^3 menisci in the two capillaries. This difference in height was measured with a cathetometer to an accuracy of about 1%, the menisci being illuminated with a low power neon lamp. It was assumed that the angle of

[1]*Manuscript received October 22, 1954.*
Contribution from the Department of Physics, University of Toronto, Toronto, Ont.
[2]*Now at the National Research Council of Canada, Ottawa, Ont.*

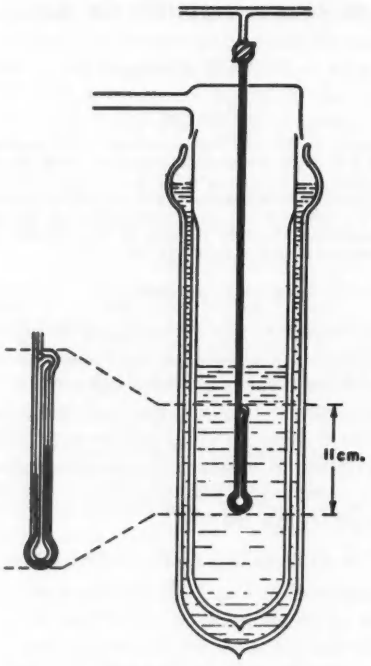

FIG. 1. The cryostat and the capillary tubes containing He^3.

contact was zero and the following formula for the surface tension was applied to each capillary:

[1] $$\sigma = \tfrac{1}{2}g(\rho_L - \rho_v)r(h + \tfrac{1}{3}r)$$

so that

[2] $$\sigma = \frac{[\Delta + \frac{1}{3}(r_1 - r_2)](\rho_L - \rho_v)g}{2(1/r_1 - 1/r_2)}$$

where Δ is the measured difference in heights, ρ_L and ρ_v are the densities of liquid and vapor respectively, taken from the work of Grilly, Hammel, and Sydoriak (2) (1949), and r_1 and r_2 are the radii of the narrower and wider capillaries respectively.

Above 1.3°K. the He^3 had a strong tendency to bubble on changing the temperature. The bubbles persisted and in many cases could only be removed by lowering the temperature below 1.3°K. again. In the range 1.5 to 2.1°K. the bubbling was particularly troublesome so that only one reading was obtained in this region.

3. RESULTS

In Fig. 2 the experimental points are plotted. The absolute values of the surface tension have a probable error of 3% mainly as a result of the uncer-

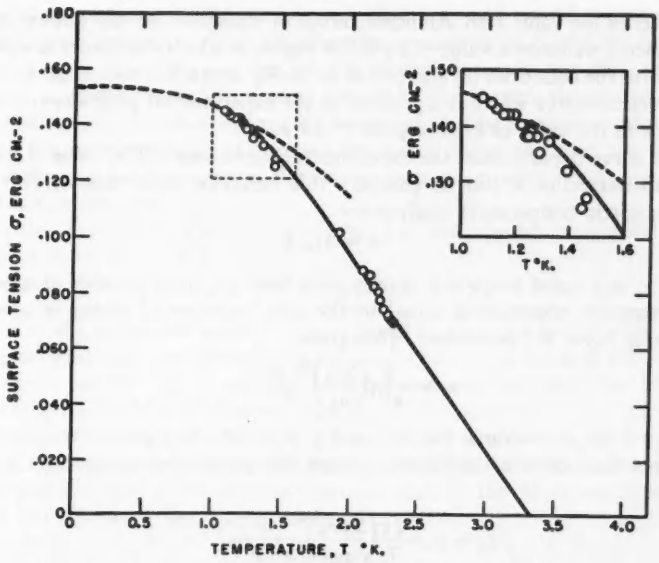

FIG. 2. Variation of surface tension of He^3 with temperature. Full line is the experimental curve (and its linear extrapolation to the critical temperature). Broken line is the curve based on Atkins' theory.

tainty in the measurement of the bore. Above 1.8°K. a straight line has been drawn through the experimental points to cut the abscissa at the critical temperature of 3.34°K.

Below 1.5°K. the points are shown in the inset to Fig. 2. The single point 0.145 erg cm.$^{-2}$ at 1.08°K. has more weight than the others since it is actually the mean of five readings 0.143, 0.145, 0.145, 0.145, and 0.148 erg cm.$^{-2}$ at this temperature.

4. DISCUSSION

According to Atkins (1) (1953) the variation of surface tension at low temperatures is due to the variation of energy excited in the surface waves at these temperatures. The energy of the surface waves is determined by following a procedure similar to that adopted in the Debye theory of solids. This treatment leads to the expression

[3] $$\sigma_0 - \sigma_T = bT^{7/3}$$

where σ_0 and σ_T are the surface tensions at 0° and T°K. respectively. The constant b is given by

[4] $$b = \pi h\left(\frac{\rho_L}{2\pi\sigma_0}\right)^{2/3}\left(\frac{k}{h}\right)^{7/3}\int_0^{\theta/T}\frac{x^{4/3}}{e^x-1}\,dx$$

where θ is a characteristic temperature analogous to the Debye temperature, k is Boltzmann's constant, and h is Planck's constant. As $\theta/T \to \infty$ the integral

approaches the value 1.68. All other terms in equation [4] are known except σ_0. Hence if we know a value of σ_T in the region in which the theory is valid we may solve the equations [3] and [4] for σ_0. In Fig. 2 this has been done to obtain a theoretical curve which is a good fit to the experimental points near 1.08°K. It leads to the value of 0.154 erg cm.$^{-2}$ for σ_0.

This curve departs from the experimental curve near 1.3°K. It is of interest then to determine θ and to compare this behavior with that of He^4. The characteristic temperature is given by

$$\theta = h\nu_c/k \tag{5}$$

where ν_c is a cutoff frequency chosen such that the total number of modes in the frequency spectrum is equal to the total number of atoms in a monomolecular layer at the surface. This gives

$$\nu_c = \frac{1}{\pi^{1/4}}\left(\frac{2\sigma_s}{\rho_L}\right)^{\frac{1}{2}}\frac{1}{\delta^{3/2}} \tag{6}$$

where δ is the interatomic distance and σ_s is an effective surface tension which does not include the contribution from the zero-point energy. It is given by

$$\sigma_0 = \sigma_s + \frac{2\pi}{7}\left(\frac{2\pi\sigma_s}{\rho_L}\right)^{\frac{1}{2}}\frac{k}{\pi^{7/4}\delta^{7/2}} \tag{7}$$

at 0°K. Equations [6] and [7] are only approximate and we may solve equation [7] using for σ_0 a value estimated from the experimental curve. Doing this gives 0.04 erg cm.$^{-2}$ for σ_s, leaving 0.11 erg cm.$^{-2}$ for the contribution from the zero-point energy. Using this value for σ_s we obtain from equation [6] the value 9.5×10^{10} sec.$^{-1}$ for ν_c and from equation [5] the value 4.6°K. for θ. In the case of He^4 the characteristic temperature is 7.2°K. and the theoretical curve departs from the experimental curve near 1.8°K. where $\theta/T \sim 4$. For He^3 the corresponding point on the theoretical curve is near 1.2°K. where also $\theta/T \sim 4$.

In the case of He^4 Atkins has given reasons for the divergence of the theoretical and the experimental curves, the most important being that the frequency spectrum of the surface modes is less simple than is here assumed. Comparing this with the corresponding situation in the Debye theory of specific heats, we see that the necessary refinements to the theory would involve taking account of the discrete nature of the surface. As a consequence of this there are an increased number of modes in the higher frequencies than we have assumed and this leads to a more rapid decrease in the surface tension at higher temperatures where the higher frequency modes are being excited. It is likely then that with a more complete knowledge of the frequency spectrum of the surface modes, the theory would be improved at the higher temperatures.

However, it might be argued that the disagreement is more fundamental and springs from our ignoring the other contributions to surface energy, namely those arising from the zero-point energy of the atoms and from the interaction energy between the atoms. Changes in these contributions would

be related to changes in the interatomic distance, and would therefore be dependent on the density. Now the decrease in density of liquid He^3 from 0° to 2°K. is only 1%, whereas the surface tension decreases by 40% in this region. It is unlikely that this drastic change of the surface tension could be brought about by the small change of density and this is strong evidence in favor of the kinetic energy of the surface waves being the only important cause of the observed decrease in the surface tension, except perhaps near the critical temperature.

From the linear part of the curve in Fig. 2 it was possible to calculate the Eötvös constant k_E given by

$$k_E = -d/dT\ [\sigma(M/\rho_L)^{2/3}]$$

where M is the molecular weight. It was found to have a value of about 0.8. This agrees with the rule given by Kamerlingh Onnes and Keesom (3) (1923) according to which normal substances form a series in which the Eötvös constant increases with critical temperature.

I should like to acknowledge my gratitude to Prof. K. R. Atkins for suggesting the problem and for helpful discussions and to the National Research Council of Canada for financial assistance.

REFERENCES

1. Atkins, K. R. Can. J. Phys. 31: 1165. 1953.
2. Grilly, E. R., Hammel, E. F., and Sydoriak, S. A. Phys. Rev. 75: 1103. 1949.
3. Kamerlingh Onnes, H. and Keesom, W. H. Communs. Phys. Lab. Univ. Leiden, Suppl. No. 23. Enzyklopädie Math. Wiss. Vol. 10. 1923.

A NOTE CONCERNING THE CONDUCTIVITY OF LIQUID DIELECTRICS[1]

By John Hart and D. A. Simmons[2]

ABSTRACT

Experiments are described which show that it is not permissible to ignore electrode effects in the calculation of the mobilities of ions in liquid dielectrics. Preliminary results indicate that the fall in direct current with time is due partly to electrode polarization, and partly to the removal of ions from the liquid. It has been found that for apparent field strengths lower than 1 kv./cm., the current in the dielectric is proportional to the applied potential, and there appears to be a back-e.m.f. of about one volt. Precautionary measures are suggested for future experiments.

INTRODUCTION

A measure of the mobility of the ions in an organic liquid with low electrical conductivity may be made from observations of the decay of current with time when a constant electrical field is applied across two electrodes immersed in the liquid (1, 3). The calculation involves the assumption that the fall in conductivity is initially governed by a decrease in the ionic concentration in the main body of the liquid, rather than by electrode processes. Gemant shows that this assumption is justified, provided the field intensity is at least 10 kv. $cm.^{-1}$; Eck, on the other hand, obtains consistent results with fields as low as 1 v. $cm.^{-1}$; further, a decrease in current occurs even when the liquid in the cell is continuously replaced (5). It seems probable, therefore, that electrode effects may be relatively large and that considerable errors may occur in the calculated values of ion mobilities. There has been some controversy concerning electrode processes in true electrolytes (6), and it is even more difficult to investigate electrode effects in liquid dielectrics since very low currents are involved (4). This is a report describing typical qualitative experiments which allow electrode effects to be separated from bulk effects.

FOUR-ELECTRODE CELL

The cell employed contained two similar pairs of platinum electrodes, each pair having plates of 0.25 $cm.^2$ area, 0.5 cm. apart; the total volume of chloroform in the cell was about 2.5 ml. The apparatus was contained in a darkened thermostat. Each pair of electrodes (A and B respectively), when energized separately, showed a saturation current of about 0.25 μa. after 12 hr. with an applied potential of 600 v. Both pairs were removed from the cell and cleaned. Electrodes A and B were then energized; electrodes B were removed from the cell immediately the current had been measured, while electrodes A were left energized in the cell. Electrodes B were inserted in the cell for a short time at regular intervals, and the currents passing through

[1]*Manuscript received October 28, 1954.*
Contribution from the Division of Physics, National Research Laboratories, Ottawa. Issued as N.R.C. No. 3492.
[2]*Summer student at National Research Laboratories; present address—Chancellors Hall, University of Birmingham, Birmingham, England.*

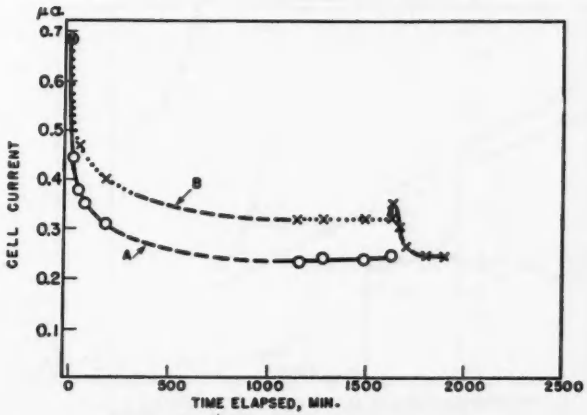

FIG. 1. Chloroform. Platinum electrodes 1.2 kv. cm^{-1}. The fall of current in the four-electrode cell. Electrodes A energized continuously, but electrodes B removed from the cell between measurements. Continuous energization of B shown at right.

each pair were measured. It was found that the current through the continuously energized electrodes decreased more rapidly than the current through those that were intermittently energized, and to a lower limiting value (Fig. 1). It is likely that the upper curve represents changes taking place within the liquid, while the lower curve includes electrode effects. Violent agitation of the liquid had no appreciable effect upon either curve. The difference between the two curves shows that the current fall due to increased resistance and reverse fields at the electrodes is of the same order of magnitude as the decrease in ion concentration and is quite important when considering ionic mobilities. When, finally, the field was applied continuously to electrodes *B*, the current rose very sharply, and then again fell regularly to the former limiting value (0.25 μa.). This sudden rise from 0.32 to 0.35 μa. may result from a sudden rush of ions from one half of the cell to the other; there was no observable compensating effect in the other half of the cell. The subsequent fall presumably arose from the building of ion and gas layers at the electrodes.

TWO-ELECTRODE CELL

The current was allowed to fall to saturation (0.09 μa.) overnight in a chloroform cell with two brass electrodes. The electrodes were then removed from the cell for one minute, and were reinserted. After this treatment, the current was found to have increased to some intermediate value (0.3 μa.) from which it fell in the usual way (Fig. 2). Similar treatment of the electrodes at regular intervals showed that there was a recovery of the current, which, after the third removal, attained a greater value (0.8 μa.) than the initial current (0.6 μa.) when the cell was new. Other experiments had shown that when the electrodes were left in the liquid with no applied potential, recovery was regular and much slower.

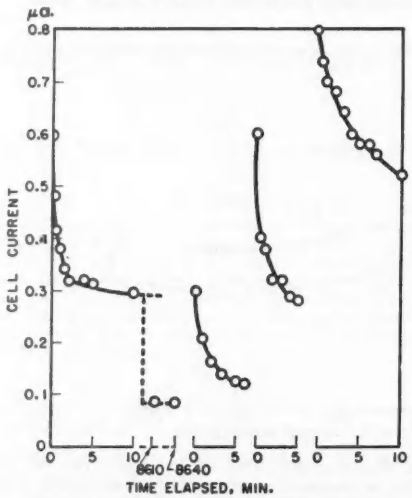

FIG. 2. Chloroform. Brass electrodes 1.2 kv. cm^{-1}. The fall of current in the two-electrode cell. Electrodes removed for one minute at discontinuities.

After subsequent removals, the current fell smoothly from about 0.6 to 0.3 μa. in three minutes, as it had during the first part of the experiment. It is clear from this behavior that there are at least two separate mechanisms occurring concurrently. These may be separated into one part which has a long time constant, and causes a rise in the general current level after successive removal of the electrodes, and another short-time part which causes the decay when the electrode is reinserted.

If the long-term part of the decay is due to an electrode process, and the short-term part, which corresponds to the upper part of the curve in Fig. 1, is a bulk process, such as a removal of ions, then Eck's contention that only the first part of the decay curve may be used for the calculation of mobilities is justified. It seems not unlikely that Gemant's separation of positive and negative ionic mobilities may in fact be a separation of bulk and electrode effects.

SATURATION CURRENT

Eck has reported some irregularities in current–voltage curves with low applied fields at current saturation. In contradiction to these results, it has now been found that the apparent resistance of a chloroform cell with platinum electrodes is constant to the lowest measurable field, and the current–voltage curve is linear up to 1.2 kv. $cm.^{-1}$ (Fig. 3). It is significant that the cell current was zero for an applied potential of somewhere between 0.5 and 1.5 v.; discharge currents were consistently observed. This is evidence that there is a significant electrode overvoltage. Current measurements were made as rapidly as possible but there is a discrepancy between readings on a rising and on a falling potential; this was evidently recovery in the cell while low potential readings were being made.

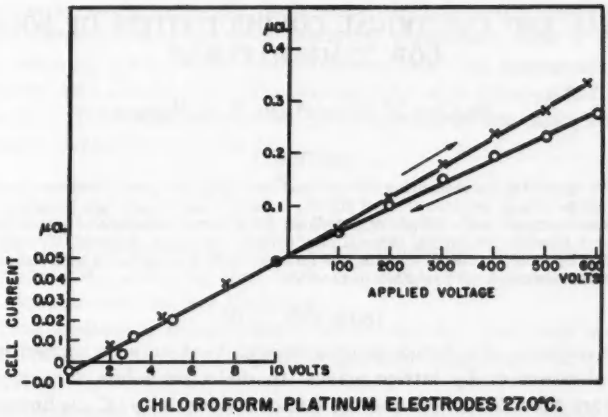

FIG. 3. Chloroform. Platinum electrodes, 0.5 cm. apart. Cell saturation current plotted against applied voltage.

Owing to the rapid current changes, it is impossible to make accurate current measurements at very low potentials during the early part of the current decay. It has, however, been possible to plot the current–voltage relationship for apparent fields of from 0.2 to 1.2 kv. cm.$^{-1}$, and in each case, the current was approximately linear with the applied voltage at all stages of current decay. This is in agreement with the results of Sambussy (7), who showed that the back-e.m.f. was of the order of 1.4 v.

PRECAUTIONS

These preliminary experiments show that there is some doubt concerning the validity of present methods of calculating ion mobilities and dimensions in organic liquids of low conductivity. The difficulty experienced in obtaining consistent results, both in the course of these experiments and previously, shows that the apparatus must be carefully designed to exclude unwanted impurities. For future experiments, it is proposed to use a sealed constant circulation system of the type generally used in breakdown measurements (2). Control of the quantity of water or other ion source present is essential. The liquid should pass successively through two or three conductivity cells connected with fine tubing; it will then be possible to examine the conductivity of the liquid intermittently by d-c., or by very low frequency a-c., both before and after passage through the d-c. field. Changes in the conductance of the d-c. cell which are not accompanied by a similar change in the other cells may be ascribed to electrode polarization.

REFERENCES

1. ECK, J.-L. Ann. phys. 4: 12. 1949.
2. EDWARDS, W. D. Can. J. Phys. 29: 310. 1951.
3. GEMANT, A. Phys. Rev. 58: 904. 1940.
4. GEMANT, A. J. Chem. Phys. 13: 146. 1945; 14: 424. 1946.
5. HART, J. Can. J. Phys. 32: 99. 1954.
6. NEWBERY, E. Trans. Faraday Soc. 43: 127. 1947.
7. SAMBUSSY, J. Compt. rend. 193: 853. 1931.

THERMAL AND ELECTRICAL CONDUCTIVITIES OF SOLIDS AT LOW TEMPERATURES[1]

By Guy K. White[2] and S. B. Woods

ABSTRACT

An apparatus for measuring the thermal and electrical conductivities of solids at temperatures between 2° and 300°K. is described. Results are presented of measurements of some dilute copper alloys, beryllium, bismuth, and germanium. Where possible the lattice thermal conductivity has been deduced, directly or indirectly from the measurements, and its magnitude and variation with temperature are discussed with relation to theory.

INTRODUCTION

In the presence of a temperature gradient, heat may be carried in a solid by free electrons or by lattice waves. In dielectric solids, lattice waves or phonons are the sole carriers and the lattice conductivity, K_g, is limited by the following processes which are assumed to be approximately additive in their effect: scattering by crystal boundaries, small scale defects (impurities, mosaic structure, etc.), and lattice waves. We denote the corresponding components of thermal resistance by W_B, W_D, W_U; a recent review by Berman (3) discusses the magnitude and temperature dependence of these processes in a number of insulators.

In a metal, K_g is reduced by an additional resistance, W_E, due to scattering by free electrons; in a pure metallic element this is a major process and it is generally assumed that the thermal conductivity due to the conduction electrons themselves (K_e) far outweighs that due to the lattice, K_g. The conduction electrons are scattered by static imperfections (chemical impurities, physical defects) and by lattice vibrations, which produce thermal resistances W_0 and W_i respectively. Considerable work on pure metals in recent years (e.g. see review by Olsen and Rosenberg (25)) has been done, which indicates that

$$[1] \qquad 1/K_e = W_0 + W_i$$

$$[2] \qquad = A/T + BT^n \text{ for } T < \theta/5$$

where $n \simeq 2$, θ is the Debye characteristic temperature, A and B are constants. The most serious conflict with the theory of Wilson and Makinson (Wilson (35), Makinson (24), Sondheimer (30)) is in the magnitude of W_i, the constant B being about five times less for the monovalent metals copper, gold silver than that given by the theory; nor is the maximum in W_i at $T \simeq \theta/4$, predicted by the various solutions of the transport equation (e.g. Makinson, Sondheimer, and Klemens (19)), found experimentally.

The work presented here was designed to investigate the thermal conductivity of metals in which K_g is comparable with, or in some cases even greater than,

[1]*Manuscript received October 29, 1954.*
Contribution from Division of Physics, National Research Council, Ottawa, Canada. Issued as N.R.C. No. 3501.
[2]*National Research Council Postdoctorate Fellow, on leave from Commonwealth Scientific Industrial Research Organization, Division of Physics, Sydney, Australia.*

the electronic conductivity K_e. Such metals include many alloys or impure metallic elements, and also poor electrical conductors with a small free-electron density, such as bismuth. Previous work on copper–nickel alloys (Estermann and Zimmerman (8), Berman (2)) and silver–palladium alloys (Kemp *et al.* (16)) has shown that at temperatures less than about $\theta/20$, the lattice conductivity is given by

$$K_g = dT^3 \qquad [3]$$

suggesting that electron scattering is dominant (cf. the theory of Makinson (24)) and the experimental values of d are comparable with those calculated by Klemens (18), assuming that both longitudinal and transverse phonons interact equally with the free electrons.

Electrical resistance measurements which are reported here were made primarily to assist in estimating the electronic component of the thermal conductivity.

A brief report of the measurements on the copper–iron alloys has been presented previously (White and Woods (34)).

APPARATUS

The cryostat shown in Fig. 1 differs in the method of temperature control and in the provision of a means of simultaneous electrical conductivity determination from one described previously by White (33). In the temperature regions between 4° and 55°K. and above 90°K., which are not covered by the vapor pressures of boiling liquid helium or liquid oxygen, the temperatures of the chamber C and radiation shield S are electrically controlled to within 0.001° of any desired temperature above that of the surrounding liquid bath. The e.m.f. from the differential thermocouple T consisting of Au + 2.10% Co, Ag + 0.37% Au alloys (Keesom and Matthijs (15)) is fed to a regulator (Dauphinee and Woods (6)), the output of which supplies the heater H_2.

A temperature gradient in the specimen, produced by the electrical heater H_1, is determined by the helium filled gas thermometers A and B which are connected by 0.3 mm. I.D. german silver capillary tubing to an oil-filled differential manometer (e.g. see Hulm (13), White (33)). For the electrical conductivity measurement a current lead, I, of lead-coated 38 B and S copper wire, is attached to the lower end of the specimen or to the copper former on which the heater H_1 is wound. The lead coating is superconducting below 7°K., thus reducing the Joule heating which is important when a large measuring current is used. The electrical potential leads, a, b, are attached to copper wires which thermally connect the thermometer bulbs to the specimen. The potential difference is measured either on a Rubicon potentiometer or on a galvanometer amplifier (MacDonald (20)), depending on the magnitude of the electrical resistance. To avoid an electrical short circuit through the german silver capillary tubes when measuring specimens of resistance greater than, say, 10^{-6} ohm, thermometer B is connected thermally but not electrically to the specimen and to the potential lead b. This is achieved by means of a sleeved junction, in which a layer of rice paper and baked formel varnish act

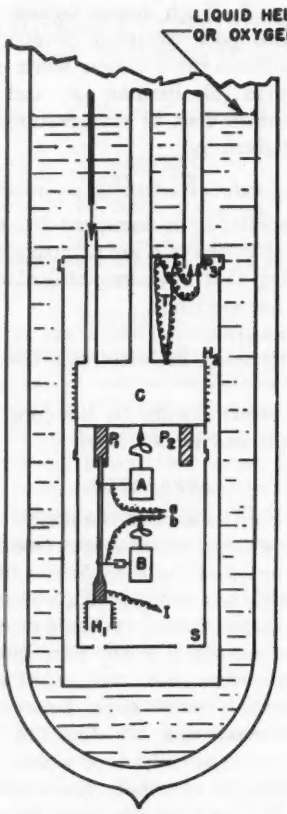

FIG. 1. Schematic diagram of conductivity cryostat.

as electrical insulation, in the thermal link from B to the specimen. All the electrical leads to the specimen are thermally anchored to the copper pillars, P2 and P3, to reduce stray heat inputs, and A, B, and S are gold-plated to reduce radiation transfer.

Although it is quite practical to measure electrical conductivity at any desired temperature between 1°K. and room temperature with this apparatus, thermal conductivity measurements are normally restricted to the region between 2° and about 160°K. This is because below 2°K., on the one hand, the vapor pressure of liquid helium which sets an upper limit for the helium gas pressure in the thermometer bulbs is small and hence accurate differential gas thermometry is difficult. Above about 150°K., on the other hand, the time required for equilibrium to be established in the gas thermometers is long and the radiation correction becomes too large to be applied with confidence. This upper temperature limit may be increased by changing the geometrical

form of the specimen, i.e. making the ratio of length to cross-section smaller, but this change makes accurate measurements in the important region below 20°K. very difficult.

The majority of the thermal conductivity observations have an estimated error of about 1% and appear to be reproducible to this accuracy. In the temperature range between 4° and 15°K., measurements on specimens of higher thermal conductivity are rather less accurate, the probable error of perhaps 5% being due largely to the necessity of using a small temperature gradient. The inaccuracy in the electrical conductivity determinations is generally less than 1%, the limit being due to the effect of seismic vibrations on the galvanometer amplifier.

SPECIMENS

(i) *Dilute Copper Alloys*

Three rods of 1 to 2 mm. diameter and about 6 cm. length were drawn from homogenized alloys of copper containing respectively 0.02 weight per cent (0.02 atomic per cent) germanium, 0.056 weight per cent (0.063 atomic per cent) iron, and 0.0043 weight per cent (0.0048 atomic per cent) iron, and subsequently annealed. Connections between the rods and the pillar P_1, the heater H_1, and the leads to gas thermometers A and B were made with soft solder.

(ii) *Beryllium*

Be 1 was a 5 mm. diameter sintered rod originally supplied by the Brush Co. to the Chalk River Atomic Energy establishment; spectrographic analyses showed strong magnesium lines and a trace of iron, the magnesium content being estimated to be approximately 2%. The second sample (Be 2) was a sintered rod of high purity from A. D. Mackay and machined to 4 mm. diameter; spectrographic analysis of the latter showed less than 0.1% magnesium and a trace of iron. The connections to the rods were made with indium solder.

(iii) *Bismuth*

Bi 1 was a rod cast and cooled quickly in a 2 mm. bore glass tube from standard bismuth supplied by Mining and Chemical Products (London); the original purity was stated to be 99.97% but this material had previously been cast and handled in the laboratory before recasting so may be of lower purity. Etching and metallographic examination showed the specimen to consist of columnar crystals penetrating to the center of the rod, there being 16 to 18 crystals exposed on the circular section of diameter 2 mm. Connections were made to the rod by soft soldering.

Bi 2 was a 3 mm. diameter rod, cast in a brass former and cooled slowly. The bismuth used was granular metal from General Chemical Division of Allied Chemical and Dye Corporation with the following stated impurities: Sb $<$ 0.01%; Cu, Pb, Ag, Zn each $<$0.005%; Fe $<$ 0.002%; As $<$ 0.0001%. Microscopic examination showed this rod also to consist of columnar crystals penetrating to the center with about six crystals per circular section of 3 mm.

diameter. Two copper wires were cast in the rod and the thermal and electrical potential connections were made to these wires to avoid contamination by soldering onto the rod.

(iv) *Germanium*

This specimen was of 2 mm. by 4 mm. rectangular section and 5 cm. long, cut from a single crystal grown from high purity germanium. The electrical resistivity at 22°C. was about 31 ohm cm. Connections were made by soft soldering to the rod.

RESULTS

1. *Electrical Conductivity*

(i) *Copper Alloys*

The measurement of electrical resistance, ρ, on the copper alloys (Fig. 2)

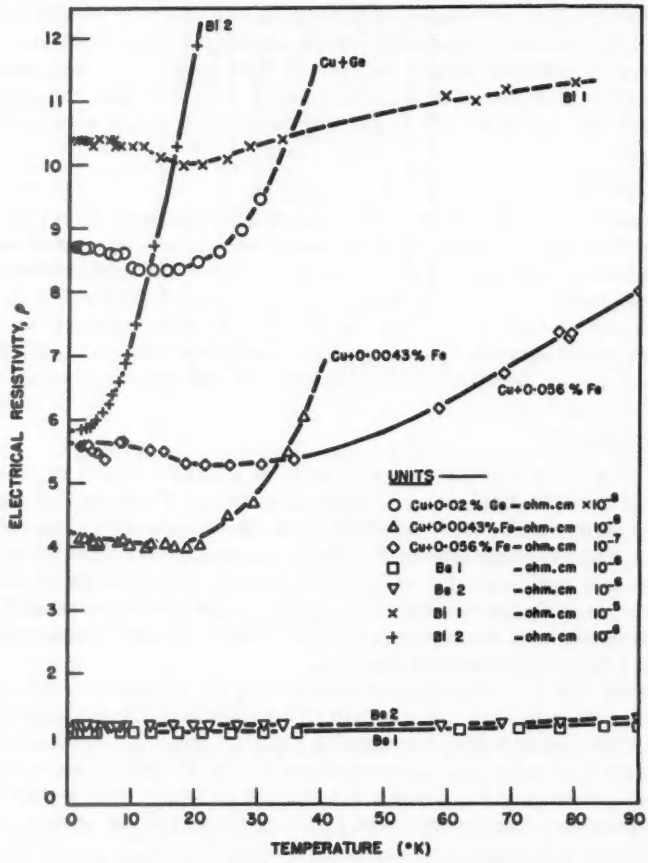

FIG. 2. Electrical conductivity of the specimens at low temperatures.

gives the values shown in Table I for the residual electrical resistivity, ρ_0, due to impurity scattering. The room temperature value of the ideal resistivity due to lattice scattering, and calculated as $\rho_i = \rho - \rho_0$, agrees within about 2% with the accepted value of 1.72×10^{-6} ohm cm. for pure annealed copper, indicating that Matthiessen's rule is reasonably well obeyed.

TABLE I

SUMMARY OF DATA ON ELECTRICAL RESISTIVITY AND ELECTRONIC THERMAL CONDUCTIVITY AT LOW TEMPERATURES

	$\frac{\rho_{min}}{\rho_{295}-\rho_{min}}$	$\frac{\rho_{4.2}-\rho_{min}}{\rho_{min}}$	T_{min} (°K.)	$\rho_{min}=\rho_0$, ohm cm.	$\rho_{295°K.}$, ohm cm.	K_0/T, watts per cm. deg.^{2}	L_0, watt ohm per deg.^{2}
Cu+0.02% Ge	0.046	0.04	~13	0.084×10^{-6}	1.92×10^{-6}	0.30$_8$	2.68×10^{-8}
Cu+0.056% Fe	0.32	0.06	~25	0.53	2.18	0.046	2.45
Cu+0.0043% Fe	0.024	~0.03	12–18	0.041	1.75	0.66	2.70
Be 1	0.28	<0.01	—	1.11	5.08	0.022$_3$	2.48
Be 2	0.32	<0.02	—	1.20	4.95	0.022$_0$	2.64
Bi 1	—	0.04	~18	104	136	—	—
Bi 2	0.051	<0	—	5.9	120	—	—

All three dilute alloys exhibit a shallow minimum in the electrical resistance as expected from previous work on the effect of small quantities of germanium and iron in copper (MacDonald and Pearson (22)). The approximate temperature of the minimum and its depth as expressed by the ratio $(\rho_{4.2}-\rho_{min})/\rho_{min}$ are shown in Table I together with the ratio of the residual resistance at the minimum to ideal resistance at room temperature (295°K.) as given by $\rho_{min}/(\rho_{22°C.}-\rho_{min}) = \rho_0/\rho_i$.

(ii) *Beryllium*

Both specimens of beryllium (Fig. 2 and Table I) have a comparable high residual electrical resistance despite the difference in chemical purity between them. This presumably indicates that the major scattering is due to the physical impurities, structural irregularities, and perhaps occluded oxygen and nitrogen which result from the process of producing the rods, viz. sintering.

Up to a temperature of about 130°K. ($T \simeq \theta/8$), the resistance of the two specimens may be represented by

$$\rho = (\rho_0 + 6.4 \times 10^{-8} \times T^{3.2}) \times 10^{-6} \text{ ohm cm.}$$

The ideal resistivities, ρ_i, of 3.97×10^{-6} ohm cm. (Be 1) and 3.73×10^{-6} ohm cm. (Be 2) at 22°C. appear to be within a few per cent of the value obtained by Grüneisen and Adenstedt (10) and Erfling and Grüneisen (7) on single crystals of pure beryllium.

(iii) *Bismuth*

Bi 2, the purer specimen of larger grain size, has an electrical resistivity which at temperatures below 10°K. ($\sim\theta/10$) fits the expression

[4] $$\rho = (5.9 + 2.20 \times 10^{-3}T^{2.5}) \times 10^{-6} \text{ ohm cm.}$$

and has an ideal resistivity at room temperature (see Table I) within 1% of that obtained by Kaye (14) for the resistivity of a pure single crystal measured perpendicular to the trigonal axis.

However, the results obtained on Bi 1 shown in Table I and in Fig. 2 indicate a very high residual resistance, a strong departure from Matthiessen's rule, and an apparent minimum in the residual resistance at low temperatures. This may be due to the intrinsic impurities or to the introduction of impurities when mounting (by soldering), although no appreciable change in the electrical or thermal properties was observed when the specimen, having broken near the end, was remounted in the cryostat.

2. *Thermal Conductivity*

(i) *Copper Alloys*

The copper–germanium and more dilute copper–iron alloy (Fig. 3) both have a thermal conductivity which increases approximately proportionally to temperature at low temperatures ($T < 15$°K.), reaches a maximum at 25° to 30°K. and then falls, finally attaining an almost constant value of about 4 watts/cm. degree at temperatures above 100°K. The conductivity of the Cu + 0.056% Fe alloy increases rather more rapidly than the linear relation with T would suggest and does not pass through the maximum characteristic of the high purity copper.

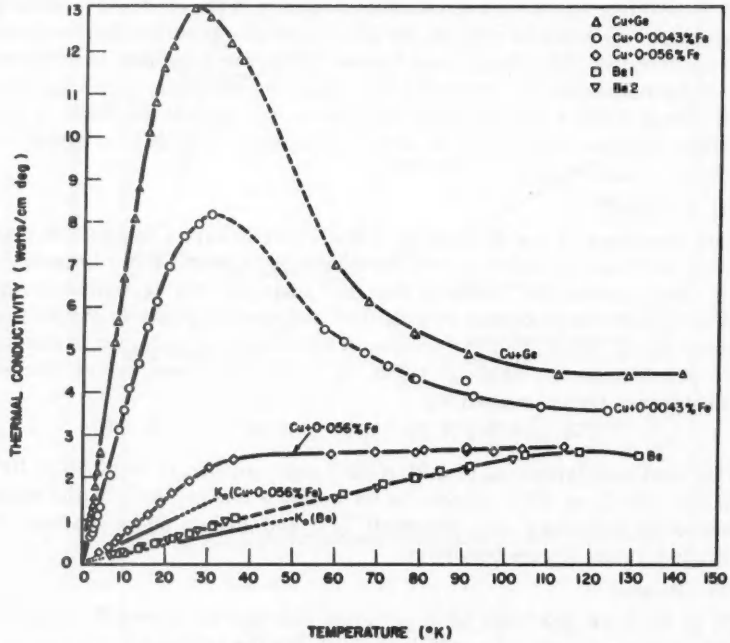

FIG. 3. Thermal conductivity of dilute copper alloys and beryllium at low temperatures.

(ii) *Beryllium*

As in the case of the less dilute copper–iron alloy, the thermal conductivity of both sintered beryllium rods (Fig. 3) rises more quickly at low temperatures than is predicted by equation [2], but reaches a maximum at about 115°K. and then appears to fall. The position and magnitude of this maximum are not inconsistent with the detailed results obtained by Powell (26) on various samples of beryllium at temperatures above room temperature, which indicate a thermal conductivity of 1.5 to 2.0 watts/cm. degree at 50°C., falling to about 1 watt/cm. degree at 400°C.

(iii) *Bismuth and Germanium*

As shown in Fig. 4, these two elements—a semimetal and a semiconductor—exhibit the behavior more typical of crystalline dielectric solids (see e.g. Berman (3)) in that the thermal conductivity increases rapidly at low temperatures, being approximately proportional to T^3, and then passes through a maximum. At higher temperatures the conductivity of the bismuth appears to

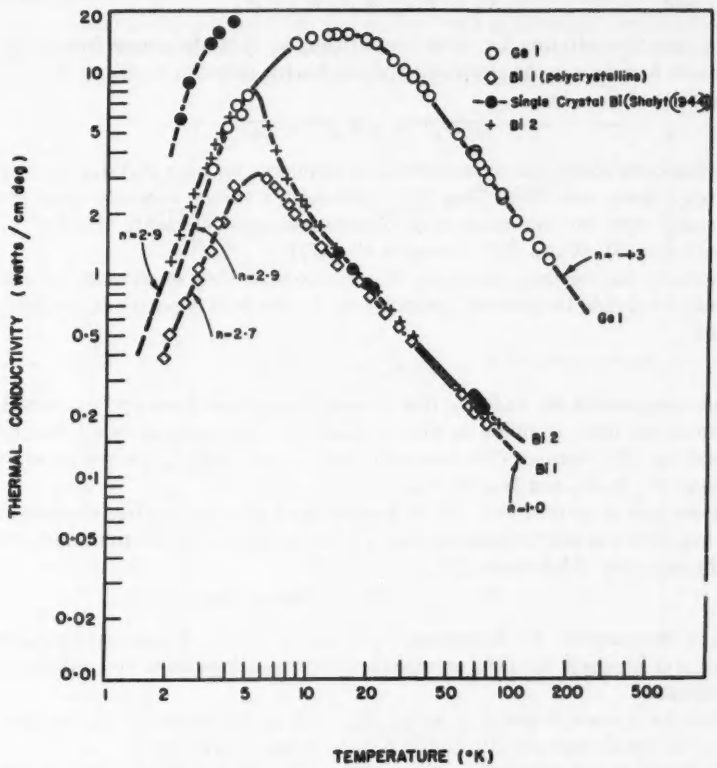

FIG. 4. Thermal conductivity of germanium and bismuth at low temperatures.

be inversely proportional to T, similar to that of an insulating crystal, whereas the germanium has a conductivity proportional to $T^{-1.3}$.

ANALYSES OF RESULTS

General Remarks

The principal aim in these experiments is to deduce the lattice conductivity of the elements investigated. In the case of the two more dilute alloys we expect the electronic conductivity, K_e, to be much greater than K_g, which will prevent any accurate estimate of the latter. On the other hand, we might reasonably expect germanium and bismuth to be predominantly lattice conductors. Between these extremes are the sintered beryllium and Cu + 0.056% Fe alloy for which we expect K_e and K_g to be comparable. In general we may write

[5] $$K = K_e + K_g$$

[1] where $$1/K_e = W_0 + W_i$$

[6] and $$1/K_g = W_B + W_E + W_D + W_U.$$

W_0 is due to scattering by static impurities, so that the mean free path is constant; hence since the electronic specific heat is linear in T, $W_0 = A/T$ and W_0 is related to ρ_0 by

[7] $$\rho_0/W_0T = \rho_0K_0/T = L_0.$$

This has been confirmed by numerous experiments on pure metallic elements (see e.g. Olsen and Rosenberg (25)) although a minor anomaly may exist associated with the minimum in ρ_0 observed in some elements (Herlin (11), Rosenberg (28), White (32), Kemp *et al.* (17)).

Similarly the thermal resistance, W_B, due to scattering of phonons by grain boundaries should be inversely proportional to the heat capacity of the lattice waves,

[8] i.e. $$W_B = C/T^3.$$

The components W_i and W_U, due to scattering of electrons and phonons by phonons, are more complex in their temperature dependence (see Olsen and Rosenberg (25), Berman (3)), but fortunately at sufficiently low temperatures we have $W_i \ll W_0$ and $W_U \ll W_B$.

In the case of metals, W_E, due to scattering of phonons by free electrons, is also important at low temperatures and is theoretically related to temperature by the equation (Makinson (24))

[9] $$W_E = D/T^2 \qquad (D \text{ constant}).$$

Recent experiments by Estermann and Zimmerman (8) on copper–nickel alloys and Kemp *et al.* (16) on silver–palladium alloys seem to confirm this dependence.

Thus for a normal metal in which $W_E \gg W_B$ at sufficiently low temperatures, the total conductivity should reduce to the expression

[10] $$K = K_0 + K_E$$

[11] $$= aT+dT^3 \qquad (a, d \text{ constants}),$$

while for an insulator, semiconductor, or metal containing very few free electrons we expect $K_e \gg K_s$, and hence

[12] $$K \simeq K_B = cT^3.$$

Copper Alloys

For the two more dilute alloys, K/T is sensibly constant below 10°K. and measurements of K and ρ in the liquid helium region confirm that $\rho K/T(=L)$ has a value within 2–3% of the theoretical figure. Up to about 50°K. ($\theta/5$) the measured conductivity can be well represented by

[13] $$K = 1/W = (A/T + 7.1 \times 10^{-6}\, T^{2.4})^{-1} \text{ watts/cm. degree.}$$

The second term in equation [13] is that deduced from previous measurements on high purity copper by Berman and MacDonald (4) and White (33). In Fig. 6 are shown the experimental values for K together with K_e calculated from equation [13], the values for W_i above 50°K. (where equation [13] is no longer valid) being derived from the earlier work of Berman and MacDonald, and White. The difference between K and K_e is presumably the lattice component but is too small to allow any accurate deduction of K_g.

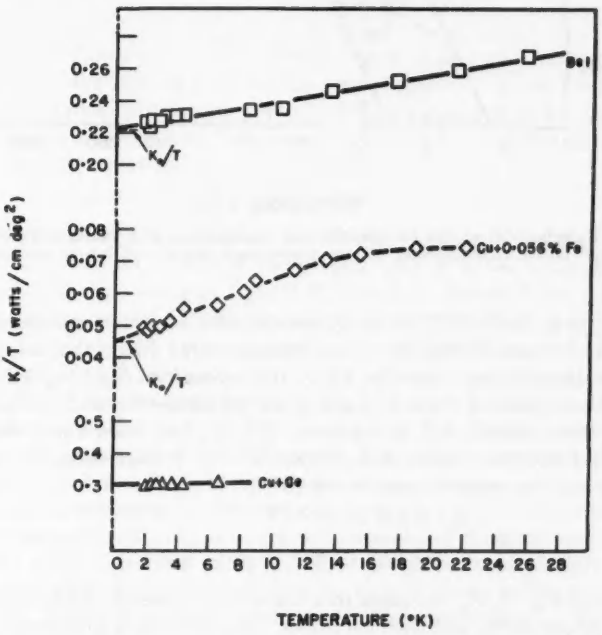

FIG. 5. Graph of the ratio K/T versus temperature T, illustrating the method of determining the constant K_0/T.

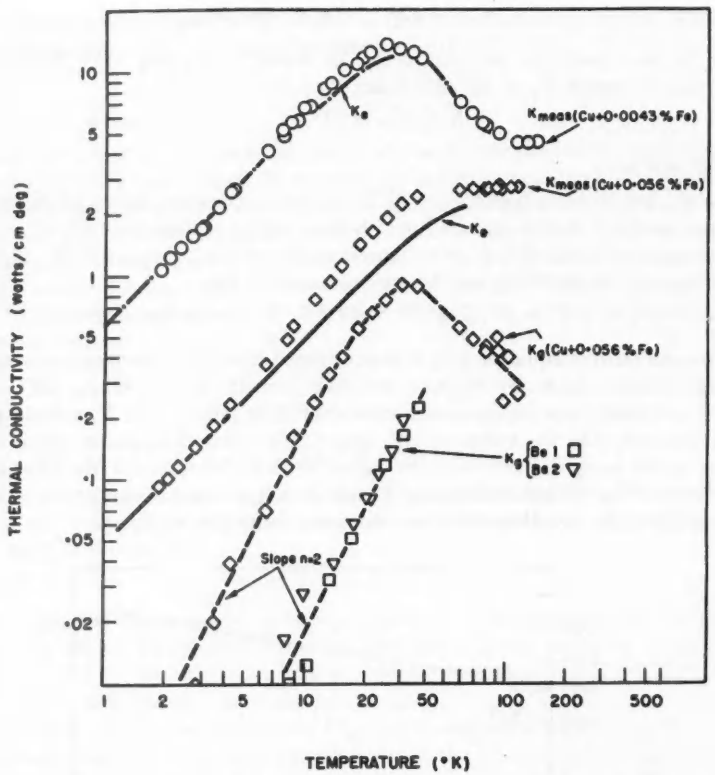

FIG. 6. Experimental results for the thermal conductivity and values deduced for the electronic and lattice conductivities of two copper–iron alloys, and lattice conductivity of beryllium.

In the case of the 0.056% Fe alloy, however, K_0 is reduced considerably and plotting K/T versus T (Fig. 5) at low temperatures yields the values $K_0/T = 0.046$ watts/cm. deg.^{2} and $d = 1.8 \times 10^{-3}$ watts/cm. deg.^{3} (equation [11]). Since this extrapolated value of K_0/T is indeed consistent with the measured $\rho_0 = \rho_{min}$ when substituted in equation [7], K_g has been calculated from equation [1] and the values of K_g shown in Fig. 6 were deduced assuming $K_g = K - K_e$. For temperatures below 15°K.

$$K_g = 1.8 \times 10^{-3}\, T^2 \qquad [14]$$

$$= 17.8\, (T/\theta)^2 \qquad (\theta = 315°\text{K.}). \qquad [14a]$$

As seen in Fig. 6, K_g increases to a maximum value of nearly 1 watt/cm. degree at about 35°K. and then decreases. This decrease is presumably due to scattering processes other than free electrons, i.e. defects and impurities (W_D) or phonon–phonon interaction (W_U). It would be of considerable interest

to obtain more accurate experimental information on the magnitude and temperature variation of K_g at higher temperatures to see whether it falls as $1/T$ as predicted for anharmonic coupling between the lattice waves, but the fact that $K_g = K - K_e \ll K_e$ at these temperatures makes the problem a difficult one.

Beryllium

From the two samples of sintered beryllium, the resistance, W_0, due to the scattering of the electrons by impurities, is large and K_g may be deduced as for the 0.056% Fe alloy. However, this is only correct when $W_0 \gg W_i$ since, in contrast to the case of copper, there is no available information on W_i for beryllium. Thus Fig. 6 only shows the lattice thermal conductivity of beryllium up to 40°K. ($\sim\theta/20$). From previous work on another group II element, magnesium (Kemp *et al.* (17)) for which $W_i = 8.6(T/\theta)^2$ for $T < \theta/5$, we may estimate crudely the magnitude of W_i for beryllium, and for $T \leqslant 40$°K. it appears to be negligible in comparison with W_0. For both Be 1 and Be 2, the lattice conductivity (Fig. 6) is then apparently given by

$$K_g \simeq 2 \times 10^{-5}\, T^2 \qquad [15]$$

$$\simeq 20(T/\theta)^2 \qquad [15a]$$

using a value of 1000°K. for θ_D (see Hill and Smith (12)).

Bismuth

In Fig. 4 are shown the thermal conductivities of Bi 1 and Bi 2 and results obtained by Shalyt (29) on a cylindrical single crystal of radius 1.4 mm. and electrical resistance ratio $\rho_{4.2}/\rho_{273} = 0.02$ (cf. $\rho_{4.2}/\rho_{295} \simeq 0.05$ for our Bi 2).

At the lowest temperatures, K is given by cT^n where $n \simeq 3$. For the constant c we may use the equation due to Casimir (5)

$$K = 2.31 \times 10^3\, pRA^{2/3}\, T^3 \text{ watts/cm. degree} \qquad [16]$$

where p is a function of the phonon velocities and has a value of about 1.4 for most crystals, R is the radius of the crystal, and A is the constant in the expression for the specific heat $C_v = AT^3$ joules/cc. degree. Then taking the results of Armstrong and Grayson-Smith (1) for the specific heat of bismuth, we obtain $K_B \simeq 3.8\, RT^3$. Hence, substituting experimental results, values for R of approximately 0.1 mm., 0.3 mm., and 1.3 mm. are obtained for Bi 1, Bi 2, and Shalyt's single crystal respectively. In the case of Shalyt's specimen, the agreement is sufficient to indicate that below 3°K. thermal resistance is predominantly due to boundary scattering at the surface of the rod. However, in the case of Bi 1 and Bi 2, interpretation is more difficult as the grains are columnar and penetrating to the center of the rod, i.e. the cross-section for grain boundary is almost triangular; in Bi 1 two sides of the grain are of length about 1 mm. and the third is an arc of a circle of length about 0.3 mm., and in Bi 2 two sides are of length 1.5 mm. and the third is an arc of length 1.2 mm. In lieu of a proper theoretical treatment we have calculated the effective hydrodynamic radius (R_h = 2 × area/perimeter) of such a boundary and obtain

$$R_h \simeq 0.1_8 \text{ mm. for Bi 1}$$

and $$R_h \simeq 0.5 \text{ mm. for Bi 2.}$$

The agreement with the values of R calculated on the assumption of grain boundary scattering at very low temperatures is probably to some extent fortuitous.

Between 10° and about 80°K., K is given by $16/T$ watts/cm. degree, the T^{-1} relation suggesting that anharmonic coupling between phonons is the principal cause of thermal resistance. Above 80°K. in the case of Bi 2 and the Shalyt crystal, K appears to be decreasing less rapidly owing probably to the addition of an electronic component of the thermal conductivity. We may calculate the approximate magnitude of K_e from the residual electrical resistivity, ρ_0, and the ideal resistivity, ρ_i, at room temperature.

Since $$W_i \simeq \text{constant} = \rho_i/LT \text{ for } T > \theta/2$$

and $$W_0 T = \text{constant} = \rho_0/L,$$

therefore $$W_e(T) = W_0(T) + W_i$$
$$= L^{-1}[\rho_0/T + (\rho_{295} - \rho_0)/295];$$

therefore $$K_e \simeq 0.01_8 \text{ for Bi 1 at 80°K. (cf. } \theta \simeq 100\text{°K. for bismuth)}$$

and $$K_e \simeq 0.05 \text{ for Bi 2 at 80°K.}$$

This estimate receives some confirmation from Shalyt's observation that a field of 4200 oersteds increases the thermal resistance by 15–20% at liquid nitrogen temperatures, indicating that K_e is at least 15–20% of the total conductivity at about 80°K.

In the case of Bi 2, the more rapid fall of the thermal conductivity with increasing temperature at about 7°K. is similar to the behavior of high purity dielectric crystals. As discussed more fully in a recent review by Berman (3), the thermal conductivity of sapphire, quartz crystals, solid helium (see also Webb and Wilks (31)) falls rapidly as the temperature increases above that for the maximum. These results on insulators agree quite well with the prediction of Peierls (theory of Umklapp-prozessen (3)) that for $T < \theta/10$, the thermal resistance W_U should vary as $e^{-\theta/2T}$ rather than follow the T^{-1} relation characteristic of higher temperatures. In Bi 1 the presence of impurities presumably produces an additional resistance which masks this effect.

Germanium

The results on germanium (Fig. 4) are of a preliminary nature as the specimen cracked before measurements of thermoelectric power and electrical resistance were completed. However, the thermal conductivity data for this specimen are interesting for two reasons. Firstly, the conductivity has the same form as that observed by Rosenberg (27) on a slightly smaller specimen; at the lowest temperatures the conductivity varies as $T^{2.9}$ so that, substituting the experimental values in equation [16] and taking $\theta = 280$°K., we obtain $R \simeq 0.9_8$ mm., i.e. an effective diameter of about 1.7 mm. This compares well with the dimensions of the rod, viz. 2 mm. × 4 mm., suggesting an effective diameter of perhaps 2.5 mm.

The second feature of interest is the shape of the conductivity curve (Fig. 4) at temperatures above its maximum. Between 35° and 160°K., $K \propto T^{-1.8}$, thus decaying appreciably faster than the T^{-1} relation that is predicted for anharmonic coupling of the lattice waves. This might be due to the presence of holes or free electrons but, since the electrical resistivity of Ge 1 varies from approximately 2 ohm cm. at 60°K. to about 6 ohm cm. at 150°K., it seems unlikely that there are sufficient charge carriers present to cause either appreciable additional scattering of the lattice waves or to make K_e significant; nor is there any evidence of a sharp peak and rapid exponential variation of conductivity with temperature in the region between 10° and 30°K. which we might expect from a high purity material (cf. Bi 2 or Berman's results on dielectric crystals (3)). However, further results on the various transport phenomena and the Hall effect* are awaited before these questions can be adequately discussed.

Between 60° and 90°K. the thermoelectric power varies approximately as $T^{-1.5}$ having a value of about +1.8 mv./°K. at 90°K., which is close in magnitude but opposite in sign to that observed by Frederikse (9) on N-type germanium having a room temperature resistivity of 1 ohm cm.

DISCUSSION AND CONCLUSION

Electrical Conductivity

The dilute copper alloys show a resistance minimum which, in the case of germanium and iron impurities, is to be expected from the previous work of MacDonald and Pearson (22), but the amount of impurity is not sufficient to cause any serious departure from Matthiessen's rule.

The less pure specimen of bismuth has a very high residual resistance and a low temperature minimum but does not obey Matthiessen's rule.

Beryllium in the form of two sintered rods of differing chemical purity has a residual electrical resistance sensibly constant below 50°K. and the ideal resistivity at room temperature is close to that observed previously for pure single crystals.

Thermal Conductivity

In the case of copper + 0.02% germanium, and copper + 0.0043% iron, the electronic component, K_e, appears to be the dominant part of the thermal conductivity and is similar to that previously observed in pure copper (Berman and MacDonald (4), White (32)); here the following relations hold:

$$W = 1/K = W_0 + W_i$$

$$= (\rho_0/L\,T) + W_i$$

where $$W_i = BT^n,\ n \simeq 2\ (T < \theta/5).$$

In beryllium and copper + 0.056% iron, K_e and K_g are comparable at low temperatures. However, the difference in temperature dependence makes it possible to deduce the separate contributions. Thus in these specimens for $T < \theta/20$,

*We are indebted to Dr. E. Mooser for Hall effect data on this germanium specimen which indicate that it is P-type with approximately 7.7×10^{14} carriers per cc.

$$K = K_e + K_g$$
$$= K_0 + K_g$$
$$= aT + dT^2.$$

As in the more dilute copper alloys, the value of $a(=K_0/T)$ is consistent with that calculated from the equation

$$L_0 = \rho_0 K_0 / T$$

and the constant d has a value for copper which agrees with that calculated by Klemens (18). The maximum value of the lattice conductivity of copper appears to be about 1 watt/cm. degree at 30°K. These results suggest that the mean free path of the phonons in a metal at low temperatures is restricted by the free electrons present and that in the region $T \leqslant \theta/20$, the mean free path for a phonon–electron collision may be much shorter than that for a phonon–phonon collison. This raises doubt as to whether one of the fundamental assumptions of present transport theory, namely that of Bloch, that the phonons in the lattice are in thermal equilibrium with one another in the presence of an electron current, is strictly true. This question of electron–phonon interaction and its possible effect on the existing theories of thermal conductivity and thermoelectricity has been discussed more fully elsewhere by MacDonald (21) and MacDonald, Pearson, and White (23).

The specimens of polycrystalline bismuth examined show a thermal conductivity characteristic of dielectric crystals (lattice conductors), that is, a size-dependent conductivity at very low temperatures rising sharply with the temperature, and at higher temperatures decreasing as T^{-1} owing to anharmonic coupling between the lattice waves. The electronic thermal conductivity may become significant at liquid nitrogen temperatures but not below this.

At low temperatures germanium shows a lattice conductivity limited by boundary scattering similar to bismuth, but then has a broad maximum and falls rather more rapidly with rise in temperature than the T^{-1} relation would predict.

ACKNOWLEDGMENTS

The authors are grateful to Dr. W. B. Pearson for supplying the copper alloys and for metallographic examination of samples, to Dr. E. Mooser for producing the germanium specimen, and to Dr. D. K. C. MacDonald for many interesting discussions on the problems of transport phenomena in solids.

REFERENCES

1. Armstrong, L. D. and Grayson-Smith, H. Can. J. Research, A, 27: 9. 1949.
2. Berman, R. Phil. Mag. 42: 642. 1951.
3. Berman, R. Phil. Mag. Suppl. 2: 103. 1953.
4. Berman, R. and MacDonald, D. K. C. Proc. Roy. Soc. (London), A, 211: 122. 1952.
5. Casimir, H. B. G. Physica, 5: 495. 1938.
6. Dauphinee, T. and Woods, S. B. Rev. Sci. Instr. To be published. 1955.
7. Erfling, H. D. and Grüneisen, E. Ann. Physik, 41: 89. 1942.
8. Estermann, I. and Zimmerman, J. E. J. Appl. Phys. 23: 578. 1952.
9. Frederikse, H. Phys. Rev. 92: 248. 1953.
10. Grüneisen, E. and Adenstedt, H. Ann. Physik, 31: 714. 1938.
11. Herlin, M. A. Proc. 3rd Inst. Conf. on Low Temp. Phys., Houston. 1953.

12. HILL, R. W. and SMITH, P. L. Phil. Mag. 44: 636. 1953.
13. HULM, J. K. Proc. Roy. Soc. (London), A, 204: 98. 1950.
14. KAYE, G. W. C. Proc. Roy. Soc. (London), A, 170: 561. 1939.
15. KEESOM, W. H. and MATTHIJS, C. J. Physica, 2: 623. 1935.
16. KEMP, W. R. G., KLEMENS, P. G., SREEDHAR, A. K., and WHITE, G. K. Proc. Phys. Soc. (London), A, 67: 728. 1954.
17. KEMP, W. R. G., SREEDHAR, A. K., and WHITE, G. K. Proc. Phys. Soc. (London), A, 66: 1077. 1953.
18. KLEMENS, P. G. Australian J. Phys. 7: 57. 1954.
19. KLEMENS, P. G. Australian J. Phys. 7: 64. 1954.
20. MACDONALD, D. K. C. J. Sci. Instr. 24: 232. 1947.
21. MACDONALD, D. K. C. Rapp. 10e Conseil Solvay, Brussels. 1954.
22. MACDONALD, D. K. C. and PEARSON, W. B. Acta Metallurgica. To be published. 1955.
23. MACDONALD, D. K. C., PEARSON, W. B., and WHITE, G. K. Bull. Intern. Inst. Refrig. 1954 (Grenoble Conference).
24. MAKINSON, R. E. B. Proc. Cambridge Phil. Soc. 34: 474. 1938.
25. OLSEN, J. L. and ROSENBERG, H. M. Phil. Mag. Suppl. 2: 28. 1953.
26. POWELL, R. W. Phil. Mag. 44: 645. 1953.
27. ROSENBERG, H. M. Proc. Phys. Soc. (London), A, 67: 837. 1954.
28. ROSENBERG, H. M. Phil. Mag. 45: 73. 1954.
29. SHALYT, S. J. Phys. (U.S.S.R.), 8: 315. 1944.
30. SONDHEIMER, E. H. Proc. Roy. Soc. (London), A, 203: 75. 1950.
31. WEBB, F. J. and WILKS, J. Phil. Mag. 44: 663. 1953.
32. WHITE, G. K. Australian J. Phys. 6: 397. 1953.
33. WHITE, G. K. Proc. Phys. Soc. (London), A, 66: 559. 1953.
34. WHITE, G. K. and WOODS, S. B. Phil. Mag. 45: 1343. 1954.
35. WILSON, A. H. Proc. Cambridge Phil. Soc. 33: 371. 1937.

A PANORAMIC MASS SPECTROSCOPE FOR KINETIC STUDIES[1]

By Edouard G. Leger[2]

ABSTRACT

A mass spectroscope capable of recording the trend of many chemical species in rapid gas-phase reactions is described. The instrument represents a departure from analytical mass spectrometric practice by using a molecular streaming source, rapid electric scanning, an electron multiplier ion detector amplifier, and a cathode ray tube display. A 40 peak spectrum can be scanned in five milliseconds and recorded by a motion picture camera. A few results obtained with this instrument in the study of diethyl ether cool flames are given.

INTRODUCTION

For some time mass spectrometry has been employed to investigate the kinetics of gas-phase chemical reactions. In the case of slow reactions, micro-samples can be drawn and chilled at convenient time intervals and analyzed in a conventional instrument equipped with a capillary leak and graphic recorder. Rapid reactions, however, require continuous and practically instantaneous sampling to minimize further collisions between molecules after they leave the reaction zone and before ionization in the mass spectrometer. Instantaneous sampling has been achieved in the spectrometers designed by Eltenton (4), Robertson (23), Lossing and Tickner (14), by allowing the molecules (and free radicals) to leave the reaction vessel through a microscopic hole in a thin membrane, preferably quartz, and to travel in a molecular stream to the ionization chamber. Since the recording of a mass spectrum usually takes several minutes, the reactions studied so far took place in flow systems.

The problem of obtaining analytical data on reactions of one-second duration taking place in a static system arose in the studies on rapid oxidations in the cool flame region (20). The mass spectrometer appeared to be a suitable instrument, provided the mass spectra obtained with a "collision-free" source could be recorded at repeated intervals during a small fraction of a second. Fast recording with normal sources has been reported in mass spectroscopes designed by Siri (24), Guthrie and Wakerling (8), and more recently by Ezoe (5) and Cook-Yarborough (1). In these investigations the spectra were displayed on a cathode ray oscilloscope by varying the spectroscope accelerating voltage synchronously with the horizontal sweep voltage of the cathode ray tube and placing the detected pulses on the vertical axis of the same tube.

The construction of such an instrument, briefly described in a previous publication (11), involved a number of exacting design requirements. Com-

[1]*Manuscript received November 1, 1954.*

The development of this instrument was carried out at Laval University under DRB Grant 129 to Dr. C. Ouellet. This research assignment was part of a general investigation of gas phase oxidations by new instrumental techniques conducted in the Physical Chemistry Section at Laval University.

[2]*Present address: Canadian Armament Research and Development Establishment, P.O. Box 1427, Quebec, P.Q.*

parative characteristics of the proposed and of a normal mass spectrometer were such that a new instrument seemed preferable to modification of existing designs. The requirements included:

(1) A fast, intense, "collision-free" entry of gas from the reaction vessel into the ionization chamber,

(2) A fast electric scanning of the mass spectrum (approximately 40 peaks in five milliseconds),

(3) Fast and extremely sensitive detection and amplification of the pulsating peaks of the spectrum,

(4) Recording with a motion picture camera of the changing spectrum from a cathode ray oscilloscope.

Recording was required up to an approximate mass of 125 (O = 16) which is in the range of the base peaks of some peroxides capable of playing a major role in oxidation reactions. These features may be compared with those of a normal mass spectrometer using capillary tube gas inlet, magnetic scanning, Faraday-cup detection of the pulsating peaks, amplification by electrometer tube techniques, and finally recording of the spectrum on a pen and ink chart recorder.

The interpretation of changing spectrum was not believed difficult since, in addition to the normal calibration with pure compounds, the information furnished by comparison of the various curves of peak intensity versus time permits positive identification of peak origin. A compound whose concentration changes with time will give peaks which will vary with time while keeping the same relative intensity to one another. Moreover, by conducting the same reaction at various ionization potentials, further qualitative data are provided by changes in the relative intensity of the peaks of a compound. Free radicals can also be detected by their lower ionization potentials.

The purpose of this paper is to present the instrumentation techniques used in the first rapid panoramic spectroscope constructed at Laval University. Detailed analysis of reaction studies and instrument improvements will be reported in subsequent papers.

GENERAL DESIGN

The "collision-free" gas inlet was comprised of a molecular jet or stream made by passage of gas through a microscopic hole in a reaction vessel close to an ionization chamber. The jet entered the ionization chamber via slits in the chamber walls. The excess non-ionized gas was evacuated by a high capacity pump. Thus, two vacuum systems were required—one for the source and one to maintain the spectroscope evacuated.

To produce oxidation reactions of the cool flame type in a static system that could be easily correlated with the cool flame reactions in similar vessels previously studied in our laboratories, a cylindrical reaction vessel (4.5×12.5 cm.) was believed preferable. To avoid as much as possible the influence of the chamber walls on the reaction mixture, a re-entrant cone having a microscopic hole in a thin membrane at the apex was used for gas sampling from the reaction vessel. The cold premixed fuel and oxidizer were ducted into the heated,

evacuated reaction chamber. The vessel temperature and pressure required vary with the type of fuel but are generally between 325° and 200°C. and 25 and 500 mm. of mercury, respectively (25). Therefore a heating system was incorporated into the source chamber to maintain the reaction vessel at the required temperature.

A sector type magnet was used to simplify geometric construction because of the necessity of placing the reaction vessel close to the ionization chamber. An inflection focusing magnet was chosen to increase the beam luminosity (6) with $\theta = 29.3°$ (9). The resulting pole piece was easily constructed with $\alpha = 90°$ and was readily faced with a circular piece of magnetic material. The beam angle was set at 9° and the width at 1.25 cm. The maximum mass measurement considered necessary for oxidation studies being in the 125 region, a radius of 15 cm. was chosen to permit focusing of the 125 mass ions at magnetic fields of approximately 3000 gauss and electrical accelerations of approximately 500 volts. The formula for the deflection of singly charged ions is:

$$M = \frac{H^2R^2}{V}\,\frac{1}{20700},$$

where M is the mass of the particle (O = 16),
H is the magnetic field in gauss,
R is the radius in centimeters,
V is the acceleration voltage in volts.

Based on this formula, the above values give a theoretical maximum of 150.

The vacuum system, the source, and the spectroscope geometrical arrangements are illustrated in Fig. 1. A permanent magnet was selected, since magnetic scanning, in spite of certain advantages (21), is limited to relatively low frequencies because of the electrical inertia of electromagnets. Electrical scanning was accomplished in this case by superimposing a saw-tooth wave form upon the d-c. ion-accelerating voltage. The same wave form was placed on the horizontal axis of a cathode ray tube. The output of the detector of the ionic pulses which pass sequentially through the exit slit was placed on the vertical axis of the same tube. The mass spectra were thus inscribed panoramically on the cathode ray oscilloscope where they could be recorded conveniently by a motion picture camera and subsequently studied in detail, image by image.

A sweep time of approximately four milliseconds representing a saw-tooth frequency of 260 cycles per second was chosen to permit photography at 128 images per second by a motion picture camera, not synchronized to the sweep, without losing trace sections due to shutter action. This high sweep time permitted determination of reaction concentration curves with 13 points for reactions lasting 1/10 of a second. In reality the system constructed will permit speeds of 500 cycles and higher if decreased sensitivity is acceptable.

The d-c. accelerating voltage on which the saw-tooth was superimposed was adjustable from 2000 to 500 v. A maximum of 2000 v. was chosen to facilitate insulation and availability of parts. The saw-tooth wave form used in

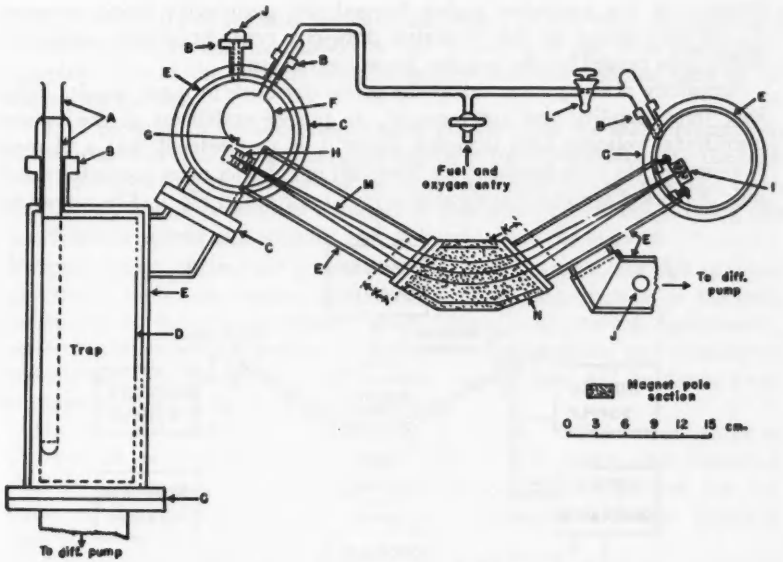

FIG. 1. Mass spectroscope geometry.

A Glass tube
B Wax seals
C "Teflon" or aluminum gaskets
D Cylindrical copper pipe
E Brass tubing silver soldered
F Heated reaction vessel
G Quartz re-entrant cone with a microscopic hole at the apex
H Slit system
I Be–Cu ion electron multiplier in brass box lined with mica
J Mountings for ionization gauges
K Fringing magnetic field
L Stopcock permitting pressure equalization in reaction vessel during pumping down, protecting the thin membrane containing the microscopic hole
M Path of ion beams
N Pole piece geometry. The vacuum chamber was made $\frac{1}{2}$ in. longer to permit easy adjustment of magnet for maximum resolution. The flat face is $\frac{1}{4}$ in. brass, silver soldered on $\frac{1}{4} \times \frac{1}{4}$ in. rectangular brass stock.

the acceleration of the ions was adjustable in amplitude from 1800 to 50 v. This readily permitted a 40 peak scan on one cathode ray tube display. A d-c. filament was used to obviate 60 cycle modulation of the ion beams.

This sweep speed imposed design difficulties due to reduced luminosity. Under these conditions the detector received ions of a given mass at time intervals in the order of 10^{-5} seconds. A high sensitivity and short response time are required and thus a high fidelity response of the detector and amplification systems in the range d-c. to 10^{+5} cycles per second is necessary. The detector was an ion–electron multiplier fulfilling these requirements. In order that the multiplier will receive enough ions during the short peak scan time to permit accurate recording of peak intensity, a relatively intense ion beam is required. For 4% accuracy 7500 ions, representing an ion current of 10^{-11} amp., are necessary with multiplier efficiency of 15% and a peak scan time of 50×10^{-6} sec. This necessitated a rapid rate of gas intake and a correspondingly fast evacuation of the non-ionized molecules. This increased the gas

pressure in the ionization region beyond the permissible static pressure. An efficient source of the focalizing draw-out type diminished luminosity restrictions caused by the angular beam limitations.

Simplicity of design was set as the prime objective in most circuits. Since long term stability was not required, no precise stabilizers of the various operational voltages were included. Later it was considered that a filament stabilizer of the type described by Nier (18) might offer more accurate recordings. A block diagram of the circuits required is given in Fig. 2. The panoramic

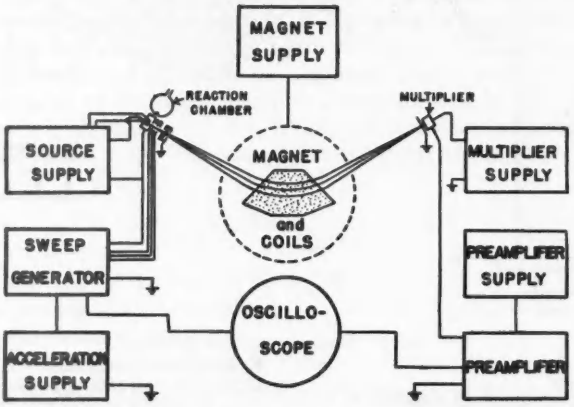

FIG. 2. Circuits.

spectrum was displayed on a Tektronix 512 oscilloscope. Its wide band characteristics and high overload limit permitted easy handling (without distortion) of pulses whose ratio may vary from 1:1 to 1000:1 in amplitude and from tens of microseconds to tens of milliseconds in duration. A preamplifier was used to transfer the pulses from the multiplier to the oscilloscope without distortion, to limit the height of the larger pulses so that the smaller peaks, of amplitude one ten thousandth that of the larger peaks, may be observed without base line distortion, and to provide added gain up to the noise level of the electronic tubes. A separate sweep generator slave driven by the oscilloscope sweep gate circuit superimposed the saw-tooth wave form on the d-c. accelerating voltage. This facilitated circuit construction. The other circuits required were mainly d-c. sources. Detailed descriptions of circuits are given in succeeding sections.

GAS INLET SYSTEM

The introduction of gas into the ionization chamber by molecular streaming from a high pressure region in a fast scanning instrument requires close control of the gas entry system. If used correctly, this technique permits:

(1) A "collision-free" entry of gas which immunizes the reaction mixture from chemical changes caused by collisions of the molecules on the walls.

(2) A fast entry of gas into the ionization region at near sonic velocities and a correspondingly fast evacuation of the non-ionized gas, thus providing a sampling time of the gaseous mixture smaller than the response time of the measuring circuits.

(3) A pressure in the ionization region greater than the static pressure in the source chamber. The gas expands conically from the orifice into the high vacuum region and by placing the ionization chamber in the expansion cone, a relatively higher pressure is obtained in this chamber without flooding the spectroscope proper and without risk of burning out the filament.

By means of an efficient slit system and ionization chamber, the high pressure produces a high ionic current permitting accurate measurement of the ionic pulses seen by the detector within a short, limited time interval. Additionally, since the decomposition products resulting from combustion and cracking on the filament are formed in a low pressure region, they will be swept away without contaminating the reaction mixture.

The various factors that contribute to an intense, "collision-free" entry of gas are the relative geometric arrangements of the orifice and ionization chamber, the membrane thickness and microscopic orifice diameter, the distance of the orifice from the ionization chamber, and, finally, pumping capacity.

The geometric arrangement, designed to yield a high pressure in the ionization chamber, is illustrated in Fig. 1. The reaction vessel was placed on the opposite side to the high vacuum inlet and as close as possible to the rectangular slit system, with the microscopic orifice concentric with the slits in the ionization chamber walls. This arrangement permitted easy evacuation of the non-ionized gas molecules, with the expansion cone at 90° to the acceleration slits. This prevented too large an entry of gas into the spectroscope proper, and located the gas cone directly in the electron stream before the expansion gas cone was lost by turbulence in the static gas. The microscopic orifice was placed as close as possible to the electron stream, as it is doubtful if the expansion cone extends more than a few centimeters from the orifice even with large capacity pumps. The diameter of the orifice must be such as to permit the maximum gas inlet that can be handled by the diffusion pump thus providing a suitable gas expansion cone when the fuel/oxygen mixture is introduced into the reaction vessel without increasing the static pressure in the source region beyond the efficient operating pressure. The normal reaction must also not be affected by the pressure decrease in the reaction vessel due to the leak through the orifice. It is preferable that the capacity of the pump be sufficient to permit a large gas intake. Since few data are available on gas expansion cones functioning under molecular stream conditions, no reasonable calculation of the required pumping capacity can be made. In our case a 100 liters/sec. at 10^{-4} mm. of mercury oil diffusion pump was used for the source. The maximum static pressure acceptable in the source region was 10^{-4} mm. of mercury. The pumping capacity in the source chamber was found by calculation to be 50 liters per second at this pressure after deducting the effect of the trap. The diameter, d, of the microscopic orifice was calculated by

using the hydrodynamic flow formula given by Guthrie and Wakerling (7) and modified for equimolecular oxygen/fuel mixtures:

$$d(\text{cm.}) = \left(\frac{2}{7} \times \frac{P_2 S_2 T_1}{T_2 P_1}\right)^{\frac{1}{3}},$$

where P_1 is the pressure in reaction vessel,
P_2 is the pressure in source chamber,
S_2 is the pump capacity in liters per second at pressure P_2,
T_1 is the temperature in reaction vessel in °K.,
T_2 is the temperature at which pumping is effected in °K.

This yields an orifice diameter of 25μ with a reaction vessel pressure of 100 mm. of mercury and a temperature of 200°C. Pumping was usually carried out at room temperature with the liquid air trap held in reserve as a safety factor. Calculations agreed with experimental results.

The membrane at the apex of the cone must be as thin as possible and always thinner than the diameter of the orifice for a "collision-free" gas entry. Assuming uniform distribution,* an orifice diameter of 25μ yields, by calculation, gas expansion cones whose angles may not exceed 100° before the gas is lost by turbulence in the static gas pressure at 1 cm. from the microscopic hole (see Fig. 3). The gas does not exit in molecular effusion since the microscopic

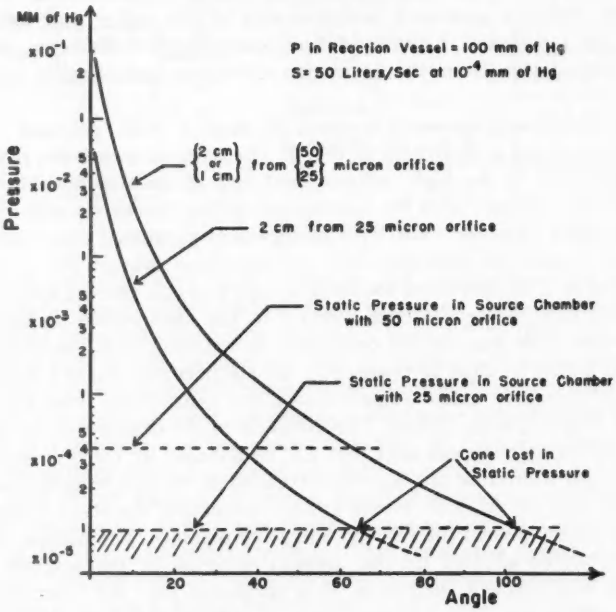

FIG. 3. Pressure in expansion cone for various cone angles.

*This hypothesis is undoubtedly ideal and should be considered in that light.

orifice has a diameter which is 100 times the mean free path of the molecules in the reaction vessel (2).

In this case the amount of gas leaking out of the reaction vessel during a one-second reaction was calculated to be 0.15%, which is sufficiently small to prevent the resulting pressure change from affecting the normal reaction course. Fig. 3 shows the pressure in the jet at a distance of 1 and 2 cm. from the orifice for various expansion cone angles. Uniform distribution was assumed and calculations were based on the expansion ratio.* It may be concluded that with the orifice and ionization chamber in close proximity, together with large pumping capacity and a reasonable orifice diameter, the possibility of higher pressure in the ionization region is real.

THE VACUUM SYSTEM (Fig. 1)

As previously discussed, two vacuum systems are required for a fast-scanning mass spectroscope. These are interconnected by the spectroscope accelerating slits. Two pumps were used, one with a capacity of 100 liters per second at 10^{-4} mm. of mercury in the source as outlined in the preceding section, and one with a capacity of 20 liters per second at 10^{-4} mm. of mercury for the spectroscope proper. This latter pump was considered adequate to maintain the spectroscope vacuum below 5×10^{-5} mm. of mercury notwithstanding the gas escaping through the slits when the source static pressure was 10^{-4} mm. of mercury.

All vacuum tubings used were of seamless brass which is readily available and can be worked easily. All joints were silver-soldered. Gaskets of "teflon" and of aluminum were used in the demountable joints. Large cylinders were provided at the gas inlet and detector ends to permit easy mounting of the equipment. No serious contamination problems were anticipated with this type of gas inlet and none were encountered. Degassing was reduced to a minimum.

Liquid air traps were provided to increase the pumping speed and to decrease occasional background peaks caused by condensable organic matter inside the vacuum tubings. The liquid air trap shown at the left of Fig. 1 was designed by Mr. Jean Lafaivre and merits special attention. It consists of a cooled $10\frac{1}{2} \times 3\frac{1}{2}$ in. cylindrical copper pipe inserted in the brass tubing and insulated by vacuum from the wall. The pipe is cooled by liquid air in a $\frac{3}{4}$ in. glass tube, and held in position by means of a copper tube snugly fitted over the glass and soldered at one side of the copper pipe. Since the mean free path of the molecules entering the trap is considerably greater than the diameter of the cylinder, all molecules traversing this section will in general collide many times with the cold walls. The advantage of the trap is that it does not drastically reduce pumping capacity while providing adequate trapping efficiency. It could be further improved by baffles at the expense of pumping capacity.

Considerable difficulty was experienced in the detection of leaks before the spectroscope was sufficiently perfected to be used for that purpose. Leaks were successfully detected by a saturated diode having a tungsten filament

*This hypothesis is undoubtedly ideal and should be considered in that light.

and connected to the vacuum system. The penetration of oxygen sprayed onto the apparatus poisons the emission of the filament. This method is described by Dushman (3), and a description of the instrument used has been published by the author (10).

THE REACTION VESSEL, IONIZATION CHAMBER, AND SLIT SYSTEM (Fig. 4)

In the early experiments a glass-cylinder reaction vessel (4.5 × 12.5 cm.) was used. A quartz thimble having a thin membrane with a 25μ hole was welded into the vessel with molten silver chloride. The quartz thimble (14) was graciously furnished by Dr. F. P. Lossing of the National Research Council of Canada. This vessel was heated by an electric current passed through a platinum film deposited on the glass. The thermal strain induced in the glass, especially at the gas inlet, was greater than it could withstand. Repeated failures were experienced. Quartz was then used to replace glass in the reaction vessel, and the quartz cone made separately with the orifice sparked in the thin membrane by a tesla coil previous to welding it directly to the quartz wall. Nichrome wire wound around the quartz vessel was used as a heating element. A copper sheath insulated by mica was placed over the vessel to equalize the temperature which was measured by thermocouples. Thermistors, capable of withstanding the temperature, could probably have been used to advantage in view of the need for changing metals when bringing thermocouple leads through hermetic seals. The reaction vessel was heated by a-c. line voltage isolated from d-c. by a transformer to permit heater operation at ionization chamber potential. This prevented attraction of the ions through the ionization chamber gas slits to the reaction vessel copper sheath and heater.

The ionization chamber was a small stainless steel box with 1/16 in. walls and with a tantalum filament at one end. Tantalum was used to reduce filament emission poisoning due to oxygen and ether when these are suddenly introduced into the reaction vessel. A small reflector was placed behind the filament at the negative filament potential to increase the quantity of electrons passing through the chamber. Small magnets supported by a grounded iron magnetic shield, insulated by glass plates, were placed over the accelerating slits and were used to force the electrons into a helical path, thereby increasing ionization efficiency. The slit geometry was developed by Nier (17) and was selected for its greater luminosity due to its focalizing action. The slits were made from brass rectangles. This permitted the location of the reaction vessel close to the slits. Arcing between the reaction vessel and shield was prevented by the use of mica insulators. The slit assembly was made as gas-tight as possible to prevent flooding the spectroscope proper by the source static pressure. Mechanical details of the slit assembly are shown in Fig. 4. The slit assembly was mounted on a brass ring held in place by a locking bolt.

At the detector end of the spectroscope the circular exit slit, 0.8 × 12.5 mm., was mounted in a manner similar to the acceleration slits. The multiplier was mounted in a mica-lined box and placed on top of the exit slit. The sizes of the slits were adjusted to permit complete peak separation at the base of peak

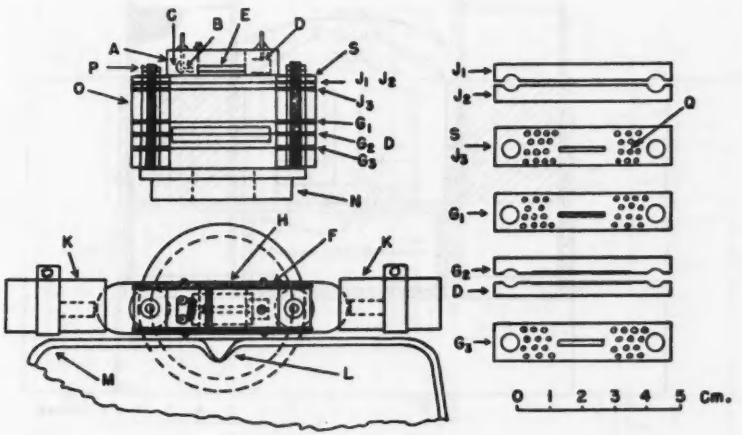

FIG. 4. Acceleration slit assembly.

A Ionization chamber
B Tantalum filament
C Electron reflector
D Collector
E Gas inlet slit 1.5 × 15 mm.; gas outlet slit 4.0 × 15 mm. covered by a grid
F Glass sheet insulator 55 × 29 mm.
H Iron magnetic shield 1.5 mm. thick
K 15 × 30 mm. cylindrical "alnico" magnets to increase ionization
L Quartz cone having a 25μ orifice
M Quartz reaction vessel 45 × 125 mm.
N Mounting plate
O Glass spacers 12 mm. O.D. and insulator 6.0 mm. O.D. over brass bolt 2 mm. O.D.
P Holding nut
Q Gas pumping orifices

Slits in brass rectangles 55 × 12 mm.
Slit spacings: S−J_1J_2, J_1J_2−J_3 2 mm.; J_3−G_1 10 mm.;
G_1−G_2D, G_2D−G_3 4 mm.; G_3−N 6 mm.
Slit widths: J_1−J_2 1 mm.; S, J_3 1.0 × 12.5 mm.; G_1 0.49 × 12.5 mm.;
G_2−D 2 mm.; G_3 0.80 × 12.5 mm.

65 which corresponds to resolution of 130 at half peak heights. A flat section, 1/13 of the total peak width, was permitted at the peak top by choosing an appropriate exit slit width to facilitate peak height measurements. No repeller plate was used in the detector-slit system in the first measurements.

THE MAGNET

The mass spectroscope magnet is illustrated in Fig. 5 while the pole piece section is shown in Fig. 1. The four half-cylindrical sections of "alnico 5" were manufactured at the Quebec Plant of Canadian General Electric. Two coils of 10,000 turns each of No. 23 varnished magnet wire were placed over the "alnico" to magnetize, to change the magnetic field strength, and to stabilize the magnet. The coils were energized by a battery source. The maximum magnetic strength attainable in the $\frac{3}{4}$ in. gap was approximately 3800 gauss with magnetization at 40,000 ampere turns. The magnet position was adjustable in relation to the slits, thus permitting easier focusing adjustment.

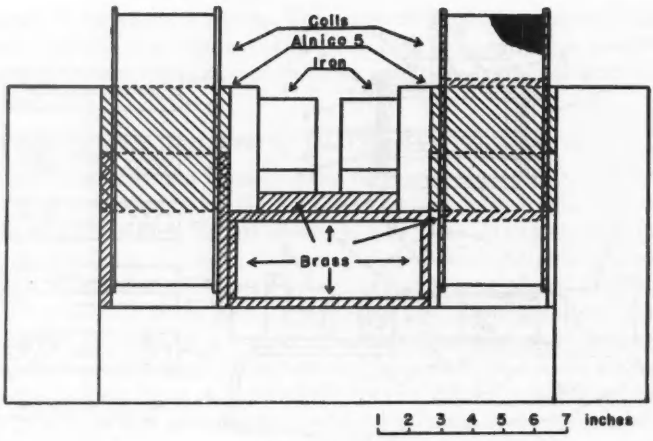

FIG. 5. Magnet.

THE ELECTRON MULTIPLIER

The detection of positive ion pulses at high speed requires an extremely low current amplifier capable of response to very rapid pulsed signals. The d-c. electrometer amplifiers normally employed are unsuitable because they use high input resistors whose wiring capacity limits the response time. Low input capacity circuits specially designed to measure small, rapid pulses often achieve this at the expense of a decreased signal to noise ratio. The beryllium–copper electron multiplier is practical in this case because of its high amplification of free ionic or electronic currents without the introduction of undue noise (13). Its main disadvantage is that the positive ions of varying energy and/or mass create a varying secondary electron yield at the first plate. Various methods of estimating this effect have been suggested (12, 22) but because of the nature of the source, calibration of the spectrometer against pressure and mass for a given acceleration is necessary. Since the electron multiplier forms part of the analytical train, the calibration with known gas mixture obviates this disadvantage.

The beryllium–copper electron multiplier (modelled after RCA 931A phototube) was graciously given to us by Dr. Hin Lew of the National Research Council of Canada and is similar to the model he used in experiments at M.I.T. (13). It provided a gain of approximately 100,000 when operated at 300 v. per dynode, and was sensitized by oxidation in air after heating to 600°C. for 15 min. in a simple oven in an atmosphere of commercial argon as described by Osborne (19).

CIRCUITS

The Preamplifier (Fig. 6)

A special low-input-capacity circuit, somewhat similar to that previously described by Moody (15), comprised of tubes V_1 and V_2 and associated parts located near the multiplier, was used to transfer the pulses from the multiplier to the electron tubes without introducing capacitance distortion. Negative

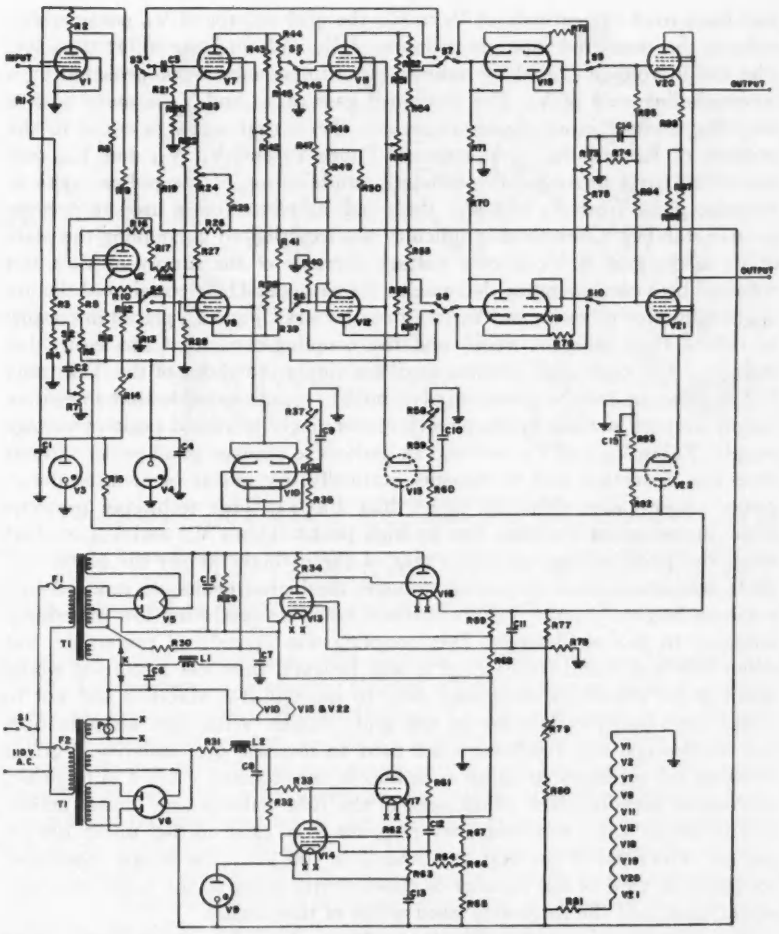

FIG. 6. Preamplifier.

C_3, C_{14} 0.1 μf. 600 v.; C_1, C_4 0.5 μf. 600 v.; C_5, C_8 80 μf. 600 v.; C_6 4000 μf. 25 v.; C_2, C_7, C_9, C_{10}, C_{15} 0.05 μf. 600 v.; C_{11}, C_{12}, C_{13} 0.01 μf. 600 v.

R_1 chosen to adjust the circuit gain, maximum value approximately 5 megs, in our set-up 50 kΩ; R_2, R_{11}, R_{20}, R_{28}, R_{50}, R_{63} 33 kΩ 2 w.; R_3 190 kΩ 1 w.; R_4 50 kΩ 1 w.; R_5 155 kΩ 1 w.; R_6, R_{41}, R_{48}, R_{54}, R_{55} 66 kΩ 1 w.; R_7 500 kΩ 2 w. pot.; R_8, R_{17} 100 kΩ 1 w.; R_9 15 kΩ 4 w.; R_{10} 27 kΩ 1 w.; R_{12}, R_{19}, R_{32}, R_{34}, R_{35}, R_{60}, R_{77}, R_{82}, R_{83} 1 meg 1 w.; R_{13}, R_{29}, R_{44}, R_{53}, R_{87} 22 kΩ 1 w.; R_{14} 2 megs 2 w. pot.; R_{15} 10 kΩ 4 w.; R_{16}, R_{67}, R_{69} 47 kΩ 1 w.; R_{18}, R_{33} 5 kΩ 2 w. pot.; R_{21}, R_{38}, R_{46}, R_{49}, R_{56}, R_{64}, R_{70}, R_{71}, R_{72}, R_{74}, R_{76}, R_{84}, R_{85} 470 kΩ 1 w.; R_{22}, R_{47}, 400 Ω 2 w.; R_{23}, R_{27} 4.7 kΩ 2 w.; R_{24} 2 kΩ 2 w. pot.; R_{26} 4 kΩ; R_{39}, R_{52} 220 kΩ 2 w.; R_{39} 560 kΩ 1 w.; R_{31} 80 Ω 4 w.; R_{37}, R_{58} 1 meg 2 w. pot.; R_{36}, R_{42}, R_{51}, R_{66} 19 kΩ 2 w.; R_{43} 4 kΩ 2 w. pot.; R_{45}, R_{40} 6 kΩ 2 w.; R_{61} 1 kΩ 25 w.; R_{62} 1 kΩ 2 w.; R_{65} 56 kΩ 2 w.; R_{68} 10 kΩ 2 w. pot.; R_{81} 10 kΩ 1 w.; R_{73} 20 kΩ 2 w. pot.; R_{75} 50 kΩ 1 w.; R_{78} 447 kΩ 2 w. pot.; R_{79} 75 kΩ 2 w. pot.; R_{80} 600 kΩ 2 w.; R_{81} 250 Ω 10 w.; R_{86} 20 kΩ 2 w.; R_{87}, R_{88} 15 kΩ 2 w.

V_1, V_2 6AK6; V_3, V_4 0B2; V_5 5T4; V_6 5U4; V_7, V_8, V_{11}, V_{12}, V_{20}, V_{21} 12AU6; V_9 5651; V_{10}, V_{18}, V_{19} 12AU7; V_{13}, V_{14} 6AU6; V_{15}, V_{22} ½ 12AU7; V_{16}, V_{17} ½ 6AS7.

T_1 trans. 310–0–310 v. 70 ma. 5 v. 2 amp. 6.3 v. 2.4 amp.; T_2 trans. 400–0–400 v. 200 ma. 5 v. 3 amp. 6.3 v. 6 amp.; L_1 0.5 h. 4 Ω d-c.; L_2 30 h. 200 ma.; K selenium rectifier 12 v. 2 amp.; F_1, F_2 fuses 3 amp.; P pilot lamp 6.3 v.

feed-back from the cathode of V_2 to R_1, the grid resistor of V_1, considerably reduces the measured input impedance of R_1 and thus the input capacity. The loss in voltage caused by reduced input impedance is compensated by a corresponding gain of V_1. The combined gain of V_1 and V_2 is unity with a resulting lowered input capacitance—i.e., the output signal is equal to the product of R_1 and the input current. Tubes V_7 and V_8, V_{10} and V_{12}, and associated parts provide d-c. push–pull amplification of the pulses taken in opposite phase from R_9 and R_{11}. Push–pull amplification is used to provide greater stability. Considerable difficulty was experienced in coupling the plate of V_2 to the grid of V_7, since a voltage decrease of the supply of V_2 is not reflected by a corresponding decrease at the cathode. This necessitated the use of gas regulator tubes V_3 and V_4 (with condensers C_1 and C_4 placed in parallel to reduce their inherent noise) and the coupling-capacity C_3 to assure d-c. stability. The push–pull circuits used are similar to those of the Tektronix 512 oscilloscope and the power supply similarly compensated so that a negative supply voltage increase produces a correspondingly increased positive voltage supply. Tubes V_{18} and V_{19} are used as limiters to observe small peaks without base line distortion and to measure statically, by means of an attenuator, peaks whose ratios differ by more than 1000:1. This technique prevents scope distortion of the base line by high peaks. Tubes V_{18} and V_{19} conduct when the plate voltage surpasses that of the cathode. When the plates and grids are connected to the signal voltage, the higher peaks are reduced to a common height. V_{20} and V_{21} are cathode followers producing low impedance coupling to the oscilloscope. D-c. coupling was considered preferable, but when this was found impractical it was believed that less distortion would result if the capacities were used only to increase d-c. stability and not to avoid large positive voltages on the grid circuits. With high amplification, the oscilloscope a-c. condensers are used to increase d-c. stability. Various resistors are necessary to adjust tube bias to the required -3.5 v. A large a-c. test signal permits exact adjustment of the tube balance and limiter action.

The circuit has a flat frequency response from close to d-c. up to 100 kc. per sec. The noise of the first two stages is 100 μv. This is not considered excessive in view of the number of tubes contributing to the noise on a near equal basis, and the frequency band width of this circuit.

The over-all plan of this circuit was designed by the author. For detailed design and construction the author is indebted to E. Vaillancourt.

Saw-Tooth Acceleration (Fig. 7)

The saw-tooth generator and acceleration supply for the mass spectroscope are illustrated in Fig. 7, together with their connection to the acceleration slits. A sweep was required varying in amplitude and time from 2000 to 50 v. and from 20 to a few milliseconds, respectively, superimposed on a d-c. acceleration voltage 500 to 2000 v. The oscilloscope sweep could have been amplified to 2000 v. and a special technique employed to superimpose it on d-c. voltage, but this would have necessitated either the use of a special high fidelity step-up transformer and a very high-voltage supply or special high-voltage amplifier tube circuits. It was considered preferable to construct an

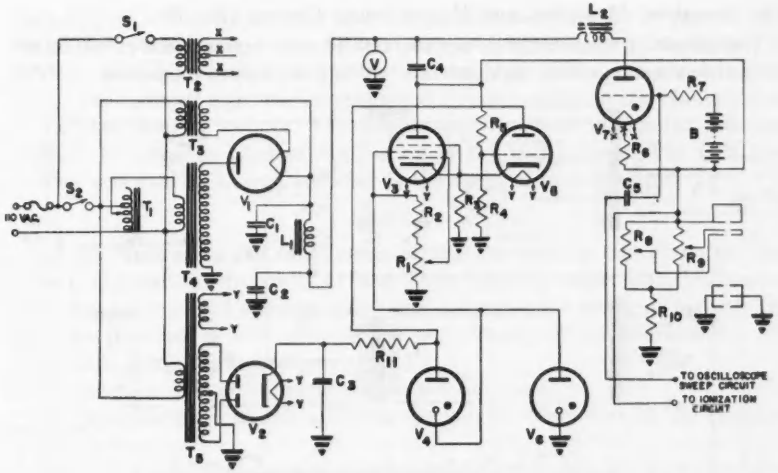

FIG. 7. Saw-tooth acceleration.

C_1, C_2 4 μf. 2000 v.; C_3 10 μf. 450 v.; C_4 0.02 μf. 2000 v.; C_5 0.0025 μf. 2000 v.; R_1 20 kΩ 2 w. pot.; R_2, R_7 100 kΩ 1 w.; R_3 3.5 kΩ 10 w.; R_4 50 kΩ 1 w.; R_5 6 × 2 megs 2 w.; R_6 500 Ω 10 w.; R_8, R_9 1 meg 2 w. pot.; R_{10} 2 megs 4 w.; R_{11} 2.5 kΩ 1 w.; T_1 variac G.R. 200B 1.5 amp.; T_2 2.5 v. 10 amp.; T_3 2.5 v. 5 amp.; T_4 2000 v. 10 ma.; T_5 325–0–325 v. 50 ma. 6.3 v. 4 amp.; L_1 30 h. 20 ma. insulated at 2000 v.; L_2 0.35 h. 10 Ω d-c. insulated at 3000 v.; V_1 2X2; V_2 6X5; V_3 802; V_4, V_6 0D3; V_5 6J5; V_7 5557; B battery 13 v.

adjustable sweep voltage generator slave-driven from the oscilloscope gate circuit. A condenser, C_4, is charged through a high voltage pentode, V_3, whose curves are linearized by feed-back through V_5. The condenser is discharged through a mercury thyratron, V_7, when a positive pulse of sufficient amplitude is applied to the grid. The high voltage operating point is adjusted by changing the power supply voltage by variac T_1. An instant after the thyratron fires, both sides of the condenser are at the same high voltage. The current passing through the constant current generator V_3 lowers linearly with time the voltage of the plate of C_4 connected to V_3. Since the oscilloscope sweep controls the instant of condenser discharge or sweep frequency, a change in the charging current is effected by adjusting R_1 which controls the sweep amplitude. With the given constants, the d-c. high voltage operating point is adjustable from 2000 to 100 v., the sweep amplitude voltage from 1800 to 50 v., and the frequency from 50 to 500 cycles.

The draw-out potential and the focusing on the geometrical limitation slit are adjusted by varying R_8 and R_9 together, and varied independently, they serve to deflect the beam from right to left to give greater luminosity. A disadvantage of this system is that the draw-out potential varies with the accelerating voltage, producing a decrease in peak intensity of the high masses caused by a reduction in the draw-out potential at the lower accelerating voltages. By calibration this disadvantage is obviated. A constant voltage draw-out could have been provided by the use of another slit connected to the ionization source.

The Ionization, Multiplier, and Magnet Source Circuits (Fig. 8)

The remaining circuits are power sources. The multiplier and d-c. ionization potential were regulated against line voltage variation to permit faithful

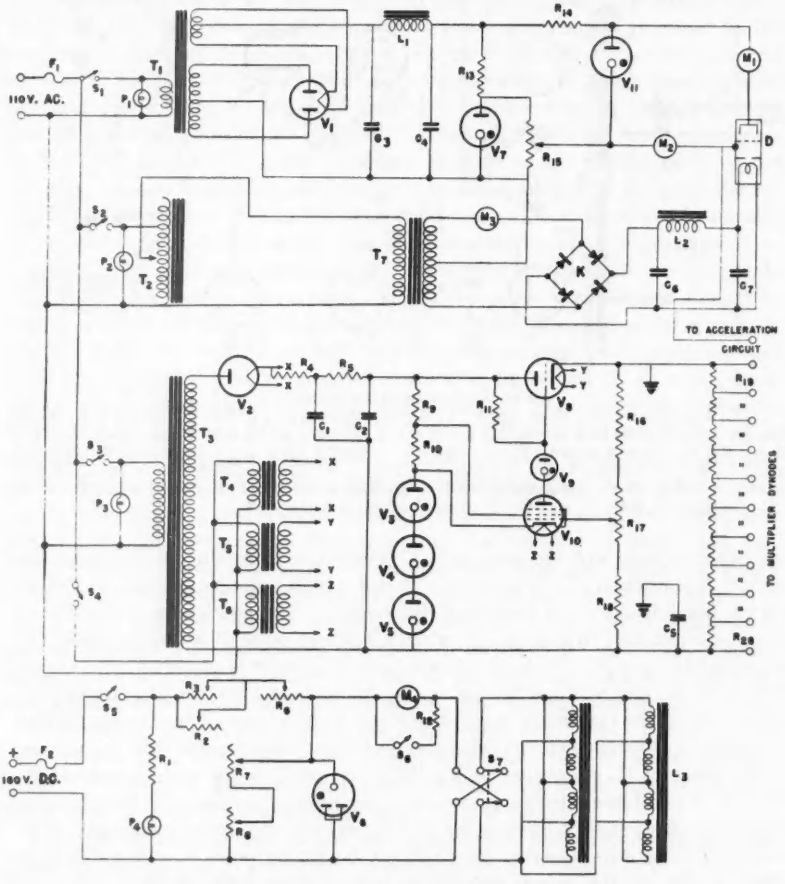

FIG. 8. Ionization multiplier and magnet source circuits.

R_1 3000 Ω 10 w.; R_2, R_3 22 Ω 4.5 amp.; R_4 20 kΩ 10 w.; R_5 50 kΩ 10 w.; R_6 190 Ω 1.5 amp.; R_7 8 Ω 10 amp. carbon; R_8 45 Ω 3.1 amp.; R_9 400 kΩ 30 w.; R_{10} 100 kΩ 8 w.; R_{11} 1 meg 5 w.; R_{12} ammeter shunt 15 amp.; R_{13} 10 kΩ 30 w.; R_{14} 50 kΩ 10 w.; R_{15} 10 kΩ 4 w. pot.; R_{16} 7 × 500 kΩ 2 w.; R_{17} 300 kΩ 2 w. pot.; R_{18} 1 meg 2 w.; R_{19}–R_{28} 400 kΩ 1 w.

C_1, C_2 1.5 μf. 4000 v.; C_3, C_4 8 μf. 600 v.; C_5 1.5 μf. 4000 v.; C_6 2000 μf. 25 v.; C_7 2000 μf. 25 v.

T_1 300–0–300 v. 40 ma. 5 v. 3 amp. insulated at 2000 v.; T_2 variac GR 200B 1.5 amp.; T_3 4000 v. 10 ma.; T_4 2.5 v. 3 amp.; T_5 6.3 v. 2 amp.; T_6 6.3 v. 2 amp. insulated at 4000 v.; T_7 12 v. 10 amp.

L_1 30 h. insulated at 2000 v.; L_2 50 mh. 0.45 Ω d-c.; L_3 magnet coil 2500 turns per section.

V_1 5Y4; V_2 2X2; V_3, V_4, V_5 0D3/VR 150; V_6 0Z2; V_7 0C3/VR 105; V_8 6L6 G; V_9 30 × 1/25 w. neon; V_{10} 6SH7; V_{11} 5651.

D ionization chamber; S_1, S_2, S_3, S_4, S_5, S_6 SPST switch; S_7 DPDT switch.; M_1 0–250 μa. d-c.; M_2 0–1 ma. d-c.; M_3 0–10 amp. d-c.; M_4 0–1.5 amp. d-c.; P_1, P_2, P_3, P_4 6 w. 110 v. pilot lamp; F_1 fuse 5 amp.; F_2 fuse 20 amp.; K selenium rectifier 115 v. 10 amp.

reproduction of voltage settings and spectroscope sensitivity. To permit the use of a standard tube in the 3000 v. supply for the electron multiplier, a series of neon lamps were used to reduce the plate voltage to a reasonable value. The reduced gain was compensated by an increase in the ohmic value of the plate loading resistor. The magnet supply circuit eliminated induced voltages by allowing gradual diminution of the coil current. The OZ4 gas rectifier was used as a surge adsorber in the event of power failure.

RESULTS

Results illustrating the functioning of the spectroscope are given in this section. Detailed kinetic study of cool flame reactions made with this instrument will be reported subsequently. The following are essential features of mass spectroscopic records showing the performance of the instrument:

(1) Sufficient peak separation;

(2) Duration of stability greater than reaction time;

(3) Response time of the spectroscope shorter than that of the motion picture camera.

No attempt was made to attain the theoretical resolution of 65. However, the spectra of ether–oxygen mixtures show that the resolution attained was approximately 55. By more accurate adjustment of the exit and inlet slits in parallel to one another, theoretical resolution could have been obtained. In stability tests no peak variations were observed during an interval of some seconds other than those caused by the small change in reaction vessel pressure. It is difficult to devise a test other than a flame to verify the resolving time of the mass spectroscope. Sudden introduction of gas into the reaction vessel is limited by the mechanical inertia of the inlet stopcock and the damping action of the inlet tubings to a sharp pressure pulse. Notwithstanding these limitations, recordings of pressure-rise curves were made. A sample pressure-rise curve for an equimolecular ether–oxygen mixture is reproduced in Fig. 9 (photographed

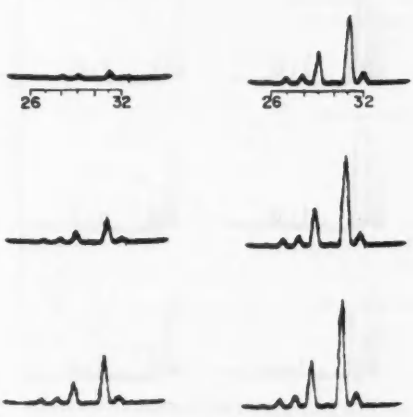

FIG. 9. Effect of a sudden introduction of gas into the reaction vessel.

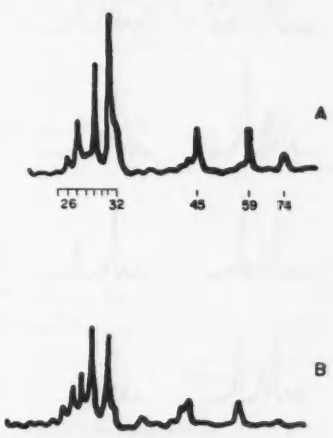

FIG. 10. Passage of a flame in front of the orifice.

at 16 images per second) and it can be seen that in this case gas inlet was accomplished within one quarter of a second. The passage of a travelling flame in front of the microscope orifice illustrates more clearly the high response speed of the system. After the introduction of the gas in the experiment recorded in Fig. 10, all photographs preceding Image A are entirely similar to Image A and those subsequent to Image B are similar to Image B. This can be explained by the passage of a fast travelling flame in front of the orifice between Images A and B. An equimolecular ether–oxygen mixture at an approximate pressure of 100 mm. of mercury served as fuel. The reaction vessel temperature was beyond 220°C. and the ionization voltage was 20 v. This verifies the complete independence of two successive images taken at that particular camera speed (16 images per second). No further experiments of this nature were carried out, since in theory the only memory effect is that produced by gas stagnation in the source chamber resulting in simultaneous measurement of this gas and the gas in the expansion cone. However, the gas stream from the orifice creates a definite positive pressure in the gas expansion cone which should sweep away the stagnant gas. In theory, the molecules leaving the reaction vessel at different times could be ionized at the same in-

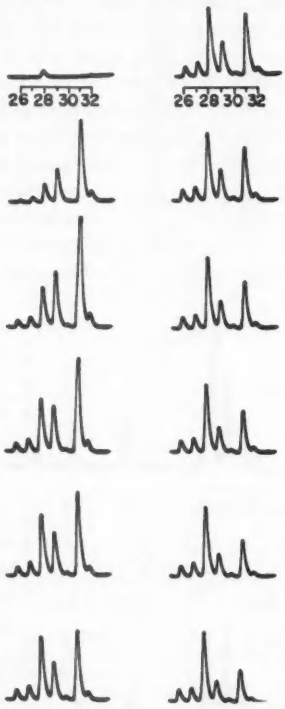

FIG. 11. Mass spectra of a 'slow' cool flame.

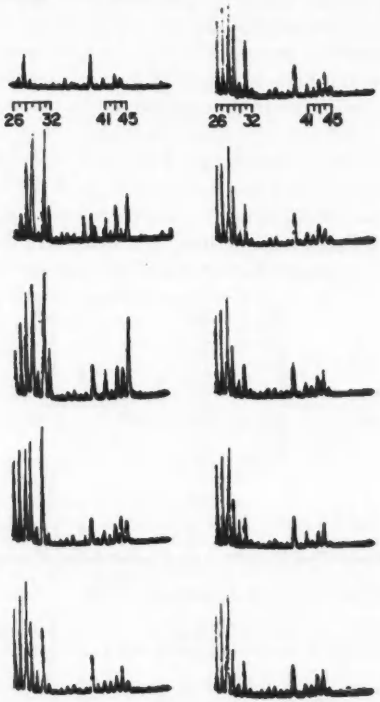

FIG. 12. Varying mass spectra of a 'rapid' cool flame.

stant by the electron stream and thus limit the response time. Since the gas exits from the orifice at near sonic velocities and the maximum diameter of the electron stream is less than one centimeter, this effect should only be noticeable at approximately 0.1 μsec. It is therefore believed that the time response of the source is sufficiently great that every peak is independent.

To illustrate its function as a kinetic investigation apparatus for gaseous reactions, two cool flame spectra are recorded in Figs. 11 and 12. The spectra reproduced in Fig. 11 are at 2 images per second. The capacity distortion, which is apparent, was due to a cathode follower input which was later replaced by the preamplifier whose excellent response is apparent in Fig. 9. The spectra reproduced in Fig. 12 are at 4 images per second. The temperature was approximately 215°C. These are for cool flames of equimolecular mixtures of ether–oxygen under 50 mm. of mercury pressures. Ether has been chosen as the fuel in this investigation because its cool flame is produced at relatively low temperatures and pressures. Figs. 13 and 14 show the relative variation of some of the peak heights during these cool flames. Figs. 11 and 13 represent a three second reaction, Figs. 12 and 14 a one-half second reaction. The higher peaks are undoubtedly caused by products and reactants. The peaks of the intermediate chemical species would be lower because of their short life and consequent low concentration. These peaks would present a time pulse initially of zero height, rising during a rapid change of reactants and products and then returning to zero. The peaks of the reactants and products of a dynamic cool flame of an equimolecular mixture of diethyl ether and oxygen, as reported in the literature (26, 17), are indicated in Table I. Although the ionization voltage was kept low in these flames in order to enhance the recording of

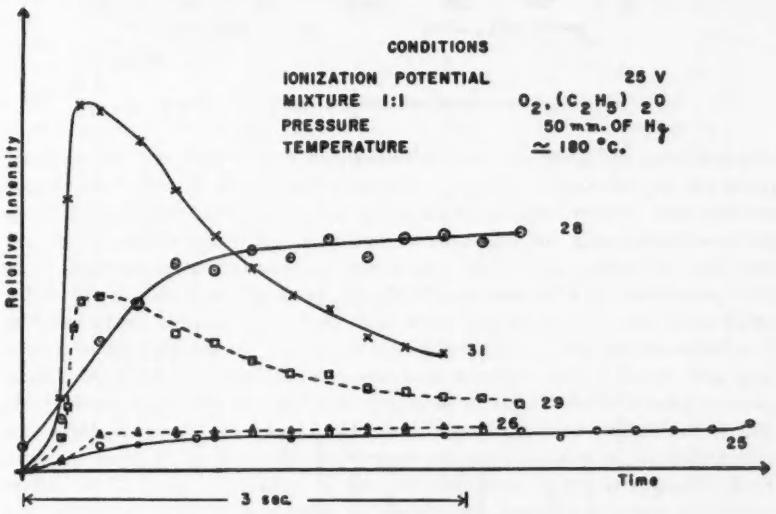

FIG. 13. Peak variations during a 'slow' cool flame.

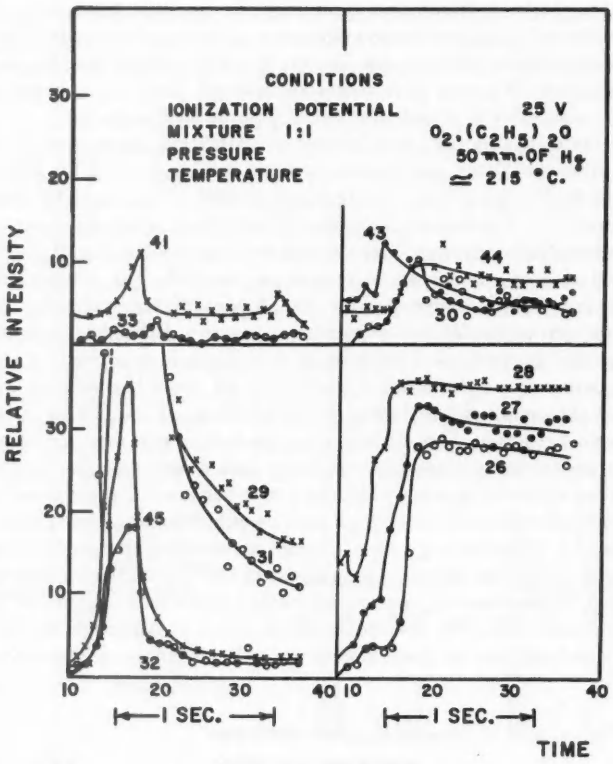

FIG. 14. Peak variations during a 'rapid' cool flame.

intermediates and although the multiplier and source were not linear, some peaks can be tentatively identified from the table. Peaks 45 and 31 are almost entirely due to ether while peak 32 is due to oxygen. The variation of these peaks indicates that the reactants rushed into the hot reaction vessel and decreased uniformly but did not reach zero as the reaction progressed. Peak 43 is attributed to ether and acetaldehyde, peak 44 to acetaldehyde and a small amount of carbon dioxide. Since peak 46 does not appear on the records, it is believed that very little formic acid is present. In the absence of formic acid and ethane in the reported analyses, peak 30 has been assigned principally to formaldehyde. It can be seen that after the formation of formaldehyde and acetaldehyde at the maximum rates of change of the reactants, these two compounds act as reactants and decrease eventually to a stable concentration. Peak 29 is due to ether, acetaldehyde, and formaldehyde; peak 28 to carbon monoxide, residual nitrogen, formaldehyde, some acetaldehyde and ethylene; peaks 27 and 26 to ether, acetaldehyde, ethylene, and acetylene; and peak

TABLE I

CONCENTRATION (26) AND MAJOR PEAKS (16) OF COOL FLAME REACTANTS AND PRODUCTS

		Concentration, %		Major mass spectrometer peaks, %															Relative sensitivity n-butane
		Reactants	Products	25	26	27	28	29	30	31	32	42	43	44	45	46	59	60	74	
Ether		50	22	—	3.1	17.7	6.1	39.5	1.8	100	1.0	1.3	6.9	3.5	37.5	—	46.9	—	30.4	65.0
Oxygen		50	10	—	—	—	—	—	—	—	100	—	—	—	—	—	—	—	—	—
Water		—	22	—	—	—	—	—	—	—	—	—	—	—	—	—	—	—	—	—
Carbon monoxide		—	11.5	—	—	—	100	1.2	—	—	—	—	—	—	—	—	—	—	—	80.3
Acetaldehyde		—	11.0	—	5.6	3.5	9.0	100	—	—	—	14.9	50.0	88.2	—	—	—	—	—	65.0
Formaldehyde		—	6.6	—	—	—	30.0	100	88.5	1.9	—	—	—	—	—	—	—	—	—	140
Hydrogen		—	5.7	—	—	—	—	—	—	—	—	—	—	—	—	—	—	—	—	—
Non-saturated hydrocarbons	C_2H_4	—	3.6	11.7	62.3	64.8	100	2.2	—	—	—	—	—	—	—	—	—	—	—	39.9
	C_2H_2			20.1	100	52.8	—	—	—	—	—	—	—	—	—	—	—	—	—	49.4
Peroxides		—	2.7	—	—	—	—	—	—	—	—	—	—	—	—	—	—	—	—	—
Carbon dioxide		—	1.5	—	—	—	8.17	—	—	—	—	—	—	100	—	—	—	—	—	64.4
Acids	HCOOH	—	1.3	—	—	—	17.2	100	1.7	—	—	—	—	9.97	47.6	60.6	—	—	—	40.64
	CH_3COOH	—		1.75	7.16	—	28.8	15.6	1.0	8.51	—	28.2	100	34.5	98.1	—	—	100	—	65.0

25 to ethylene and acetylene. The constant level of peaks 26 and 27 compared with peak 44 and with the curve of the ether peaks leads to the tentative conclusion that considerable unsaturated hydrocarbons are formed during the reaction. Peaks 41 and 33 seem to indicate the presence of intermediates or free radicals. Other free radicals may be present but are masked by the superimposition of peaks from stable compounds. Sufficient data are not yet available to provide more definite conclusions.

The apparatus has proved wholly satisfactory for kinetic studies of fast gaseous reactions. Its range could be considerably increased by the use of a larger capacity pump in the source and correspondingly higher pressures up to one atmosphere in the reaction vessel. No difficulty is anticipated with the quartz cone since the thin membrane is spherical and small (pinhead size) and the eggshell principle applies, permitting higher pressures. A few cones constructed and used in the spectroscope were submitted to atmospheric pressure without deterioration. For much faster reactions, a spectroscope remaining stationary on one peak and giving high speed response should provide measurements to the microsecond range. It is hoped that by means of this mass spectroscopic technique it will be possible to elucidate the kinetics of rapid oxidations which have proved somewhat elusive with former methods.

ACKNOWLEDGMENTS

The author wishes to acknowledge the advice and helpful suggestions of his research director, Dr. Cyrias Ouellet. Appreciation is also expressed to Defence Research Board for Grant 129 and to Canadian Armament Research and Development Establishment for permission to complete this work after the author entered their employ.

Appreciation is also extended to Jean Lafaivre for the design of a low impedance liquid air trap and to L. P. Blanchard for the measurements on cool flames used in this report.

The helpful suggestions of Drs. Larkin Kerwin, C. Geoffrion, E. M. Clark, F. P. Lossing, P. A. Giguère, and Hin Lew are also gratefully acknowledged.

REFERENCES

1. Cook-Yarborough, E. H. and Russel, M. C. B. J. Sci. Instr. 30: 474. 1953.
2. Dushman, S. Scientific foundations of vacuum technique. John Wiley & Sons, Inc., New York. 1949. p. 93.
3. Dushman, S. Scientific foundations of vacuum technique. John Wiley & Sons, Inc., New York. 1949. p. 372.
4. Eltenton, G. C. J. Chem. Phys. 15: 455. 1947.
5. Ezoe, H. J. Sci. Research Inst. (Tokyo), 47: 1311. 1953.
6. Geoffrion, C. Rev. Sci. Instr. 23: 224. 1952.
7. Guthrie, A. and Wakerling, R. K. (*Editors.*) Vacuum equipment and techniques. McGraw-Hill Book Company, Inc., New York. 1949. p. 16.
8. Guthrie, A. and Wakerling, R. K. (*Editors.*) Vacuum equipment and techniques. McGraw-Hill Book Company, Inc., New York. 1949. p. 208.
9. Kerwin, L. Rev. Sci. Instr. 20: 36. 1949; 21: 96. 1950.
10. Leger, E. Can. J. Technol. 32: 199. 1954.
11. Leger, E. and Ouellet, C. J. Chem. Phys. 21: 1310. 1953.
12. Leland, W. T. Phys. Rev. 77: 634. 1950.
13. Lew, H. Phys. Rev. 76: 1087. 1949.
14. Lossing, F. P. and Tickner, A. W. J. Chem. Phys. 20: 907. 1952.
15. Moody, N. F. Rev. Sci. Instr. 22: 236. 1951.

16. National Bureau of Standards in co-operation with American Institute of Petroleum. Tables of mass spectrometric data. Washington, 1953.
17. NIER, A. O. Rev. Sci. Instr. 18: 398. 1947.
18. NIER, A. O. and WINN, E. B. Rev. Sci. Instr. 20: 773. 1949.
19. OSBORNE, F. J. F. Can. J. Phys. 30: 658. 1952.
20. OUELLET, L., LEGER, E., and OUELLET, C. J. Chem. Phys. 18: 383. 1950.
21. PHILBERT, G. and VALENTIN, R. J. phys. radium, 13: 50A. 1952.
22. PLOCH, W. and WALCHER, W. Rev. Sci. Instr. 22: 1028. 1951.
23. ROBERTSON, A. J. B. Trans. Faraday Soc. 48: 228. 1952.
24. SIRI, W. Rev. Sci. Instr. 18: 540. 1947.
25. TOWNEND, D. T. A. Chem. Revs. 21: 259. 1937.
26. TOWNEND, D. T. A. and MACCORMAC, M. J. Chem. Soc. 143, 151. 1940.

MEASUREMENTS OF SPECTRAL AND ANGULAR DISTRIBUTIONS OF SECONDARY GAMMA-RAYS IN MATTER[1]

By G. N. Whyte

ABSTRACT

The distribution in energy and angle of the secondary gamma radiation emerging from the face of a concrete barrier containing a point source of cobalt-60 has been measured as a function of barrier thickness. Results on energy spectra and angular distributions are presented, and some of their features are compared with theoretical predictions. The operation of the two-crystal spectrometer and the photographic system for recording pulse-height distributions are described in some detail.

INTRODUCTION

Nature of the Problem

When a point source of monoenergetic gamma radiation is imbedded in a homogeneous medium, it gives rise to a complex distribution of primary and secondary radiation throughout the medium.

The distribution of the primary radiation is straightforward: if the origin of coordinates is taken at the source, the primary radiation at the point $\mathbf{r}$ is in the direction $\mathbf{r}$ and its intensity is proportional to $\exp(-\mu_0 r)/r^2$, μ_0 being the total absorption coefficient at the primary quantum energy. Compton and pair-production interactions of the primaries with the atoms of the medium result in secondary gamma-rays of reduced energy and altered direction. These in turn can be absorbed and scattered with a different probability from that of the primaries. The result for an arbitrary source function is a distribution $I(\mathbf{r}, h\nu, \mathbf{\Omega})$ which might be called the differential energy and angle distribution of the secondary gamma-ray intensity.[2] $I(\mathbf{r}, h\nu, \mathbf{\Omega})\, d(h\nu)\, d\Omega$ is the energy in the form of quanta in the energy interval $d(h\nu)$ at $h\nu$ and in the element of solid angle $d\Omega$ at $\mathbf{\Omega}$ crossing a square centimeter normal to $\mathbf{\Omega}$ per second at the position $\mathbf{r}$ in the medium.

In the case of a point isotropic source the dependence on position reduces to a dependence on the distance from the source, r, and the angular dependence involves only the angle θ between the direction of the gamma-ray and $\mathbf{r}$. Thus for a point isotropic source the intensity can be written $I(r, h\nu, \theta)$. A complete description of the gamma-ray distribution then consists of a specification of the energy spectrum as a function of the angle θ for any value of r.

By integrating over one or more of the independent variables, one may obtain other quantities of interest. Thus integration over θ yields the function $I_0(r, h\nu)$, the "omnidirectional" energy spectrum at the distance r; this is the quantity measured by an isotropic detector that can distinguish quantum energies, such as a single scintillation crystal. Integration instead over $h\nu$ gives $I_A(r, \theta)$, the total intensity of all energies as a function of angle. And

[1]*Manuscript received October 18, 1954.*
Contribution from the Division of Physics, National Research Council, Ottawa, Ontario. Issued as N.R.C. No. 3503.

[2]*These definitions are based on the much more complete discussion given in Reference (2).*

integration over both θ and $h\nu$ gives the total omnidirectional intensity $I_T(r)$, as measured approximately by an ordinary air-wall ionization chamber.

Previous Measurements

A number of measurements of some of the integrated quantities defined above have been made in the last few years. Measurements of broad-beam attenuations and build-up factors are essentially determinations of I_T; several such experiments have been listed by Garrett and Whyte (1). Hayward (3) has measured the omnidirectional secondary *electron* spectrum from cobalt-60 gamma-rays in water with an anthracene crystal. This electron spectrum can be calculated from a knowledge of I_θ, and such a calculation, based on values of I_θ derived theoretically by Spencer and Fano (6), yields results agreeing well with the experiment. Weiss and Bernstein (7) measured the low-energy portion of the spectrum, I_θ, due to cobalt-60 gamma-rays in water directly, using a single sodium-iodide crystal. Again the agreement with theory was satisfactory.

To date no work seems to have been done on the complete differential energy and angle spectrum, I.

Experimental Approach

In the experiments described here a gamma-ray spectrometer was used to measure the differential energy spectrum as a function of angle at a number of different distances from a cobalt-60 source imbedded in concrete. Since it was not possible to have the spectrometer imbedded in the concrete as well as the source, the actual spectra observed were those emerging from a plane boundary of the medium. This restricted the angle, θ, at which measurements could be made to values less than 90°. The spectrum emerging from the face of the barrier differs from what would be present at the same point in an infinite medium only in the absence of those gamma-rays which would otherwise have back-scattered twice or more across the plane of the barrier surface, first back toward the source and then away from it again. These backscattered rays would almost all have energies well below 0.3 Mev., so that the spectrum emerging from the barrier above this energy should be the same as would be present in an infinite medium.

APPARATUS

The apparatus consisted of a cobalt-60 source imbedded in a concrete barrier, and a gamma-ray spectrometer. (Fig. 1.)

Sources

In order to provide usable counting rates over the range of barrier thickness studied, four different cobalt-60 sources were used; their approximate strengths were 0.5, 1, 40, and 700 curies.

Barrier

The source to be used was placed in a hole in a concrete block centered in a wall of similar blocks (dimensions 30 × 20 × 10 cm., density 2.37 gm./cm.^{3}) built to a height of 150 cm. and a width of 200 cm. The piled blocks were backed

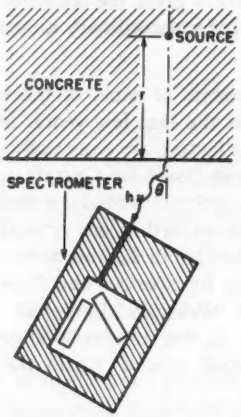

FIG. 1. Experimental arrangement.

by a 50-cm. thick wall of solid concrete, so that the source was surrounded in all but the forward direction by an effectively infinite scattering medium. The depth of the source within this "semi-infinite" medium could be varied by piling further layers of blocks up the front face. Successive layers were staggered horizontally and vertically so as to prevent the cracks between the blocks from lining up.

The exact atomic composition of the concrete was not determined. Since the element of highest atomic number present in any quantity was calcium ($Z = 20$), the photoelectric cross-section for the primary radiation was completely negligible; at these energies the medium acted as a pure Compton scatterer. In fact photoelectric absorption should only affect the energy spectrum below about 0.3 Mev., and since the behavior of the spectrometer was not considered to be reliable below this energy, the exact composition of the medium was not significant. (The situation is different where build-up factors are being considered, since even the lowest-energy portion of the spectrum contributes to the total build-up.)

Spectrometer

The energy spectrum of the gamma radiation emerging from the barrier was measured with a two-crystal scintillation spectrometer of the type first proposed by Hofstadter and McIntyre (4). The advantage of this instrument for the present work is that, for monoenergetic gamma-rays, it gives a pulse-height distribution in the form of a simple peak rather than the familiar photo-peak-plus-Compton distribution of a single sodium-iodide crystal. Consequently the shape of the pulse-height distribution due to a continuous gamma-ray spectrum of the type encountered here can be simply related to the shape of the spectrum itself.

The general arrangement of the spectrometer is shown in Fig. 2. The in-

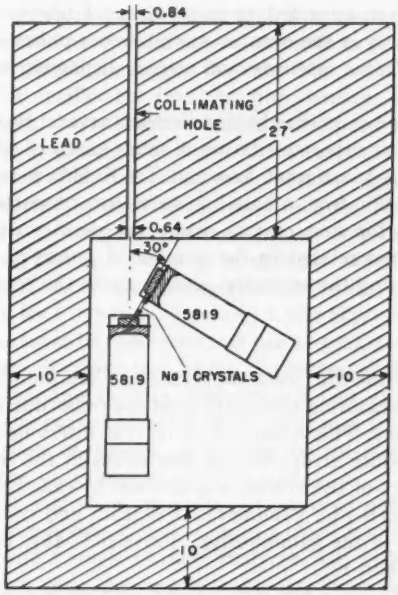

FIG. 2. Scintillation spectrometer.

coming beam of gamma radiation was first collimated to a half-angle of 1.6° by a slightly conical hole in the lead shield at the front of the instrument and then allowed to strike the center of a sodium-iodide crystal, ½ in. thick by 1 in. in diameter, coupled to an RCA 5819 photomultiplier tube. A second sodium iodide crystal, ½ in. thick by 1½ in. in diameter, was located as shown in Fig. 2, with its center 5.9 cm. from the center of the first crystal. This second crystal detected gamma-rays that had scattered back through an angle of roughly 150° from the first crystal, imparting most of their energies to Compton electrons in the first crystal. The energies of these Compton electrons, and hence the sizes of the resulting pulses from the first photomultiplier, bore a fixed relation to the energies of the incident gamma-rays, determined by the Compton scattering formula. Thus, by examining only those pulses from the first crystal that were accompanied by pulses in the second, one could determine the energies of the incident gamma-rays.

Pulse Selection and Recording

The arrangement for selecting these pulses was fairly simple. The pulses from the first crystal were passed through a preamplifier and linear amplifier and then applied to the vertical-deflecting plates of a Tektronix 511A oscilloscope—without, however, triggering the sweep. At the same time the outputs of both photomultipliers were fed into a two-channel coincidence circuit, and

the coincidence pulses were fed to the "external trigger" terminal of the oscilloscope. Thus, only in the event of simultaneous pulses in the two crystals did the oscilloscope trace intensify and sweep, displaying the pulse from the first crystal.

In order to obtain a pulse-height distribution, several thousand such pulses were photographed in superposition on a single piece of film. (A Wollensak 75-mm. f/1.9 Oscillo-Anastigmat lens and Tri-X film were used.) Distances along the developed film from a base line were then proportional to Compton-electron energies in the first crystal, while the density at a given distance from the base line was related to the number of pulses of the corresponding energy occurring during the exposure, and hence to the counting rate at that energy.

Calibration

Displacements on the film were converted to Compton-electron energies in the first crystal by measuring the positions of the peaks due to the two primary cobalt-60 gamma-rays. This was done at regular intervals during the experiment in order to reduce errors due to slow drifts in the over-all gain of the system. The linearity of the system was checked by examining the positions of the peaks in the Ra(B+C) gamma-ray spectrum and comparing them with the known energies of the gamma-rays. Above 0.3 Mev. the deviations from linearity were less than 1%.

The relationship between film density and number of pulses was established for each box of film by exposing successive portions of one film from each box to successively greater numbers of sweeps on the oscilloscope screen, the number of sweeps being determined exactly by a scaler. The procedure was to set the vertical position of the trace on the screen so that its image fell near the top of the film. The first crystal was then exposed to some of the radiation from the barrier and the resulting pulses were fed through the linear amplifier to an integral discriminator, which was set to give an output rate of, say, 150 counts per hour. This output was used to trigger the oscilloscope sweep with pulses occurring at the desired average rate but distributed randomly in time to simulate actual operating conditions. At the same time the vertical position of the trace was varied slowly over a range of a few millimeters by applying a saw-tooth voltage to the vertical-deflecting plates. (The sweep output of a second oscilloscope provided a convenient signal for this purpose.) In this way the traces were made to occur randomly over a narrow band of film, in further imitation of the experimental conditions.

The film was exposed for an hour, then the trace position was shifted vertically, the pulse rate was increased by a factor of two or three, and a second exposure was made, and so on. The result on the film was a series of bands of different densities, corresponding to different known numbers of pulses. The film was finally cut into strips at right angles to the exposed bands, and whenever a film from the same box was to be developed, one of these strips was developed along with it and used to provide a calibration curve. Thus differences in the age and temperature of the developer from film to film were taken into account.

One further point must be considered in this connection. For the long exposure times involved here (from several minutes to several hours) the reciprocity law does not hold: the longer the time over which a given number of pulses is spread, the smaller the resulting film density. Thus the calibration curves obtained from the calibration strips, which were based on one-hour exposures, had to be modified according to the actual duration of the exposure. This necessitated a set of correction curves, made by exposing a film to a fixed number of pulses spread over different times ranging from a few minutes to several hours and repeating the process for several different numbers of pulses. The resulting curves of density vs. exposure time for fixed number of pulses were then used to correct the experimental calibration curves (number of pulses vs. density for a one-hour exposure) to the appropriate exposure time. An idea of the importance of this correction can be gathered from the fact that a typical film density obtained in a 24-hr. run corresponded to roughly twice as many pulses as the same density obtained in a 1-hr. run.

With the aid of the corrected calibration curve and the energy calibration mentioned earlier, plots of density vs. position on the film were converted to plots of counting rate vs. Compton-electron energy.

The photographic system of pulse-height analysis outlined above allows one to measure a pulse-height distribution in a small fraction of the time that would be required with a single-channel analyzer, and with less distortion due to drift. At the same time the cost is much less than that of an electronic multichannel analyzer to do the same job. The chief disadvantage lies in the inferior accuracy of the photographic method. Variations in film sensitivity, non-uniform development, and changes in beam intensity in the cathode-ray tube can all introduce error. Comparisons of the same spectrum analyzed by the photographic method and with a single-channel pulse-height analyzer showed the accuracy of the former to be about $\pm 10\%$. (This applies, of course, to the *counting-rates* in the spectrum; measurements of the energies of peaks are accurate to about 1%.)

Efficiency of the Spectrometer

In order to convert a pulse-height distribution from the spectrometer to a gamma-ray intensity distribution, it is necessary to know the efficiency of the spectrometer as a function of quantum energy.

The efficiency is proportional to the quantity

$$\epsilon = P_1 P_2$$

where P_1 is the probability of an incoming gamma-ray scattering in the first crystal in the direction of the second crystal and then escaping from the first crystal, and P_2 is the probability of its being detected in the second crystal. To a fair degree of approximation these probabilities are given by

$$P_1 = \int_0^d \exp[-(\tau+\kappa)x]\, N_e\, dx\, k(150°)\, d\Omega \exp(-\mu' x/\cos 30°)\,,$$

$$P_2 = \frac{1}{R}\int_0^R [1-\exp(-2\mu'\sqrt{R^2-y^2})]\, dy$$

where d = thickness of first crystal,
x = depth inside front face of first crystal,
τ, κ = photoelectric and pair-production coefficients for primary gamma-rays in sodium iodide,
$k(150°)d\Omega$ = probability per electron of Compton scattering into the solid angle $d\Omega$ at 150°, as given by the Klein-Nishina formula,
N_e = electron density in sodium iodide,
μ' = total absorption coefficient for backscattered ray in sodium iodide,
R = radius of second crystal,
y = distance from central axis of second crystal.

The quantity $\tau+\kappa$ is used rather than the total absorption coefficient μ because a gamma-ray scattered in any direction in the first crystal is still available for scattering into the second crystal. In fact such a ray has a somewhat higher probability of being scattered into the second crystal, so that $\tau+\kappa$ is, if anything, a bit high. Of course, the pulse size produced by a gamma-ray scattering through a net angle of 150° in two or more interactions is not quite the same as that produced by a single scatter through 150°, but the size is comparable and will contribute to the same region of the pulse-height distribution.

A plot of the relative efficiency of the spectrometer as a function of incident quantum energy, calculated with the aid of the above equations, is presented in Fig. 3. It differs somewhat from that found by Maienschein (5) for a similar spectrometer, mainly because of differences in the sizes and shapes of the crystals used. The fall-off toward high energies is due to the decreasing probability of scattering in the first crystal, whereas the decline at low energies is due to the increasing fraction of the backscattered rays that fail to escape from the crystal.

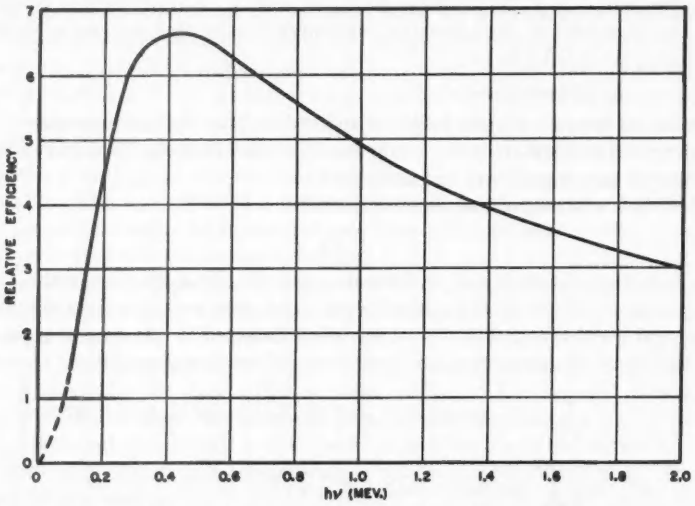

FIG. 3. Efficiency of spectrometer as a function of gamma-ray energy.

Determination of Gamma-ray Intensity Spectrum

The Compton-electron energies in the first crystal were converted to the corresponding gamma-ray energies by means of the relation

$$E = \frac{a\gamma}{1+a\gamma} \cdot h\nu$$

where $h\nu$ = gamma-ray energy,
E = energy of Compton electron associated with a coincidence in the spectrometer,
$a = 1-\cos 150°$,
$\gamma = h\nu/mc^2$.

When plotted in terms of $h\nu$ rather than E, the counting rates must be multiplied by the factor $dE/d(h\nu)$, given by

$$dE/d(h\nu) = a\gamma(a\gamma+2)/(a\gamma+1)^2.$$

Further, since it is the gamma-ray *intensities* that are of interest, the counting rates must be multiplied by the corresponding quantum energy, $h\nu$.

Performance of Spectrometer

The intensity spectrum from a small cobalt-60 source, as measured with the spectrometer, is shown in Fig. 4. The resolution of about 12% at 1.2 Mev. is

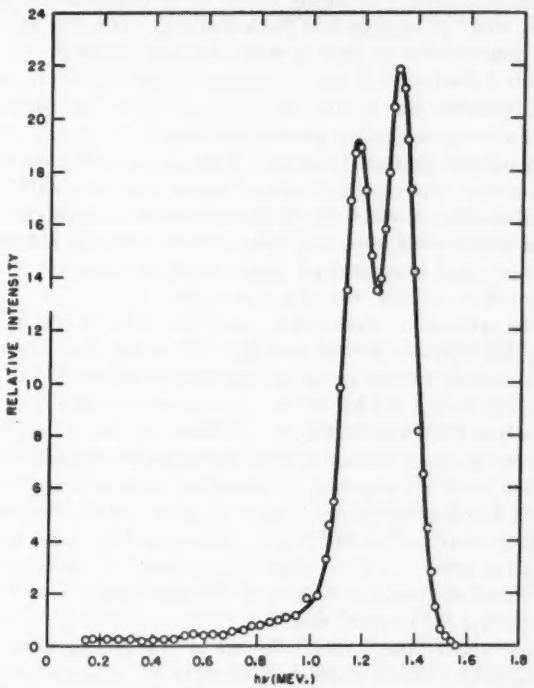

FIG. 4. Intensity spectrum of the gamma radiation from a cobalt-60 source, as measured by the spectrometer.

adequate for the continuous spectra to be examined. (Of this 12%, 8% is due to the well-known statistical variation in the number of light quanta detected by the first photomultiplier, and 4% is due to the finite range of angles around 150° at which backscattered gamma-rays can cause coincidences, as a result of the finite size of the second crystal.)

The continuous low-energy "tail" on the spectrum seems to be characteristic of spectrometers of this type; attempts to reduce it below the size shown in Fig. 4 were not successful. The possibility that it was due to chance coincidences was ruled out by reducing the resolving time of the coincidence circuit, and the possibility that it was associated with high counting rates in the amplifier was ruled out by reducing those rates. The introduction of appropriate absorbers showed that it was not due to low-energy scattered quanta from the source nor to radiation multiply scattered inside the spectrometer. The possibility that some of the Compton electrons associated with coincidences were losing only a fraction of their full energies within the first crystal was not completely ruled out because of the difficulty of eliminating such an effect, but an attempt to shield the second crystal so that it could "see" only a limited region in the center of the first crystal resulted in no significant reduction in the number of low-energy pulses. And the production of bremsstrahlung in the first crystal is hardly likely to be large enough to account for the observed effect. It may be that the low-energy tail is due to a combination of several different effects, each of which by itself is small.

A few incidental matters may bear mentioning. The 27 cm. of lead on the front of the spectrometer was found to be necessary to cut out the background counting rate due to gamma-rays penetrating directly to the crystals. Additional shielding beyond that used had very little further effect on the residual background of about three counts a minute, which was presumably caused by cosmic rays and natural radioactivity in the lead itself. To eliminate the effects of this residual background, each run was repeated with the collimating hole closed by a 10-cm. lead plug, and the pulse-height distribution obtained was subtracted from that obtained with the hole open.

In some of the preliminary runs it was found that the film was blackened by light from the filament of the cathode-ray tube which was not completely stopped by the coating on the screen of the tube. This effect was eliminated by selecting a tube with a thicker screen coating and by placing over the lens of the camera a blue filter matched to the emission spectrum of the P11 screen.

Another possible cause of unwanted film blackening is the direct action of the gamma radiation itself. By exposing a calibration strip to a controlled dose of radiation it was found that the resulting increase in density depended on the density already present, so that the shape of the calibration curve was changed. Since a dose of the order of 100 mr. can produce a noticeable blackening, care was taken to shield the camera so that the film was exposed to considerably less than this during the longest runs.

As mentioned above, the errors involved in the photographic system of obtaining pulse-height distributions may amount to as much as 10%. Additional sources of error are the calculated efficiency curve of the spectrometer,

drifts in the gain of the photomultipliers and amplifier, and inaccuracies in the aligning and positioning of the instrument. Consequently the measured intensities are not considered to be reliable to better than 20%.

EXPERIMENTAL PROCEDURE

At each barrier thickness the energy spectrum emerging from the point on the barrier face directly opposite the source was measured at angles to the normal to the face of 0°, 10°, 20°, 30°, 45°, and 60°. At each angle the spectrometer was lined up optically with a spot on the barrier, with the front end of the collimator 30 cm. from the spot. (See Fig. 1.) Under these conditions the first crystal "saw" an area around the spot about 3 cm. across; over this region the variation in the gamma-ray distribution was negligible. Measurements at different angles were made, in effect, by swinging the spectrometer about the fixed spot on the barrier face, keeping the distance constant.

The barrier thicknesses and source strengths used are listed in Table I. The relative gamma-ray outputs of the sources (to which the effective contents

TABLE I

BARRIER THICKNESSES AND SOURCE STRENGTHS USED

Barrier thickness (cm.)	Effective source strength (curies)
7.6	0.58
17.9	1.10
38.3	44
48.5	44
69.0	690

are proportional) were checked by comparing the sources, in position in the barrier, with the aid of a Victoreen condenser ionization chamber.

RESULTS AND DISCUSSION

Distribution in Energy and Angle

At each thickness a series of curves of gamma-ray intensity vs. quantum energy for different angles was obtained. A typical set is shown in Fig. 5, where the quantity plotted is $4\pi r^2 I(r, h\nu, \theta)$. The spectrum at 0° is dominated by the high-intensity primary peaks, which obscure the secondary distribution; it has been omitted from Fig. 5.

Since the measurements did not yield absolute values of the intensity, the results were normalized to the theoretical calculations, as described below.

Except at the smallest thicknesses investigated, the distributions at the various thicknesses proved to be sufficiently similar that the differences were masked by the uncertainties in the measurements. This is not surprising, since the secondary radiation is expected on theoretical grounds to approach an equilibrium distribution in the first few mean-free-paths. Fig. 5 thus gives a rough picture of the distribution, apart from a constant factor depending on the distance, at any point beyond about two mean-free-paths from the source.

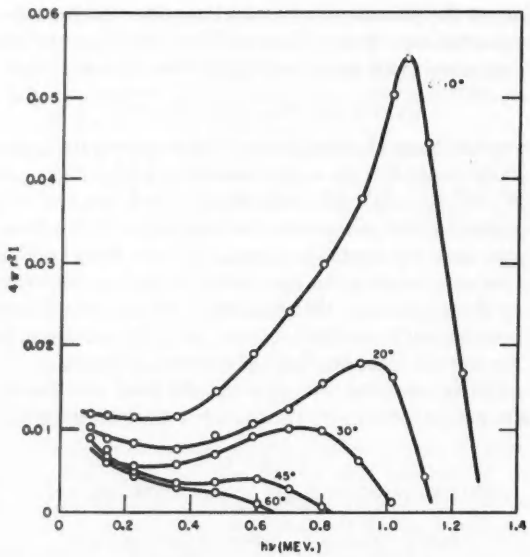

FIG. 5. Differential energy and angle distribution at $\mu_0 r = 6.52$.

Distribution in Energy

The omnidirectional energy spectrum $I_0(r, h\nu)$ at each thickness was obtained by graphical integration over θ of the values of $I(r, h\nu, \theta)$. The results, corrected to the same source strength, are indicated by the points in Fig. 6. The dashed and solid curves are the theoretical distributions for water and iron respectively, interpolated from the calculations of Goldstein and Wilkins (2). As one would expect, the spectra in the two media differ significantly only at low energies; the calculated values for concrete would lie somewhere between the two. The quantity plotted in Fig. 6 is $4\pi r^2 I_0$, where $I_0(r, h\nu)$ is the energy per unit energy interval at $h\nu$ crossing a sphere of cross-sectional area 1 cm.^{2} at the point r from any direction, and refers to a cobalt-60 source undergoing one disintegration per second.

The *relative* positions of the experimental curves were fixed by the experiments, but, as mentioned above, the *absolute* values were not. The array of experimental curves was therefore normalized to agree with theory at one value of the penetration ($\mu_0 r = 6.52$). This procedure seems justified because the absolute positions of the theoretical curves largely determine the theoretical build-up factors, and these have already been checked by experiment for the case of cobalt-60 gamma-rays in water (8) and iron (1).

By working back from the normalization of Fig. 6, it was possible to plot Fig. 5 in terms of absolute intensities as well. Again the values apply to a source undergoing one disintegration per second.

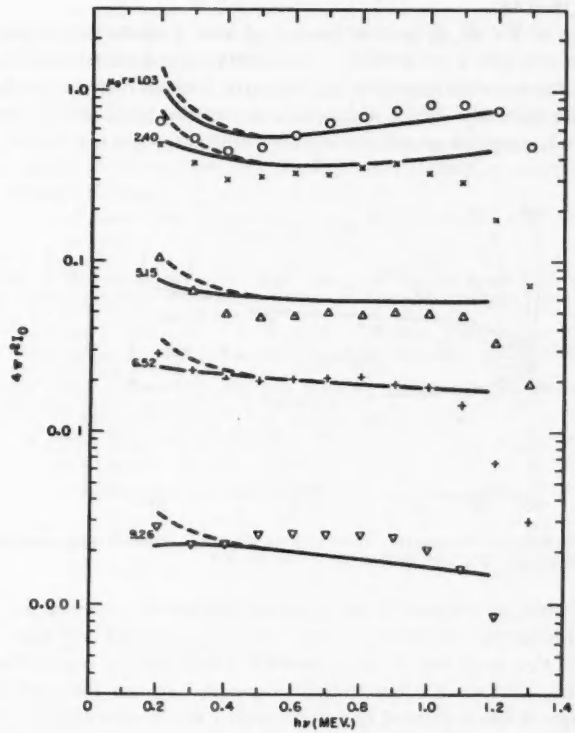

FIG. 6. Omnidirectional energy spectra at different penetrations. The dashed and solid lines are the theoretical distributions in water and iron respectively; the points are the experimental results in concrete.

The agreement between experiment and theory in Fig. 6, while not good, is probably within the accuracy of the measurements. As far as the relative intensities at different penetrations go, the discrepancies appear to be more random than systematic: there is no very marked tendency for experiment and theory to diverge steadily with increasing penetration. Except at the smallest penetration investigated ($\mu_0 r = 1.03$), the general shape of the experimental distribution agrees reasonably well with the theoretical one below 1 Mev. Above this energy the finite resolution of the spectrometer causes a gradual fall-off in the measured intensities, smearing over the sharp drops that must actually be present at 1.17 and 1.33 Mev.

The quite good agreement between the shapes of the experimental and theoretical distributions at $\mu_0 r = 6.52$ suggests that the detailed spectra of Fig. 5, from which the curve of I_0 vs. $h\nu$ at $\mu_0 r = 6.52$ was calculated, are not seriously in error.

Distribution in Angle

Integration of $I(r, h\nu, \theta)$ over $h\nu$ instead of over θ yields the total intensity as a function of angle, $I_A(r, \theta)$. Since the angular distributions so obtained for different penetrations did not differ significantly, a mean distribution is plotted in Fig. 7. The quantity shown is proportional to the total energy per second of all quantum energies crossing a square centimeter per unit solid angle at the angle θ.

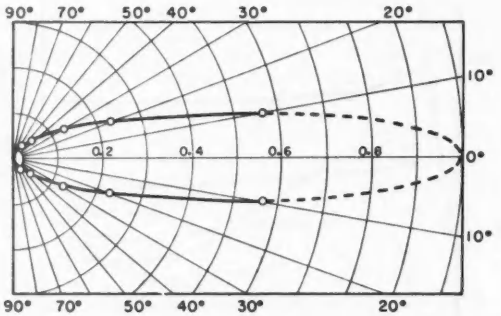

FIG. 7. Mean angular distribution. Distance from the origin represents the relative intensity of all quantum energies per unit solid angle at the angle θ.

The most striking feature of the angular distribution is its strong concentration in the forward direction. Over half the scattered intensity emerges within 30° of the direction of the primaries. Three factors contribute to this result: (1) the scattering cross-section is greatest in the forward direction; (2) the energy of the scattered quantum is greatest in this direction; and (3) in general, the greater the angle of scatter, the greater the thickness of absorber that must be penetrated before the scattered ray can get out.

A re-examination of Fig. 5 will show how this total angular distribution is made up with respect to quantum energy. The high-energy radiation is entirely in the forward direction—as it must be, by the nature of the scattering process —while the low-energy radiation is much more widely distributed in angle. This is not unreasonable since radiation below, say, 0.4 Mev. appearing in the forward hemisphere will mostly have undergone two or more scatterings and will tend to have "forgotten" its original direction.

Summary

To sum up, the curves of Fig. 5 should represent approximately the "equilibrium" distribution in energy and angle of the scattered radiation produced in a medium of low atomic number by a source of cobalt-60 gamma-rays imbedded in the medium. Fig. 6 gives the total energy distribution, integrated over angle, for a number of values of the penetration in the medium, and Fig. 7 gives the "equilibrium" angular distribution, integrated over energy.

ACKNOWLEDGMENTS

The experiment was conceived in co-operation with Mr. W. R. Dixon, who also contributed to the preliminary stages of the work and made a number of helpful criticisms of the final manuscript; his assistance is gratefully acknowledged. It is also a pleasure to thank Mr. C. D. Cox, who processed the films and assisted with many other phases of the experiment. The 700-curie source was obtained on loan through the kindness of the Commercial Products Division, Atomic Energy of Canada Limited.

REFERENCES

1. GARRETT, C. and WHYTE, G. N. Phys. Rev. 95: 889. 1954.
2. GOLDSTEIN, H. and WILKINS, J. E. Calculations of the penetration of gamma rays. NDA 15C-41. Nuclear Development Associates, Inc., White Plains, New York. 1954.
3. HAYWARD, E. Phys. Rev. 86: 493. 1952.
4. HOFSTADTER, R. and MCINTYRE, J. A. Phys. Rev. 78: 619. 1950.
5. MAIENSCHEIN, F. C. Multiple-crystal gamma-ray spectrometer. ORNL-1142. Oak Ridge National Laboratory, Oak Ridge, Tennessee. 1952.
6. SPENCER, L. V. and FANO, U. J. Research Natl. Bur. Standards, 46: 446. 1951. Phys. Rev. 81: 464. 1951.
7. WEISS, M. M. and BERNSTEIN, W. Phys. Rev. 92: 1264. 1953.
8. WHITE, G. R. Phys. Rev. 80: 154. 1950.

NOTES

A NOTE ON THE X-RAY SPECTRUM OF A 70 MEV. SYNCHROTRON

By L. E. H. Trainor and S. B. Brown

The X-ray spectrum of the 70 Mev. synchrotron at Queen's University was determined by McDiarmid (2) from measurements on electron pairs produced in photographic plates exposed to the beam, making use of the Bethe–Heitler (1) cross sections for pair production. Although his results above 25 Mev. are in reasonable agreement with the expected Schiff spectrum (3), they are in serious disagreement below this value, showing a markedly lower intensity of low energy X-rays. The question naturally arises as to whether this disagreement is real. The purpose of the present note is to show that the requirement of consistency of the experimental data with the Bethe–Heitler cross sections indicates a discrimination against low energy X-rays which may be sufficient to account for the disagreement between theory and experiment.

McDiarmid employed two methods: in the first, pairs were required to have track lengths $\geqslant 1300\mu$ in the emulsion; in the second, this requirement was reduced to $\geqslant 300\mu$. The results obtained by the first method are less reliable since the statistics are not as good, and the assumption that all pairs are produced in the forward direction breaks down completely at low X-ray energies. In Fig. 3 of Reference 2, a series of histograms based on the results of the second method is presented, showing the distribution of X-ray energy between pairs for each 5 Mev. interval of X-ray energies from 5 to 45 Mev. As noted by McDiarmid, the experimental distributions are considerably more peaked than the Bethe–Heitler curves. This feature of the distributions is sufficiently pronounced to be considered statistically significant, as is borne out by the analysis described below. It suggests that discrimination was made against those pairs having at least one low energy member. It is then interesting to enquire whether the discrimination is sufficient to account for the reported deviation from a Schiff spectrum.

We proceed as follows. Assume that the measured number of pairs (as corrected by McDiarmid for multiple scattering) having positron energy in a small range about E_1 and electron energy in a small range about E_2 can be corrected by multiplication with an expression of the form

$$f(E_1)\, f(E_2)$$

where $f(E)$ is a function to be determined. One cannot obtain the product $f(E_1)\, f(E_2)$ directly from the histograms of Fig. 3, Reference 2, since the low energy discrimination implies that the theoretical distribution shown there for each X-ray energy k requires a further "relative" normalization $N(k)$ which depends upon k only, and which is unknown at the outset. In fact, $N(k)$ is the desired correction to the spectrum. However, we can write

$$f(E_1)\, f(E_2) = N(k)\, g(E_1, E_2)$$

where $g(E_1, E_2)$ is the ratio of the experimental and theoretical ordinates, corresponding to X-ray energy division $k = E_1+E_2$, which appear in Fig. 3 of Reference 2. Hence the ratios

$$\frac{f(E_1)\,f(E_2)}{f(E_1')\,f(E_2')} = \frac{g(E_1, E_2)}{g(E_1', E_2')},$$

where $E_1+E_2 = E_1'+E_2'$, can be determined. The problem is then to determine $f(E)$ from the resulting set of ratios, with the requirement that $f(E)$ approach unity for sufficiently large values of E.

An elaborate analysis of this problem is scarcely justified, since the experimental statistics are poor, and the assumed form of the correction factor has only a rough justification. The approach used was to compare the experimental ratios with the ratios determined from each of a series of smooth curves having wide variations in form. The choice between curves was based upon several simple criteria, e.g. least mean absolute deviation, least mean algebraic deviation. One can establish beyond doubt that the best-fit curve has the general shape of the curve shown in Fig. 1, i.e. a rapidly decreasing negative slope as a function of energy E; but the data are relatively insensitive to rather wide variations in the details of shape. Hence, the corrections applied here have only a rough quantitative significance and should not be interpreted too literally.

Identifying $f(E)$ with the curve shown in Fig. 1, the experimental results of McDiarmid can be corrected below 45 Mev. X-ray energy, in accordance with the above remarks. As expected, the corrections are large at the low energy end of the spectrum, decreasing from a factor of 5.6 at 7.5 Mev. to about 1.1 at 45 Mev. Presumably the corrections above 45 Mev. would be

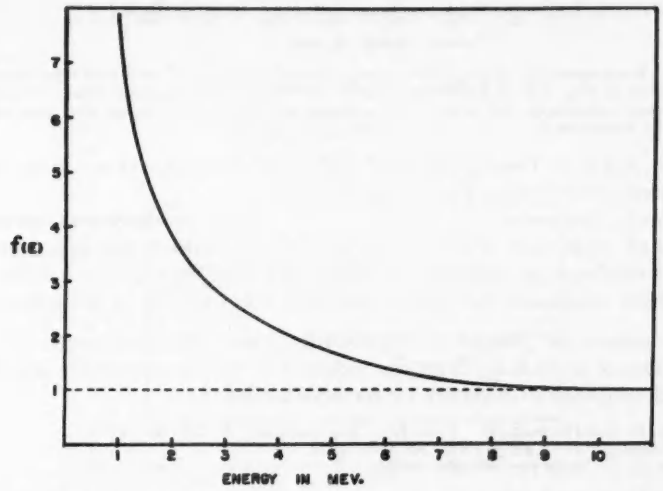

FIG. 1. The function $f(E)$. If E_1 is the positron energy and E_2 the electron energy for each of a measured number of pairs, the corrected number is obtained by multiplication with the product $f(E_1)\,f(E_2)$.

negligible. The resulting spectrum, renormalized to fit McDiarmid's results at 42.5 Mev., is shown in Fig. 2 as crosses, with the vertical lines indicating the statistical errors. For comparison, McDiarmid's results (black dots)

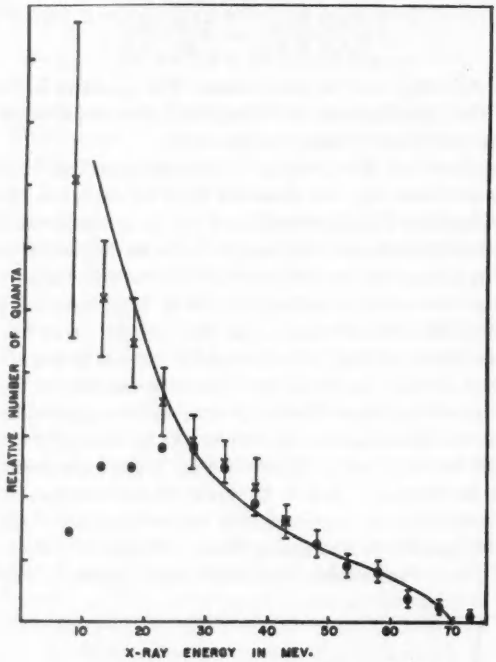

FIG. 2. X-ray spectrum of the 70 Mev. Queen's synchrotron. The black dots reproduce the results shown in Fig. 5(*b*) of Reference 2, while the crosses give the same results according to the present corrections. For comparison, a theoretical Schiff spectrum has also been reproduced from Reference 2.

and his choice of theoretical Schiff spectrum (smooth curve) have been reproduced in Fig. 2 from Fig. 5(*b*) of Reference 2.

Evidently, the present corrections lead to reasonable agreement between theory and experiment. However, in view of the indirect and approximate methods employed in obtaining the corrections used, one is only justified in drawing the conclusion that theory and experiment are not in disagreement.

The authors are pleased to acknowledge useful discussion with W. R. Dixon. One of us (S.B.B.) is greatly indebted to the Committee on Scientific Research of Queen's University for financial assistance.

1. BETHE, H. and HEITLER, W. Proc. Roy. Soc. (London), A, 146: 83. 1934.
2. MCDIARMID, I. B. Can. J. Phys. 30: 670. 1952.
3. SCHIFF, L. I. Phys. Rev. 83: 252. 1951.

RECEIVED NOVEMBER 4, 1954.
DEPARTMENT OF PHYSICS,
QUEEN'S UNIVERSITY,
KINGSTON, ONTARIO.

A NOTE CONCERNING FORCES AND TORQUES ON SPHEROIDAL BODIES IN CAVITIES*

By W. J. van de Lindt

An absolute measure of microwave power has been obtained from the force or torque on a ring in a coaxial cavity (1). A metal sphere or spheroid may be used in place of a ring and it possibly offers certain advantages in fabrication and mensuration. The calculation of the forces acting on such a body will be derived from a consideration of the energy of the body in the cavity field. The sphere is supposed to be small compared with the wavelength, so that it will effectively be in a homogeneous field. If the electric field strength is denoted by $\underline{\mathbf{E}}$ and the magnetic field strength by $\underline{\mathbf{H}}$, the energy necessary to bring a body into this field is given by (4*a*)

$$W = -\tfrac{1}{2}(\underline{\mathbf{E}}.\underline{\mathbf{P}}+\underline{\mathbf{H}}.\underline{\mathbf{M}})\,\Delta V. \tag{1}$$

In this equation $\underline{\mathbf{P}}$ is the polarization per unit volume, $\underline{\mathbf{M}}$ the magnetization per unit volume, and ΔV is the volume of the body. In the case of an alternating field, a factor $\frac{1}{2}$ has to be included so that

$$W = -\tfrac{1}{4}(\mathbf{E}.\mathbf{P}+\mathbf{H}.\mathbf{M})\,\Delta V \tag{2}$$

where now **E**, **P**, **H**, and **M** refer to peak values. By differentiating this expression with respect to one of the co-ordinates, the force or torque in that direction may be found.

Calculation of Electric and Magnetic Field Strength in the Cavity

Assume a full wavelength coaxial cavity in which the field is of the form

$$E_R = (E_0/R)\sin kz, \qquad H_\phi = (H_0/R)\cos kz \tag{3}$$

(see Fig. 1)

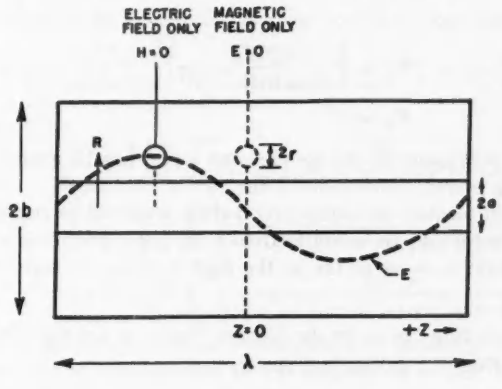

FIG. 1.

*Issued as N.R.C. No. 3500.

with the constants E_0 and H_0 related by the expression

$$H_0 = \sqrt{\epsilon_0/\mu_0}\, E_0$$

where ϵ_0 and μ_0 are the dielectric constant and permeability of a vacuum.

The stored energy in such a cavity is given by

$$W_S = \tfrac{1}{2}\int_V \mu_0 H^2 dv = \tfrac{1}{2}\int_V \epsilon_0 E^2 dv$$

where the integral extends over the volume of the cavity. Substituting [3] in this equation gives

[4] $$W_S = \frac{\pi^2\mu_0}{k} H_0^2 \ln(b/a) = \frac{\pi^2\epsilon_0}{k} E_0^2 \ln(b/a) \quad \text{(see Fig. 1).}$$

If the cavity has losses, which, in practice, is always the case, a Q can be defined as follows (2):

[5] $$Q = \frac{\omega \times \text{Energy stored}}{\text{Energy dissipated per second}} = \frac{\omega W_S}{W_D}.$$

In the case of a stationary state, the energy dissipated, W_D, must be equal to the energy supplied to the cavity, so W_D also represents the incoming power.

With the help of [4] and [5]

[6] $$E_0^2 = \frac{QW_D}{\pi^2 c\epsilon_0 \ln(b/a)\, R^2}$$

where c is the velocity of light. The calculations will be made for bodies in the planes where either $\sin kz = 1$ or $\cos kz = 1$. In the first case the electric field strength at a point R

[7] $$E_R = \left\{\frac{QW_D}{\pi^2 c\epsilon_0 \ln(b/a)\, R^2}\right\}^{\frac{1}{2}}$$

while $$H_\phi = 0,$$

and in the second case

[8] $$H_\phi = \left\{\frac{QW_D}{\pi^2 c\mu_0 \ln(b/a)\, R^2}\right\}^{\frac{1}{2}}$$

while $$E_R = 0.$$

With the help of [7] and [8] the torques and forces can be expressed in terms of the incoming power, dimensions of the cavity, and its Q.

For forces and torques on conducting bodies, it should be remembered that a perfect conductor can be considered to have a permeability $\mu_i = 0$ and a dielectric constant $\epsilon_i = \infty$ as far as the field outside the body is concerned (4*b*).

Force on a Conducting Sphere in the Electric Field of a Coaxial Cavity

The polarization of a sphere is given by (4*b*)

$$\mathbf{P} = 3\epsilon_0 \mathbf{E}\, \frac{\epsilon_i - \epsilon_0}{2\epsilon_0 + \epsilon_i}.$$

In the case of a perfect conductor

$$\lim_{\epsilon_i \to \infty} \mathbf{P} = 3\epsilon_0 \mathbf{E}$$

and [1] becomes

$$W = -\tfrac{3}{4}\,\epsilon_0 E^2 \Delta V.$$

If the sphere is situated as indicated in Fig. 1, δW, with the help of [7], becomes

$$\delta W = -\frac{3QW_D\,\Delta V}{4\pi^2 c \ln(b/a)\,R^2}.$$

For a sphere with radius r the force becomes

[9] $$F_{R_E} = -\frac{\partial \delta W}{\partial R} = -\frac{2QW_D}{\pi c \ln(b/a)}\,\frac{r^3}{R^3},$$

the sphere tending to move to the inner conductor, where the field is strongest.

Force on a Conducting Sphere in a Magnetic Field

The magnetic polarization of a sphere is given by

$$\mathbf{M} = 3\mu_0 \frac{\mu_i - \mu_0}{2\mu_0 + \mu_i}\mathbf{H},$$

which for a conducting sphere becomes

$$\mathbf{M} = \tfrac{3}{2}\,\mu_0 \mathbf{H}.$$

In the same way as before but using equation [8] instead of [7] the force on the sphere in the magnetic field is found to be

[10] $$F_{R_M} = \frac{QW_D}{\pi c \ln(b/a)}\,\frac{r^3}{R^3},$$

the sphere tending to move away from the inner conductor.

Force on a Conducting Ellipsoid

The polarization of an ellipsoid is given by (4*b*)

[11] $$P_x = \frac{\Delta V\, E_x}{L_1 + 1/(\epsilon_i - \epsilon_0)},\quad P_y = \frac{\Delta V\, E_y}{L_2 + 1/(\epsilon_i - \epsilon_0)},\quad P_z = \frac{\Delta V\, E_z}{L_3 + 1/(\epsilon_i - \epsilon_0)}$$

where

$$L_1 = \frac{u.v.w}{2\epsilon_0}\int_0^\infty \frac{ds}{(s+u^2)\sqrt{[(s+u^2)(s+v^2)(s+w^2)]}},$$

$$L_2 = \frac{u.v.w}{2\epsilon_0}\int_0^\infty \frac{ds}{(s+v^2)\sqrt{[(s+u^2)(s+v^2)(s+w^2)]}},$$

$$L_3 = \frac{u.v.w}{2\epsilon_0}\int_0^\infty \frac{ds}{(s+w^2)\sqrt{[(s+u^2)(s+v^2)(s+w^2)]}}.$$

E_x, E_y, E_z are the components of the electric field intensity taken respectively in the directions of the semiaxes of the ellipsoid, u, v, and w. In general the functions L_1, L_2, L_3 are not expressible as elementary functions. However, with two equal axes the integrals can readily be calculated. So if $v = w < u$

$$L_1 = \frac{1}{u^3e^3}\left\{\ln\left(\frac{1+e}{1-e}\right)-2e\right\}\frac{uv^2}{2\epsilon_0},$$

$$L_2 = \frac{1}{2u^3e^3}\left\{\frac{2e}{1-e^2}-\ln\left(\frac{1+e}{1-e}\right)\right\}\frac{uv^2}{2\epsilon_0},$$

where $e = \sqrt{1-(v^2/u^2)}$ is the eccentricity of the ellipsoid. If

$$P_x = \frac{\Delta V E_x}{L_1} = \alpha_x E_x, \qquad P_y = \frac{\Delta V E_y}{L_2} = \alpha_y E_y,$$

the volume of the ellipsoid being $\Delta V = \frac{4}{3}\pi v^2 u$, this gives, with the help of the expressions for L_1 and L_2,

[12] $$\alpha_x = \frac{8\pi\epsilon_0 u^3e^3}{3\left\{\ln\left(\frac{1+e}{1-e}\right)-2e\right\}}, \qquad \alpha_y = \frac{16\pi\epsilon_0 u^3e^3}{3\left\{\frac{2e}{1-e^2}-\ln\left(\frac{1+e}{1-e}\right)\right\}}.$$

From [1]

[13] $$\delta W = -\tfrac{1}{4}\mathbf{E}.\mathbf{P}\Delta V = -\tfrac{1}{4}\{\alpha_x E_x^2+\alpha_y E_y^2\}$$
$$= -\tfrac{1}{4}\{\alpha_x E^2\sin^2\psi+\alpha_y E^2\cos^2\psi\}$$

where ψ gives the direction of the electric field with respect to the orientation

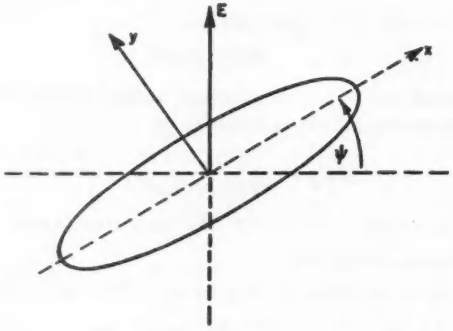

FIG. 2.

of the ellipsoid. With the major axis parallel to the electric field $\psi = \pi/2$, the energy is

$$\delta W = -\tfrac{1}{4}\alpha_x E^2$$

and the force F_{uz} on the ellipsoid, with the help of [7] and [12], becomes

[14] $$-\frac{\partial\delta W}{\partial R} = F_{uz} = \frac{-4e^3}{3\left[\ln\left(\frac{1+e}{1-e}\right)-2e\right]}\cdot\frac{QW_D}{\pi c\ln(b/a)}\cdot\frac{u^3}{R^3}.$$

Torque on an Ellipsoid in an Electric Field

From [13] it follows immediately that the torque on the ellipsoid in the electric field is given by

$$[15]\quad T_{u_E} = \frac{\partial \delta W}{\partial \psi} = \frac{\alpha_x - \alpha_y}{4} E^2 \sin 2\psi$$

$$= \left[\frac{2e^3}{3\left\{\ln\left(\frac{1+e}{1-e}\right) - 2e\right\}} - \frac{4}{3\left\{\frac{2e}{1-e} - \ln\left(\frac{1+e}{1-e}\right)\right\}} \right] \frac{QW_D}{\pi c \ln(b/a)} \frac{u^3}{R^3} \sin 2\psi.$$

Examples

To find out if the torque and force discussed will be observable in practical cases a few numerical examples will be given.

Suppose in the case of a sphere $r = 0.5$ cm., $R = 2.50$ cm., $\ln(b/a) = 1$, $Q = 3000$, $W_D = 1$ watt. The force in an electric field then becomes

$$F_{R_E} = 5\ \mu\text{gm.}$$

In a magnetic field

$$F_{R_M} = 2.5\ \mu\text{gm.}$$

Suppose for the ellipsoid $u = 0.5$ cm., $v/u = 0.5$, the other values being the same as in the case of the sphere. The force then is

$$F = 2.4\ \mu\text{gm.}$$

and the torque is found to be

$$T = 1.8 \times 10^{-2}\ \text{dyne-cm.}$$

The torsion balance used by Kalra (1) had a sensitivity of 0.01 μgm. so that the forces calculated above can be measured fairly accurately. The restoring torque of the quartz fiber used in the experiments of Solow (3) was 1.86×10^{-8} dyne-cm. per radian; it therefore appears that the torque may equally well be used as a basis for an absolute power measurement.

Finally, it should be emphasized that the above calculations are first approximations and are only applicable if the spheroid is small compared with the wavelength.

1. Kalra, S. N. J. Appl. Phys. 24: 1339. 1953.
2. Slater, J. C. Microwave electronics. D. Van Nostrand Company, Inc., New York. 1950. p. 44.
3. Solow, M. C.R.P.L. Reprint 50–15. Natl. Bur. Standards (U.S.), Jan. 12, 1950.
4. Stratton, J. A. Electromagnetic theory. McGraw-Hill Book Company, Inc., New York. 1941. (*a*) p. 114. (*b*) pp. 205–213.

Received October 27, 1954.
Division of Physics,
National Research Council,
Ottawa, Canada.

THE PHYSICAL SOCIETY

MEMBERSHIP of the Society is open to all who are interested in Physics.

FELLOWS pay an Entrance fee of £1 1*s*. ($3.00) and an Annual Subscription of £2 2*s*. ($6.00).

STUDENTS: A candidate for Studentship must be between the ages of 18 and 26, and pays an Annual Subscription of 7*s*. 6*d*. ($1.10).

MEETINGS: Fellows and Students may attend all Meetings of the Society including the annual Exhibition of Scientific Instruments and Apparatus.

PUBLICATIONS include the *Proceedings of the Physical Society*, published monthly in two sections, and *Reports on Progress in Physics*, published annually. Volume XVII, 1954, is now available (price 50*s*. ($7.15)). Members are entitled to receive many of the Publications at a reduced rate.

Further information can be obtained from:

THE PHYSICAL SOCIETY

1, LOWTHER GARDENS, PRINCE CONSORT ROAD

LONDON, S.W.7, ENGLAND

CANADIAN JOURNAL OF PHYSICS

Notes to Contributors

Manuscripts

(i) ***General.*** Manuscripts should be typewritten, double spaced, on paper 8½×11 in. **The original and one copy are to be submitted.** Tables and captions for the figures should be placed at the end of the manuscript. Every sheet of the manuscript should be numbered.

Style, arrangement, spelling, and abbreviations should conform to the usage of this journal. Names of all simple compounds, rather than their formulas, should be used in the text. Greek letters or unusual signs should be written plainly or explained by marginal notes. Superscripts and subscripts must be legible and carefully placed.

Manuscripts should be carefully checked before they are submitted; authors will be charged for changes made in the proof that are considered excessive.

(ii) ***Abstract.*** An abstract of not more than about 200 words, indicating the scope of the work and the principal findings, is required, except in Notes.

(iii) ***References.*** References should be listed **alphabetically by authors' names,** numbered, and typed after the text. The form of the citations should be that used in this journal; in references to papers in periodicals, titles should not be given and only initial page numbers are required. All citations should be checked with the original articles and each one referred to in the text by the key number.

(iv) ***Tables.*** Tables should be numbered in roman numerals and each table referred to in the text. Titles should always be given but should be brief; column headings should be brief and descriptive matter in the tables confined to a minimum. Vertical rules should be used only when they are essential. Numerous small tables should be avoided.

Illustrations

(i) ***General.*** All figures (including each figure of the plates) should be numbered consecutively from 1 up, in arabic numerals, and each figure referred to in the text. The author's name, title of the paper, and figure number should be written in the lower left corner of the sheets on which the illustrations appear. Captions should not be written on the illustrations (see Manuscripts (i)).

(ii) ***Line Drawings.*** Drawings should be carefully made with India ink on white drawing paper, blue tracing linen, or co-ordinate paper ruled in blue only; any co-ordinate lines that are to appear in the reproduction should be ruled in black ink. Paper ruled in green, yellow, or red should not be used unless it is desired to have all the co-ordinate lines show. All lines should be of sufficient thickness to reproduce well. Decimal points, periods, and stippled dots should be solid black circles large enough to be reduced if necessary. Letters and numerals should be neatly made, preferably with a stencil (**do NOT use typewriting**) and be of such size that the smallest lettering will be not less than 1 mm. high when reproduced in a cut 3 in. wide.

Many drawings are made too large; originals should not be more than 2 or 3 times the size of the desired reproduction. In large drawings or groups of drawings the ratio of height to width should conform to that of a journal page but the height should be adjusted to make allowance for the caption.

The original drawings and one set of clear copies (e.g. small photographs) are to be submitted.

(iii) ***Photographs.*** Prints should be made on glossy paper, with strong contrasts. They should be trimmed so that essential features only are shown and mounted carefully, with rubber cement, on white cardboard with no space or only a **very** small space (less than 1 mm.) between them. In mounting, full use of the space available should be made (to reduce the number of cuts required) and the ratio of height to width should correspond to that of a journal page (4½×7½ in.); however, allowance must be made for the captions. Photographs or groups of photographs should not be more than 2 or 3 times the size of the desired reproduction.

Photographs are to be submitted in duplicate; if they are to be reproduced in groups one set should be mounted, the duplicate set unmounted.

Reprints

A total of 50 reprints of each paper, without covers, are supplied free. Additional reprints, with or without covers, may be purchased.

Charges for reprints are based on the number of printed pages, which may be calculated approximately by multiplying by 0.6 the number of manuscript pages (double-spaced typewritten sheets, 8½×11 in.) and including the space occupied by illustrations. An additional charge is made for illustrations that appear as coated inserts. The cost per page is given on the reprint requisition which accompanies the galley.

Any reprints required in addition to those requested on the author's reprint requisition form must be ordered officially as soon as the paper has been accepted for publication.

Contents

Page

Mass Spectrometric Study of Natural and Neutron-irradiated-Chlorine—*A. W. Boyd, F. Brown, and M. Lounsbury* - - - 35

The Half-life of Cl^{36}—*Rosalie M. Bartholomew, A. W. Boyd, F. Brown, R. C. Hawkings, M. Lounsbury, and W. F. Merritt* - - 43

Surface Tension of He^3—*D. R. Lovejoy* - - - - - - - - - - 49

A Note Concerning the Conductivity of Liquid Dielectrics—*John Hart and D. A. Simmons* - - - - - - - - - - - - - - 54

Thermal and Electrical Conductivities of Solids at Low Temperatures—*Guy K. White and S. B. Woods* - - - - - - - - - 58

A Panoramic Mass Spectroscope for Kinetic Studies—*Edouard G. Leger* - 74

Measurements of Spectral and Angular Distributions of Secondary Gamma-rays in Matter—*G. N. Whyte* - - - - - - - - - 96

A Note on the X-ray Spectrum of a 70 Mev. Synchrotron—*L. E. H. Trainor and S. B. Brown* - - - - - - - - - - - - - - 110

A Note Concerning Forces and Torques on Spheroidal Bodies in Cavities—*W. J. van de Lindt* - - - - - - - - - - - - - 113

Printed in Canada by University of Toronto Press